JAERI-M
83-122

EFFECTS OF CORE INLET WATER SUBCOOLING ON REFLOODING PHENOMENA

— SCTF CORE-I FORCED FEED FLOODING TESTS —

August 1983

Takamichi IWAMURA, Yukio SUDO,
Makoto SOBAJIMA, Masahiro OSAKABE,
Akira OHNUKI, Yutaka ABE and
Hiromichi ADACHI

日本原子力研究所
Japan Atomic Energy Research Institute

JAERI-Mレポートは，日本原子力研究所が不定期に公刊している研究報告書です。
入手の問合わせは，日本原子力研究所技術情報部情報資料課（〒319-11茨城県那珂郡東海村）あて，お申しこしください。なお，このほかに財団法人原子力弘済会資料センター（〒319-11 茨城県那珂郡東海村日本原子力研究所内）で複写による実費頒布をおこなっております。

JAERI-M reports are issued irregularly.
Inquiries about availability of the reports should be addressed to Information Section, Division of Technical Information, Japan Atomic Energy Research Institute, Tokai-mura, Naka-gun, Ibaraki-ken 319-11, Japan.

編集兼発行　日本原子力研究所
印　　刷　㈱高野高速印刷

JAERI-M 83-122

Effects of Core Inlet Water Subcooling on Reflooding Phenomena

—— SCTF Core-I Forced Feed Flooding Tests ——

Takamichi IWAMURA, Yukio SUDO, Makoto SOBAJIMA,
Masahiro OSAKABE, Akira OHNUKI, Yutaka ABE
and Hiromichi ADACHI

Department of Nuclear Safety Research,
Tokai Research Establishment, JAERI

(Received July 9, 1983)

The major objectives of Slab Core Test Facility (SCTF) Program are to investigate the two-dimensional thermo-hydrodynamic behavior in the core and the fluid communication between the core and the upper plenum during the reflooding phase of a PWR-LOCA.

The present report describes the experimental studies on the effects of core inlet water subcooling on reflooding phenomena under forced flooding condition observed in Tests S1-04 (high subcooling test) and S1-01 (base case test). Maximum core inlet water subcoolings in the two tests were 37 and 16 K, respectively.

It was found that the higher core inlet water subcooling results in the higher quench propagation, the higher heat transfer coefficient and the lower void fraction near the quench front, the larger water accumulation in the core and upper plenum, the smaller water carryover through the hot leg, and the more significant cross flow in the core.

Keywords: Reflood, LOCA, Heat Transfer, Quench, Film Boiling, Two-phase Flow, Void Fraction, Subcooling Effects, Cross Flow, SCTF, PWR

The work was perfomed under contract with the Atomic Energy Bureau of Science and Technology Agency of Japan

再冠水現象におよぼす炉心入口サブクーリングの影響
－ＳＣＴＦ第１次炉心強制注入再冠水試験－

日本原子力研究所東海研究所安全工学部
岩村公道・数土幸夫・傍島　真・刑部真弘
大貫　晃・阿部　豊・安達公道

（１９８３年７月９日受理）

平板炉心試験装置（ＳＣＴＦ）計画は，ＰＷＲ－ＬＯＣＡ時の再冠水過程における，炉心部の２次元的な熱水力挙動や，炉心と上部プレナム間の流体挙動の相互干渉を調べることを目的としている。

本報告書では，強制注入試験シリーズのうち，試験Ｓ１－０４（高サブクーリング試験）およびＳ１－０１（基準試験）において観察された，炉心入口サブクーリングの再冠水現象に及ぼす影響についての解析結果を報告する。これらの試験における炉心入口最大サブクーリングは，それぞれ３７および１６Ｋである。

これら２つの実験結果を比較して，炉心入口サブクーリングが大きくなると，クエンチ伝播が速くなり，クエンチ点近傍の熱伝達率は改善され，クエンチ発生時のボイド率は小さくなり，炉心および上部プレナム内蓄水量は多くなり，ホットレグキャリーオーバー量は少なくなり，炉心内の横流れの強さは大きくなることがわかった。

本報告書は，電源開発促進対策特別会計法に基づき，科学技術庁からの受託によって行なった研究の成果である。

Contents

目　　次

List of Tables

List of Figures

1. Introduction

The studies of thermo-hydrodynamic behavior during the reflood phase of a postulated loss of coolant accident (LOCA) in a pressurized water reactor (PWR) have been performed with various kinds of test facilities. For example, FLECHT-SEASET tests have been performed with the bundle of 161 heater rods[1]. However, most of the simulated cores in the previous reflooding experiments have been too small in order to investigate the multi-dimensional effects expected in an actual reactor.

The multi-dimensional thermo-hydrodynamic behavior during the reflood phase is being investigated by using the Slab Core Test Facility (SCTF) which has a full height, full radial width and single bundle depth electrically heated core. The SCTF program is a part of the large scale reflood test program under contract with the Atomic Bureau of Science and Technology Agency of Japan along with the Cylindrical Core Test Facility (CCTF) program.

In the SCTF Core-I series, thirteen forced-feed flooding tests were performed in which the downcomer was isolated from the lower plenum and the emergency core cooling (ECC) water was directly injected into the lower plenum. In this way, the core inlet water temperature can be specified during each test as well as the flow rate. The core inlet water subcooling was set as low as possible for most of these tests.

In the PWR-LOCA situation, however, the ECC water is injected into the cold leg at much lower temperature than the saturation temperature. Therefore, though the ECC water is heated by contacting to the hot wall of structures and mixing with two-phase fluid or steam in the cold leg, downcomer and lower plenum before arriving at the core inlet, it is reasonably expected that the cooling water is subcooled to some degree at the inlet of core. The higher subcooling of cooling water may not only promote the core cooling but also affect the hydrodynamic behavior in the primary system through the change of steam generation rate in the core.

The present report describes the effects of core inlet subcooling on the core thermal behavior and the hydrodynamic behavior in the pressure vessel and the primary coolant system by comparing the results from Test S1-04 (high subcooling test) with those from Test S1-01 (base case test).

The measurement locations and some selected data obtained in Test S1-04 are presented in Appendixes A and B, respectively.

2. Experiment

2.1 Test Facility

The schematic diagram of SCTF and the comparison of dimensions betweeen the SCTF and a 1,100 MWe PWR are shown in Fig. 2-1 and Table 2-1, respectively.

The primary coolant loops consist of a hot leg equivalent to the four actual hot legs, a steam/water separator corresponding to the four actual steam generators, an intact cold leg equivalent to the three actual intact cold legs, a broken cold leg on the pressure vessel side, and a broken cold leg on the steam/water separator side. These two broken cold legs are connected to two containment tanks, respectively.

The flow area scaling ratio is 1/21 to a 1,100 MWe PWR, whereas the height of each component simulates the actual PWR. The emergency core cooling system (ECCS) consists of an accumulator (Acc) and a low pressure coolant injection (LPCI) systems. Fig. 2-2 shows the vertical cross section of the pressure vessel. The pressure vessel includes a simulated core, an upper plenum with internals, a lower plenum, a core baffle and a downcomer.

The simulated core consists of 8 bundles arranged in a row with full radial width. Each bundle consists of 234 heater rods and 22 non-heated rods arranged in 16×16 array. The outer diameter and the heated length of the heater rod are 10.7 mm and 3660 mm, respectively. The dimensions of rod bundle such as the rod pitch, the spacers, the end box tie plate etc., are based on those for a 15×15 fuel rod bundle of a PWR.

The core and the upper plenum are enveloped by honeycomb thermal insulators to minimize the wall effects.

More detailed information on the SCTF is available in reference (2).

The accuracy of instruments used in this report is listed in Table 2-2.

2.2 Test Conditions

The tests investigated in this report are the base case test (Test S1-01) and the high subcooling test (Test S1-04). Major test conditions for these tests are listed in Table 2-3. The BOCREC in Table 2-3 represents the time at the bottom of core recovery when the ECC water reaches the bottom of heated part.

These two tests were performed under almost the same conditions except the core inlet water subcooling. The intended values for the system pressure and the maximum cladding temperature at the start of reflood were 0.2 MPa and 973 K, respectively. The nominal flooding velocities during Acc and LPCI injection periods were 5 and 2.5 cm/sec, respectively, corresponding to 22.4 and 11.2 kg/sec of injection rates. The radial power profile was based on the initial core of a 1,100 MWe Westinghouse type PWR. The axial peaking factor is 1.4 for all bundles. The power decay curve was the sum of the ANS standard curve and the additional power generated by actinides and delayed neutron fission effect for voided core. The above-mentioned test conditions have been selected to reasonably represent the situation of reflood pahse of a PWR-LOCA.

The core inlet water subcooling was intended to be 30 K in Test S1-04, while it was set as low as possible in Test S1-01. The subcooling of 30 K is considered to be reasonable based on the cold leg injection test in CCTF core-1. However, the average subcoolings were higher than the intended values for these two tests due to the overshoot of system pressure and temperature distribution in the lower plenum. Figure 2-3 shows the transients of core inlet water temperatures for Tests S1-01 and S1-04, along with the saturation temperatures at the core center and at the lower plenum and also the water temperature at 950 mm above the bottom of heated length. As shown in Fig. 2-3, the core inlet water subcooling varied from 16 to 5 K during 100 to 500 seconds after the beginning of reflood (or Bottom of Core Recovery; BOCREC) for Test S1-01, while it varied from 37 to 32 K during the same period for Test S1-04.

2.3 Test Procedure

The test procedure for these two tests was as follows. After setting the initial conditions, core heating was initiated. When four cladding temperature signals exceeded 926 K, the Acc injection was initiated into the lower plenum and the core heating power was kept constant. After 5 seconds of power keeping time, the core heating power began to decrease along the specified decay curve from 30 seconds after shutdown. After 20 seconds from the initiation of Acc injection, the ECC injection was switched from Acc to LPCI. The time of switching

from Acc to LPCI was determined based on the analytical results for an actual PWR. The tests were terminated at 900 seconds after the initiation of LPCI.

Table 2-1 Comparison of dimensions between SCTF and 1,100 MWe PWR

Item	SCTF	PWR	Ratio (SCTF/PWR)
Quantity of Bundle	8	193	1/24.1
Number of Heater Rod	1872	39372	1/21.0
Number of Rods	2048	43425	1/21.2
Effective Length of Heater Rod (mm)	3660	3660	1/1
Rod Pitch (mm)	14.30	14.30	1/1
Diameter of Heater Rod (mm)	10.70	10.72	1/1
Diameter of Unheated Rod (mm)	13.80	13.87	1/1
Flow Area of Core (m^2)	0.259	4.76	1/17.7
Effective Core Flow Area Based on the Measured Level-Volume Relationship(m^2)	0.35	4.76	1/13.6
Fluid Volume of Core Enveloped by Honeycomb Insulators*	0.92	17.95	1/19.5
Fluid Volume of Lower Plenum (m^3)	1.305	29.62	1/22.7
Fluid Volume of Upper Head (m^3)	0.86	19.8	1/23.0
Baffle Region Flow Area (m^2)	0.10	1.76	1/17.6
Upper Plenum Fluid Volume (m^3)	1.16	23.8	1/20.5
Downcomer Flow Area (m^2)	0.121	2.47	1/20.4
UCSP Thickness (m)	76	76	1/1
Steam Generator Inlet Plenum Simulator Volume (m^3)	0.931	4.25 × 4	1/18.3
Height of Steam Generator Inlet Plenum Simulator (m)	1.595	1.595	1/1
Flow Area at the Top Plate of Steam Generator Inlet Plenum Simulator (m^2)	0.19	4.0	1/21.2
Major Axis Length of Hot Leg Cross Section	737	736.6	1/1
Flow Area of Hot Leg (4 Loops)	0.0826	1.704	1/20.6
Flow Area of Intact Loop (3 Loops)	0.0696	1.149	1/16.5
Flow Area of Broken Cold Leg (m^2)	0.0179	0.383	1/21.4
* Fluid Volume of Core Including Gaps between Core Barrel and Pressure Vessel Wall	1.74		

Table 2-2 Accuracy of instruments

Item	Range	Accuracy	Error band
Heater rod temperature	273∿1273 (K)	±1%	10 K
Fluid temperature	273∿873 (K)	±1%	6K
Liquid level above UCSP	0∿2.5 MAQ	±1%	0.025 MAQ
Liquid level above end box tie plate	0∿0.25 MAQ	±1%	0.0025 MAQ
Differential pressure across core full height	-2∿5 MAQ	±1%	0.07 MAQ
Differential pressure across end box tie plate	-0.5∿0.5 MAQ	±1%	0.05 MAQ
Horizontal differential pressure between bundles 5 and 8	-0.2∿0.2 MAQ	±1%	0.002 MAQ

Table 2-3 Test conditions for Tests S1-01 and S1-04

Test No.	Objective	Max. rod surface temperature at BOCREC (K)	Initial pressure (MPa)	Max. core inlet water subcooling (K)	ECC water injection rate (kg/s)		Radial power ratio			
					Acc max.	LPCI	Bundle 1 & 2	Bundle 3 & 4	Bundle 5 & 6	Bundle 7 & 8
S1-01	Base case	970	0.195	15.5	22	11.4	1.00	1.06	1.01	0.92
S1-04	High subcooling	966	0.202	37.2	21	10.0	1.00	1.06	1.01	0.92

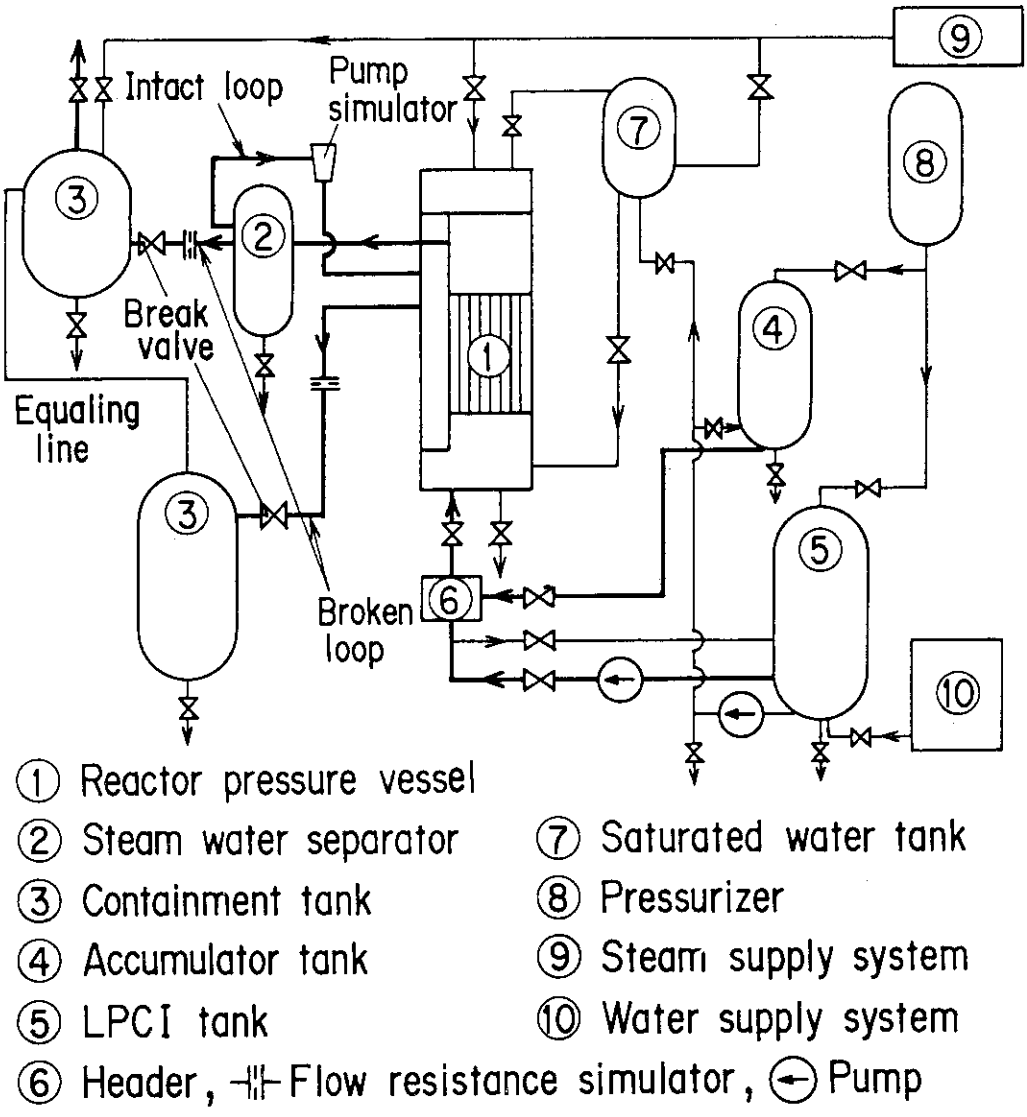

Fig. 2-1 Schematic diagram of Slab Core Test Facility

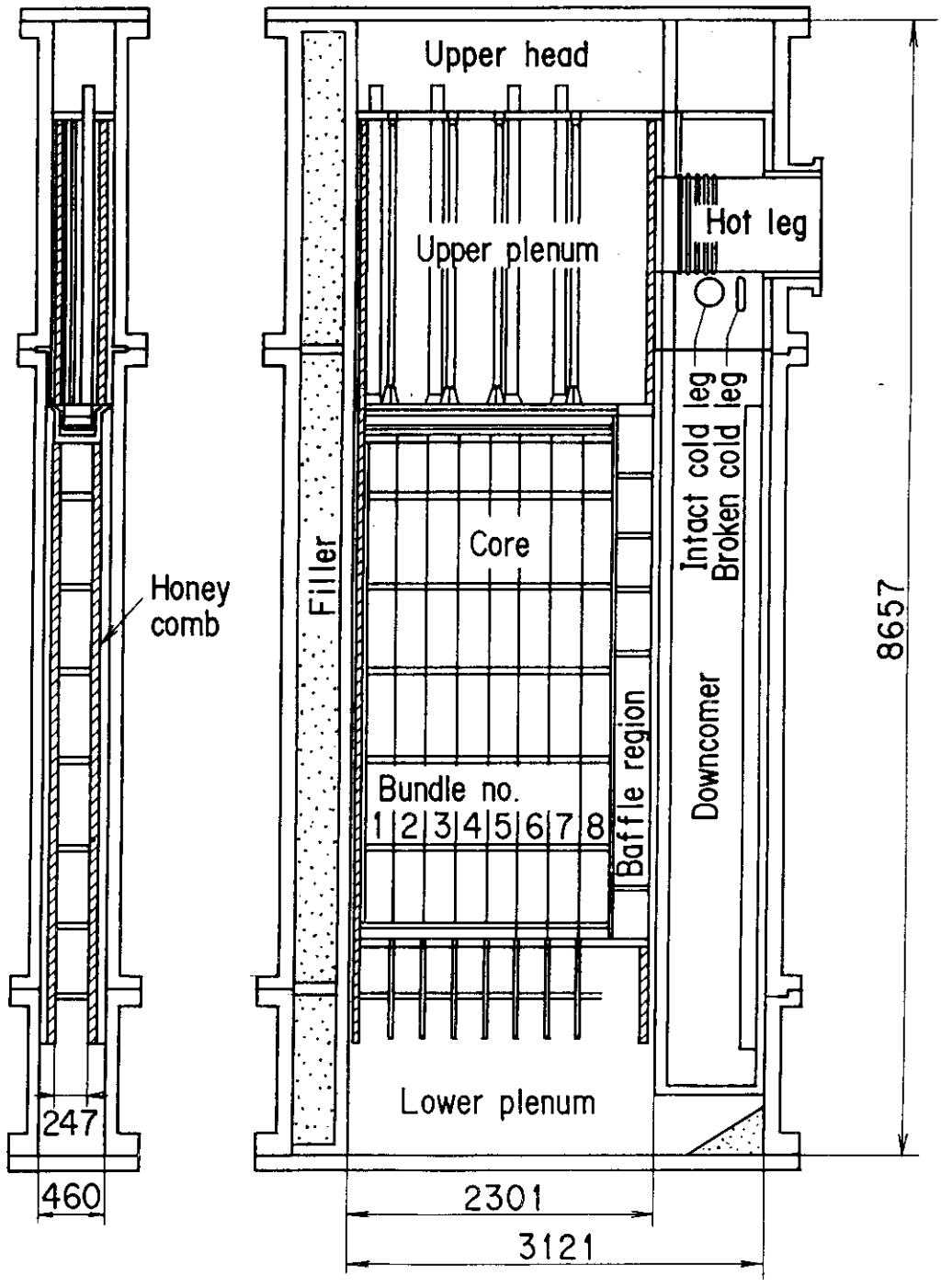

Fig. 2-2 Pressure vessel of Slab Core Test Facility

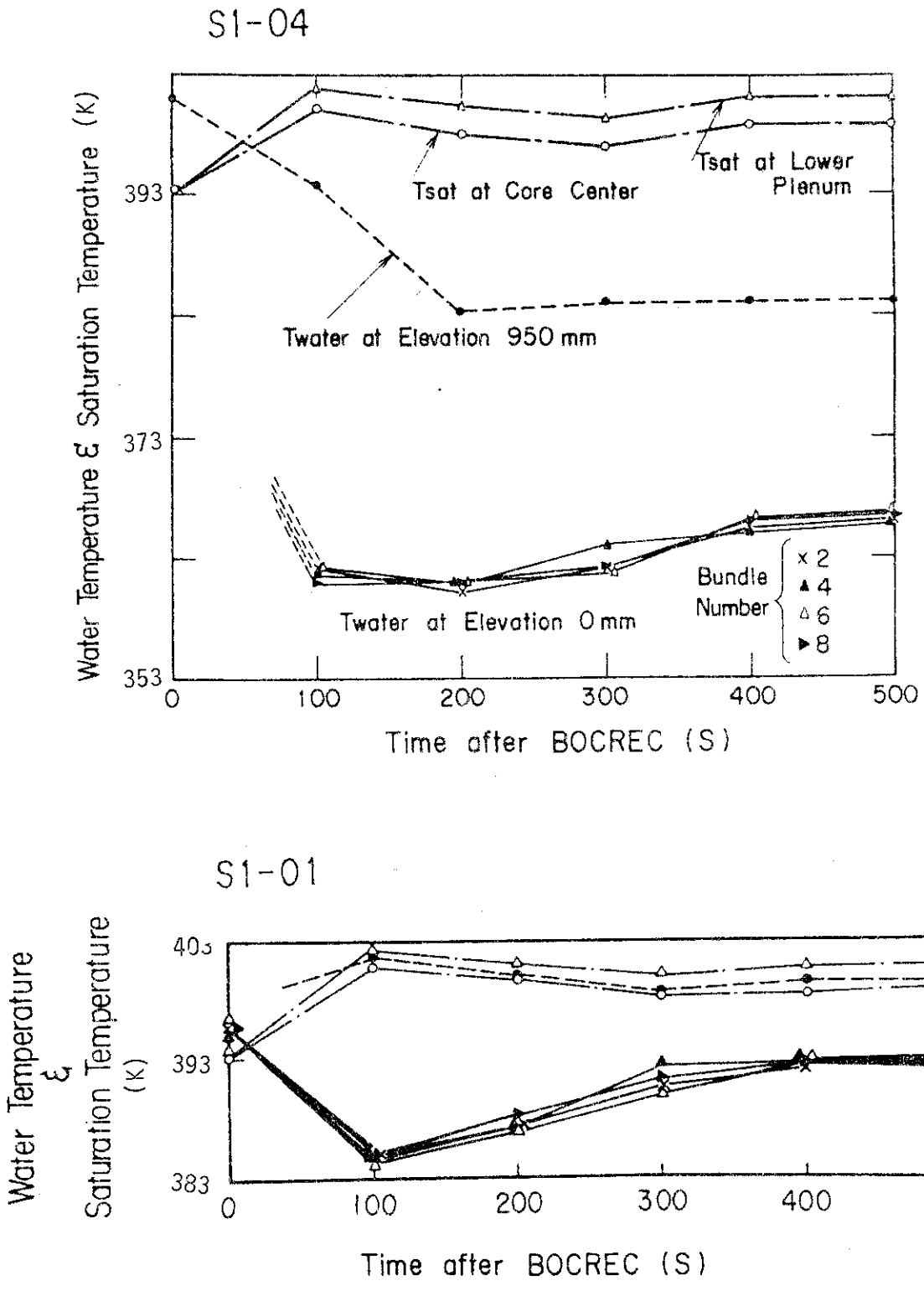

Fig. 2-3 Transients of core inlet temperatures and saturation temperatures

3. Test Results and Discussions

3.1 Core Thermal Behavior

3.1.1 Cladding Temperature

The cladding temperature histories at 1.735, 1.905, and 3.190 m above the bottom of heated length are compared in Fig.3-1 for Tests S1-01 and S1-04. The quench occurs earlier with increasing the core inlet water subcooling, indicating the heat transfer improvement above the quench front. On the other hand, the temperature history before turnaround time is little affected by the core inlet water subcooling. These characteristics are generally confirmed by almost all temperature data in these two tests.

3.1.2 Quench Characteristics

Figure 3-2 shows the comparison of quench envelopes involving all available temperature data for these two tests. As shown in this figure, the quench propagates earlier in Test S1-04 than in Test S1-01. It is also noticed that the quench front propagates upward from the bottom up to about 2.33 m while the thermocouple at 3.62 m always experiences earlier quench. Between the elevations of 2.76 and 3.19 m, the upward and downward quench propagations coexist. As shown in the shape of quench envelopes in Fig.3-2, the downward quench occurs randomly while the upward quench propagation is rather uniform throughout the core.

The effects of core inlet water subcooling on quench time and quench temperature are shown in Figs.3-3 and 3-4, respectively, by comparing the data from Test S1-04 with those from Test S1-01 for the same thermocouples. In these figures, the comparison plots are separated into two figures; the left figures for the thermocouples below 2.33 m and the right figures for the thermocouples above 2.76 m, so as to distinguish the quench characteristics in the upward quench region from those in the downward or mixed quench region.

It is indicated from Fig.3-3 that the higher core inlet water subcooling results in the shorter quench time for almost all elevations. The average ratio of the quench times of Tests S1-04 to S1-01 is about 0.94 for the thermocouples below 2.33 m.

As shown in Fig.3-4, the quench temperature becomes slightly lower

with increasing the core inlet water subcooling only between 0.52 m and 2.33 m from the bottom of heated length. No effects of core inlet water subcooling are observed on the quench temperatures above 2.76 m.

The upward quench velocities are compared in Fig.3-5 between Tests S1-04 and S1-01. The quench velocity was obtained as the average of quench velocities between the thermocouples just below and above the thermocouple elevation where the quench velocity was defined. As indicated in Fig.3-5, the upward quench propagation velocity increases with increasing the core inlet water subcooling.

3.1.3 Heat Transfer Coefficient

Core heat transfer calculation above the quench front was made by using the heat transfer calculation code "HEATT"[3] in which the temperature dependence of physical properties was considered while the axial heat conduction was neglected.

Figures 3-6 (a) and (b) show the transients of heat transfer coefficients at 1.735 m from the bottom of heated length in bundle 2 for Tests S1-01 and S1-04, respectively. The heat transfer coefficient just above the quench front is slightly higher in Test S1-04 than in Test S1-01.

The heat transfer coefficients calculated by the Dittus-Boelter's and Bromley's correlations are compared with the measured heat transfer coefficient in Fig.3-6 (b). These correlations are presented as follows.

1) Dittus-Boelter's correlation for the forced convection heat transfer

$$h = 0.023 \frac{\lambda_g}{D_h} Re^{0.8} Pr^{0.4} \qquad (1)$$

where $Re = V_g D_h / \nu_g$

λ : Thermal conductivity (W/m·k)

V : Velocity (m/s)

D_h : Equivalent diameter of subchannel (m)

Pr : Prandtle number

ν : Kinematic viscosity (m^2/s)

subscript g : vapor

The film temperature are assumed to be $(T_w + T_{sat})/2$. (T_w: Cladding temperature, T_{sat}: Saturation temperature).

2) Film boiling heat transfer correlation

Bromley[4] developed the theory for the film boiling heat transfer correlation on the vertical heated surface.

$$h = h_{sat} + 3/4\ h_R \qquad (2)$$

where $h_{sat} = C\ [\lambda_g^{\ 3}\rho_g(\rho_\ell - \rho_g)H_{fg}'G\ /\ (L_Q\mu_g\Delta T_{sat})]^{\frac{1}{4}}$

$$H_{fg}' = H_{fg}\ [1 + 0.4\ C_P\Delta T_{sat}\ /\ H_{fg}]^2$$

h : Heat transfer coefficient ($W/m^2 \cdot k$)

λ : Thermal conductivity ($W/m \cdot k$)

ρ : Density (kg/m^3)

G : Accelation due to gravity (m/s^2)

μ : Dynamic Viscosity ($Pa \cdot s$)

T_{sat} : Super heat (K)

L_Q : Distance from quench front (m)

H_{fg} : Latent heat of evaporation (J/kg)

subscript g : vapor , ℓ : liquid

h_R is the radiation heat transfer coefficient,

$$h_R = \sigma\ \{(\frac{T_w}{100})^4 - (\frac{T_{sat}}{100})^4\}\ /\ (T_w - T_{sat})$$

σ : Stefan-Boeltsman constant ($W/(m^2 \cdot k^4)$)

Constant C lies between 0.667 and 0.943 by the laminar flow theory of the vapor film.

As shown in Fig.3-6 (b), the measured heat transfer coefficient agrees well with the Dittus-Boelter's correlation in Test S1-04 as well as in Test S1-01 when the quench front is far low from the measuring location, suggesting almost the same characteristics of dispersed flow in these two tests. As the quench front approaches, the Bromley's correlation with C = 0.9 gives good agreement with the measured heat transfer coefficient.

The "C" value in Bromley's correlation can be expressed as:

$$C = (h - 3/4\ h_R)\ /\ [\lambda_g^{\ 3}\rho_g(\rho_\ell - \rho_g)H_{fg}'G\ /\ (L_Q\mu_g\Delta T_{sat})]^{\frac{1}{4}} \qquad (3)$$

By substituting the measured heat transfer coefficient, h, into equation (3), the values of "C" can be calculated as shown in Fig.3-7

for Tests S1-01 and S1-04. As the quench front approaches, the average of "C" value becomes approximately 0.9 in Test S1-04 and 0.75 in Test S1-01.

The "C" values are also plotted against local subcooling and average liquid fraction as shown in Figs.3-8 and 3-9, respectively. The average liquid fraction (1-void fraction) was obtained from the differential pressure measured between 1.365 m and 1.905 m above the bottom of heated length. As indicated in Fig.3-8, no local subcooling can be seen at the elevation of 1.735 m even in Test S1-04 in spite of the large subcooling varied from 37 to 32 K at the inlet of core. On the other hand, the void fraction is significantly lower in Test S1-04 than in Test S1-01 near the quench front as shown in Fig.3-9, indicating the difference of film boiling characteristics between these two tests.

The above-mentioned tendency is recognized at the other measurement location above 1.735 m. However, at the elevation of 0.95 m, the "C" value before the occurrence of quench is also 0.9 in Test S1-04 as well as in Test S1-01 as shown in Fig.3-10.

3.1.4 Void Fraction at Quench Front

Figure 3-11 shows the relation bewteen the quench front elevation and the void fraction at the quench front for seven forced-feed flooding tests in SCTF Core-I. The void fraction at the quench front is obtained by the interpolation of the void fractions calculated from differential pressures at the locations shown in Fig. 3-11. The void fraction at quench front increases with the elevation up to about 2.1 m. At the higher elevation above 2.1 m, on the other hand, the void fraction at quench front remains almost constant. The constant void fraction is about 0.7 for all tests except Test S1-04 in which the constant value is about 0.6.

One of the reasons of the higher quench velocity and the higher heat transfer coefficient in the higher core inlet water subcooling test can be attributed to the lower void fraction near the quench front.

3.2 Hydrodynamic Behavior

3.2.1 Water Accumulation in Core and Upper Plenum

Compared in Fig. 3-12 are the mass of water accumulated in the core including the core baffle region and that accumulated in the upper plenum for Tests S1-01 and S1-04. As the core inlet water subcooling is increased, more amount of water is accumulated in the core during the whole period and also in the upper plenum from about 160 seconds after the BOCREC (Bottom of Core Recovery).

The effect of core inlet water subcooling on the water accumulation in core can be clearly observed in the transients of core full height differential pressures as shown in Fig.3-13 in which comparisons are given for Bundles 2, 4, 6 and 8, respectively. The higher core inlet water subcooling results in the higher water accumulation in core for all bundles after the ECC injection mode is switched from Acc to LPCI at about 10 seconds after the BOCREC, because the elevation of boiling boundary is higher in the higher subcooling test. However, for about first 10 seconds, the differential pressure transients are almost the same for these two tests because the Acc injection rate, which is the same for these two tests, mainly determines the accumulated water level in core during this period.

3.2.2 Steam Flow Rate in Pressure Vessel

Figure 3-14 compares the mass of steam outflow from pressure vessel between Tests S1-01 and S1-04. The mass of steam outflow from pressure vessel is almost the same in these two tests until the quench of whole core. The relatively small effect of core inlet water subcooling on the steam flow rate can be explained by the fact that the lower steam generation rate below the quench front due to the higher core inlet water subcooling is almost canceled by the higher steam generation rate near the quench front due to the higher heat transfer coefficient and the faster quench velocity as discussed in section 3.1.

Figure 3-15 shows the estimated steam velocities at the UCSP holes for Tests S1-01 and S1-04. The higher core inlet subcooling results in the lower steam velocity from 160 seconds after the BOCREC. The time coincides with the time when the mass of accumulated water in the upper plenum begins to be greater in Test S1-04 than in Test S1-01 as shown in Fig.3-12. The comparison of integrated carryover water from the

core into the upper plenum shown in Fig.3-16 indicates that the amount of water outflow from the core is almost the same for these two tests.

It is suggested that the larger water accumulation in the upper plenum in the higher core inlet water subcooling test is not due to the difference of water flow rate from the core but due to the lower steam velocity at the UCSP (Upper Core Support Plate) holes.

3.2.3 Hot Leg Carryover

Figure 3-17 compares the integrated mass of carryover water through the hot leg between Tests S1-01 and S1-04. The higher core inlet water subcooling results in the less carryover water through the hot leg from 160 seconds after the BOCREC when the steam velocity at the UCSP hole in Test S1-04 begins to be lower than that in Test S1-01. Therefore, the difference of carryover characteristics between these two tests can also be attributed to the difference of steam velocity at the UCSP hole. Furthermore, as shown in Fig.3-18, the lower steam velocity in the hot leg in Test S1-04 also contributes to the less amount of carryover water through the hot leg.

As shown in Fig.3-17, the increasing rate of integrated carryover water in Test S1-01 is about three times larger than that in Test S1-04 from 160 to 400 seconds, while no significant difference is observed in the increasing rate of integrated carryover water after 400 seconds. The rapid increasing of carryover water is about 40 seconds earlier than the time when the mixture level in the upper plenum reaches the bottom of hot leg nozzle as shown in Fig. 3-12.

3.2.4 Two-Dimensional Hydrodynamic Behavior in Pressure Vessel

3.2.4.1 Core Full Height Differential Pressure

Figure 3-19 shows the horizontal profile of core full height differential pressure over the eight bundles at 100, 200, 300 and 400 seconds after the BOCREC for Tests S1-01 and S1-04. It is observed from this figure that the horizontal distribution of core full height differential pressure is almost uniform over the eight bundles for Test S1-04 as well as for Test S1-01 in spite of the radial power profile. The uniform distribution is induced by the equalizing effect of cross flow between bundles as discussed later. With increasing the core inlet water subcooling, the more water is accumulated in the core as discussed in section 3.2.1.

In order to investigate quantitatively how much core full height differential pressure is equalized, analytical calculation was carried out by using the correlation for void fraction derived by Cunningham and Yeh[5] with the experimental conditions for Tests S1-04 and S1-01 of core inlet water subcooling, pressure, electric power supplied to each bundle and steam mass flow rate. The calculations are carried out under the assumption that there are no fluid communication between bundles. The calculated results of horizontal distribution of core full height differential pressure over the eight bundles are shown in Figs.3-20 and 3-21 for Tests S1-01 and S1-04, respectively.

It is found by comparing these two figures that the difference of core full height differential pressure among the eight bundles is larger in Test S1-04 than in Test S1-01 especially in the early stage of the test, while from 400 seconds after the BOCREC the magnitude of pressure difference among the eight bundles becomes almost the same for the two tests with 0.12 m of water head.

The difference between experimental and analytical distributions of core full height differential pressures indicates the occurrence of cross flow from the peripheral bundles toward the center bundles.

It is also noted by comparing measured differential pressures with analytical values shown in Fig.3-22 that the analytical result of core full height differential pressure is estimated lower than the experimental results both for Tests S1-04 and S1-01.

3.2.4.2 Accumulated Water Level on UCSP

Figure 2-23 shows the comparison of liquid level transients in the upper plenum for Tests S1-01 and S1-04 above Bundles 2, 4, 6 and 8. As shown in this figure, the water level above the UCSP becomes higher for Test S1-04 than for Test S1-01 from about 160 seconds after the BOCREC as discussed in section 3.2.1. It is also noted that after about 160 seconds the water accumulation level becomes higher above Bundle 8 side than above Bundle 1 side, whereas the horizontal distribution of accumulated water level on UCSP is almost uniform until about 160 seconds.

3.2.4.3 Fluid Behavior around End Box Tie Plate

Figure 3-24 shows the comparison of liquid level transients on the end box tie plate for Tests S1-01 and S1-04 at Bundles 2, 4, 6 and 8,

respectively. This comparison also shows that at Bundle 8 more water is accumulated after 250 seconds after the BOCREC than at other bundles. In addition, it is noticed that the water level begins to increase about 60 seconds earlier for Test S1-04 than for Test S1-01.

Figure 3-25 shows the comparison of differential pressure transients across the end box tie plate for both tests above Bundles 2, 4, 6, and 8, respectively. Almost zero tie plate differential pressure above Bundle 8 in the latter half of test suggests that the water fall back from the upper plenum into the core at Bundle 8 occurs at about 250 seconds in Test S1-04 and at about 300 seconds in Test S1-01. The time when water fall back becomes significant is about 50 seconds earlier in Test S1-04 than in Test S1-01. Above Bundles 2, 4 and 6, the flow should be a co-current upflow because the differential pressure is always positive.

3.2.4.4 Fluid Density

The fluid densities at 3.235 m from the bottom of heated length between Bundles 1 and 2 and between Bundles 7 and 8 are compared in Fig.3-26 for Tests S1-01 and S1-04. As indicated in this figure, more water is accumulated at the top of the core from about 150 seconds after the BOCREC in Test S1-04 than in Test S1-01 while before that, the transient is almost the same between the two tests. The tendency that fluid density is higher between Bundles 7 and 8 than between Bundles 1 and 2 is preserved in Test S1-04 as well as in Test S1-01.

3.2.4.5 Horizontal Differential Pressure in Core

Figure 3-27 shows the horizontal differential pressures between Bundles 5 and 8 at the elevations of 1.905, 3.235, and 3.821 m from the bottom of heated length for these two tests. It is noted from these comparisons that the pressure is higher at Bundle 8 than at Bundle 5 for these two tests especially after the quench of whole core.

It is also observed in Fig.3-27 that the time when the pressure difference becomes significant is about 100 seconds earlier in Test S1-04 than in Test S1-01.

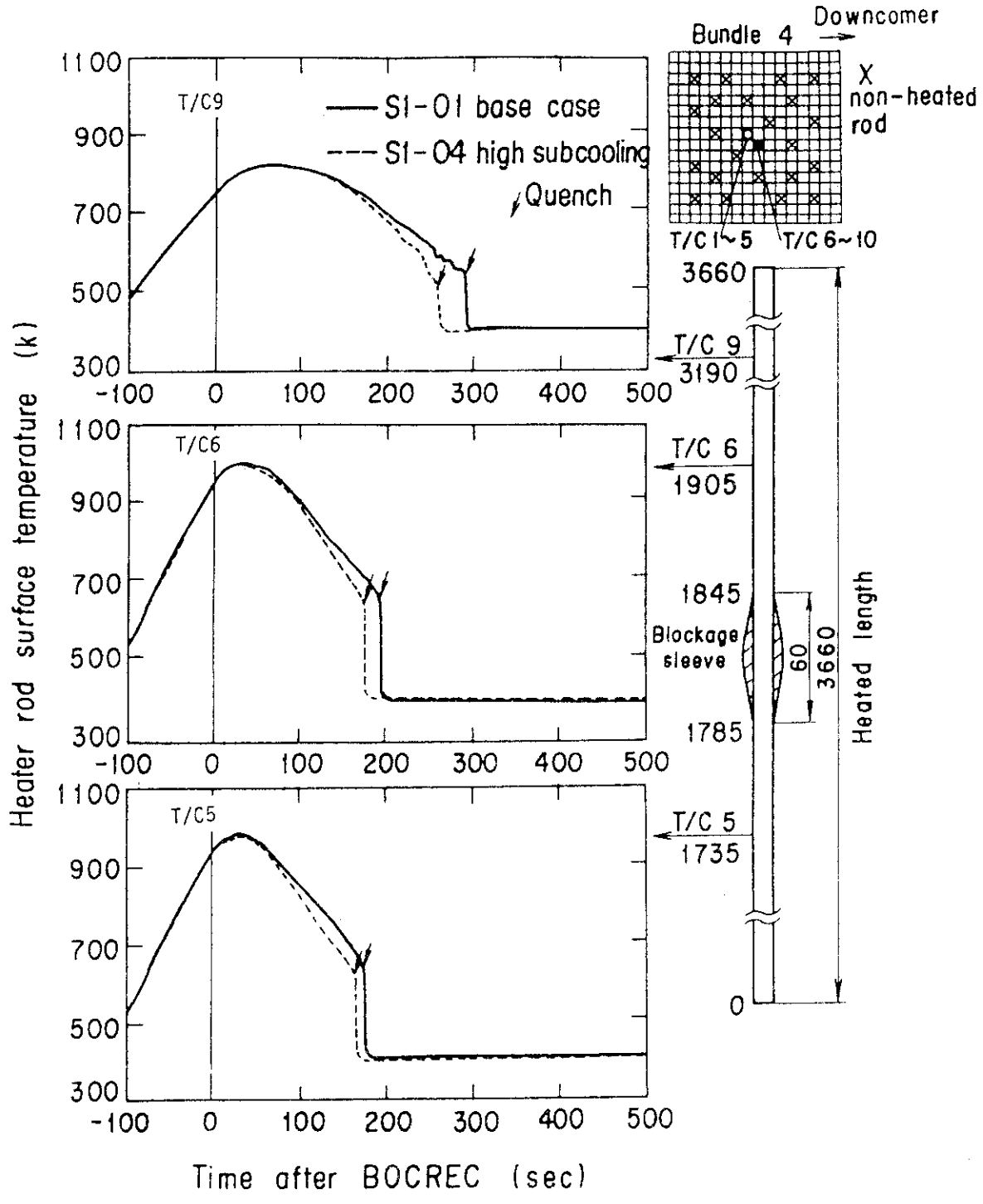

Fig. 3-1 Effect of core inlet water subcooling on cladding temperature histories

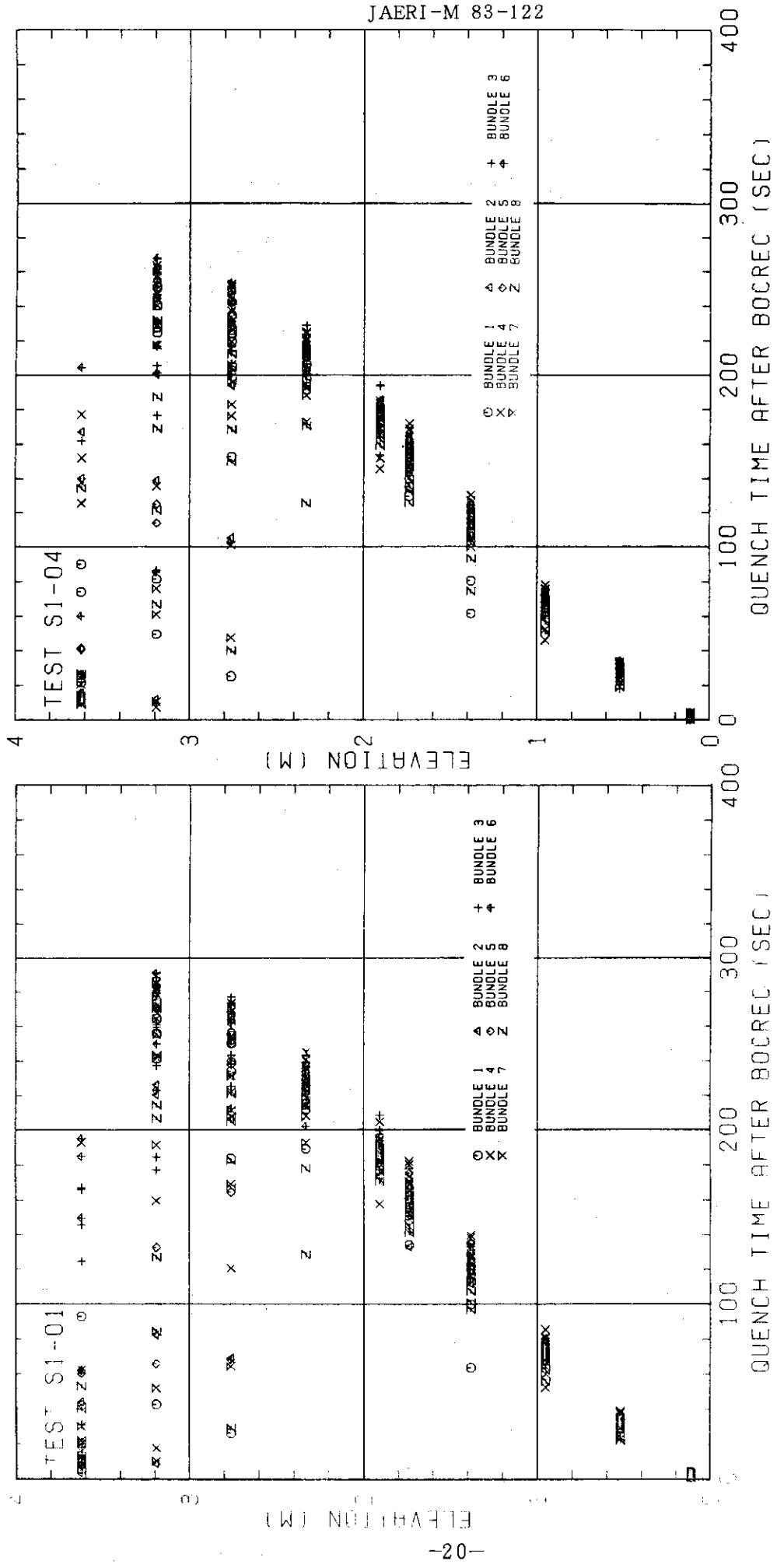

Fig. 3-2 Quench envelopes for Tests S1-01 and S1-04

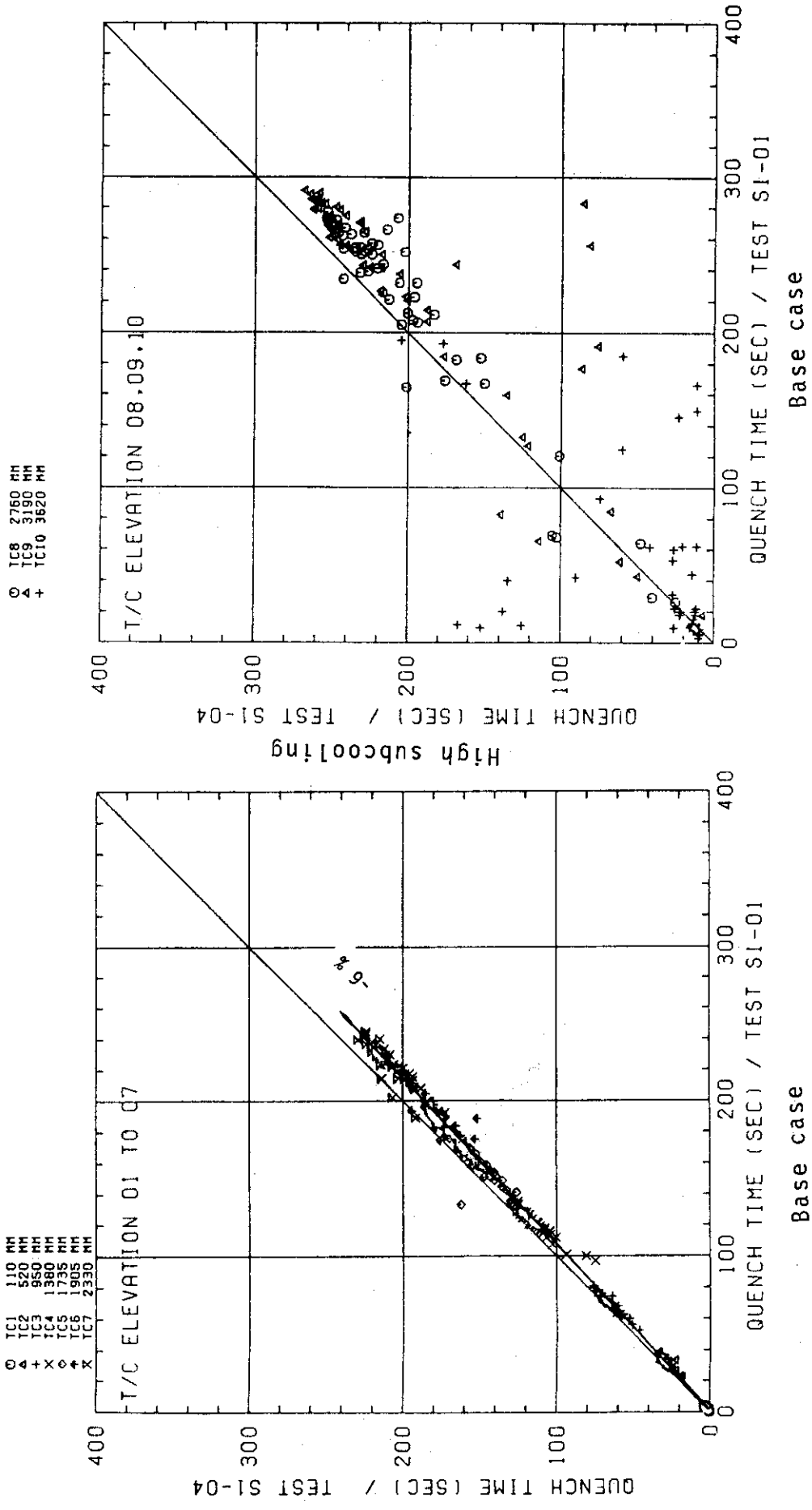

Fig. 3-3 Effect of core inlet water subcooling on quench time

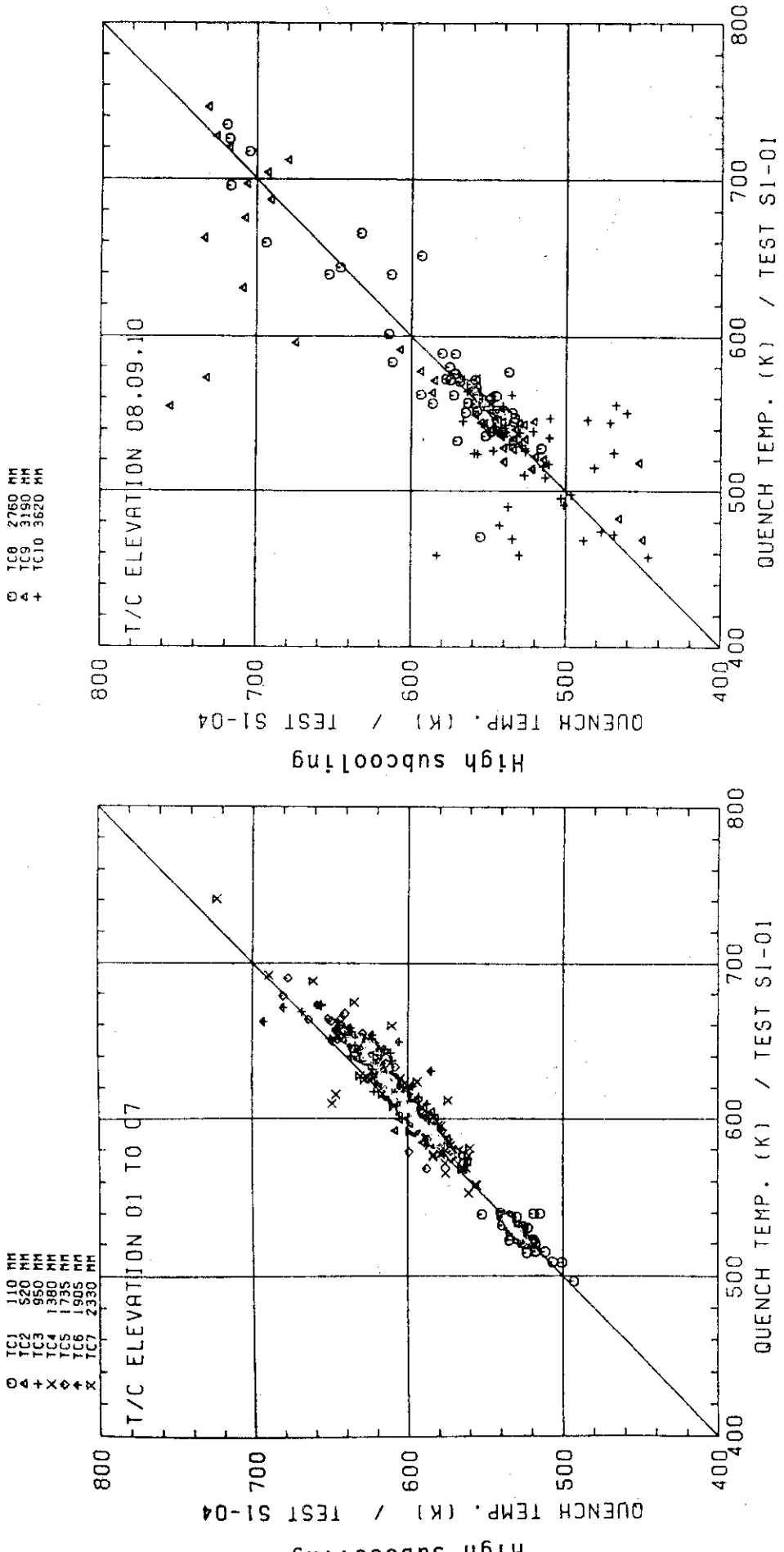

Fig. 3-4 Effect of core inlet water subcooling on quench temperature

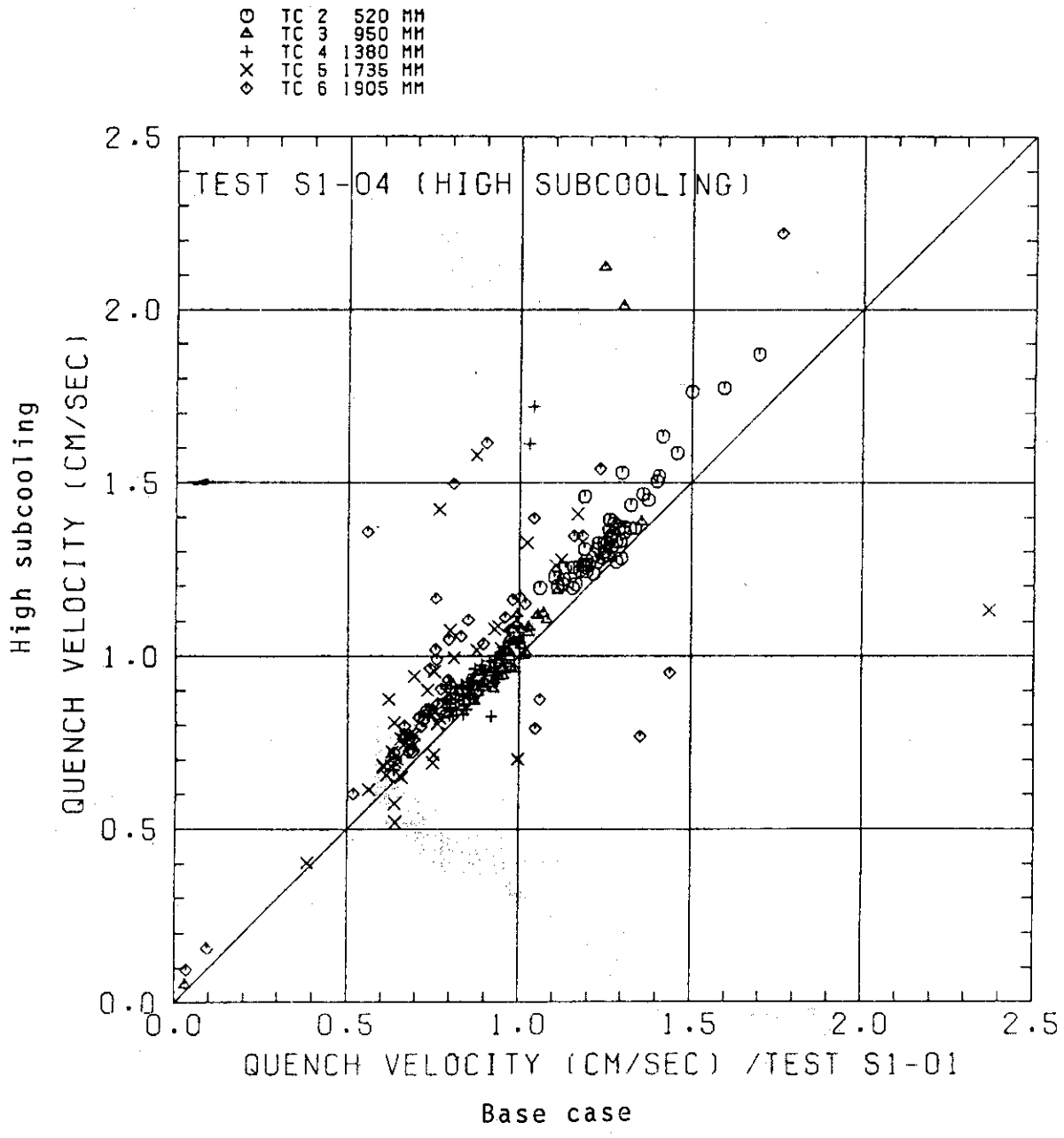

Fig. 3-5 Effect of core inlet water subcooling on quench velocity

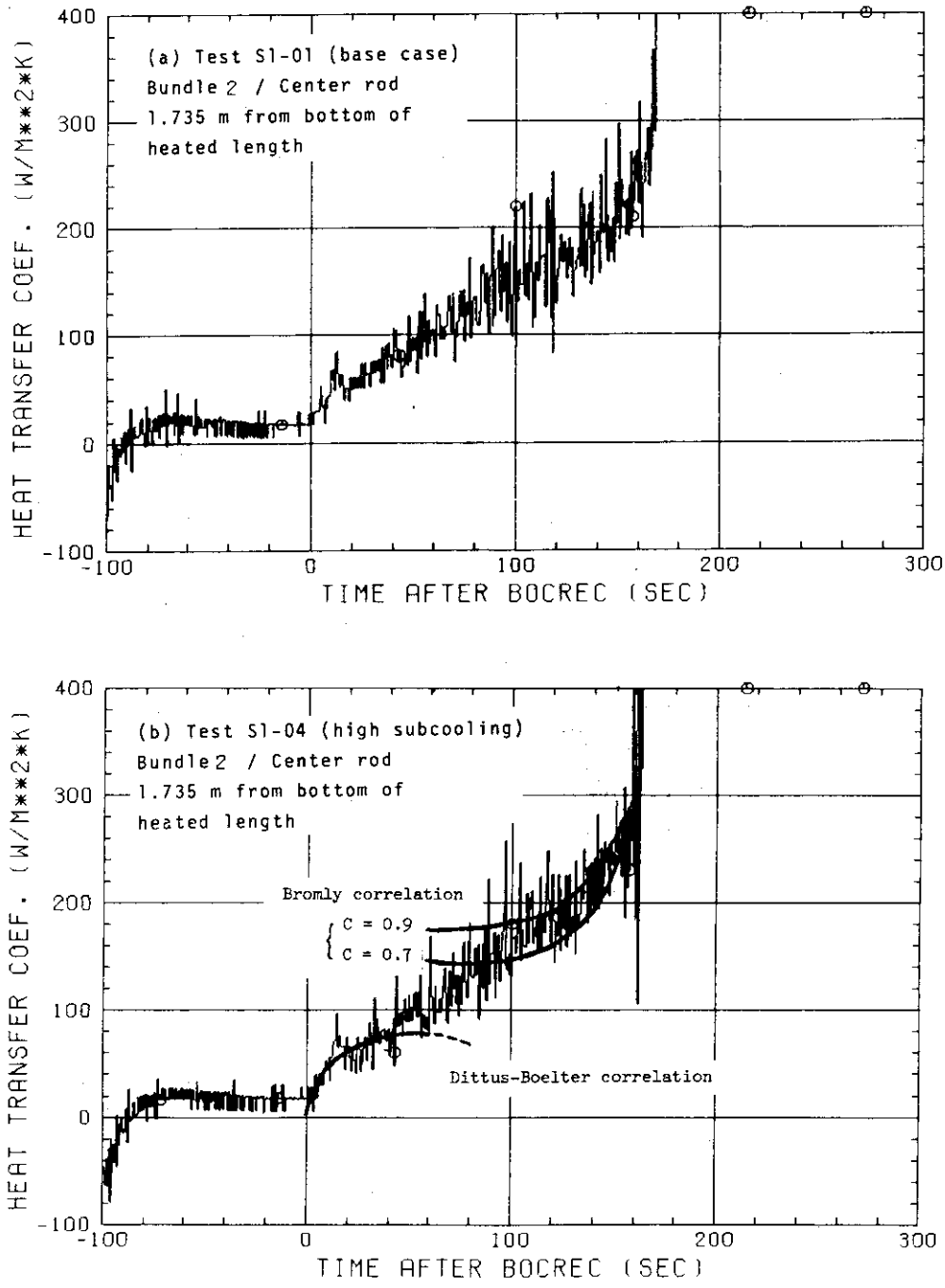

Fig. 3-6 Heat transfer coefficient at elevation 1.735 m in Tests S1-01 and S1-04

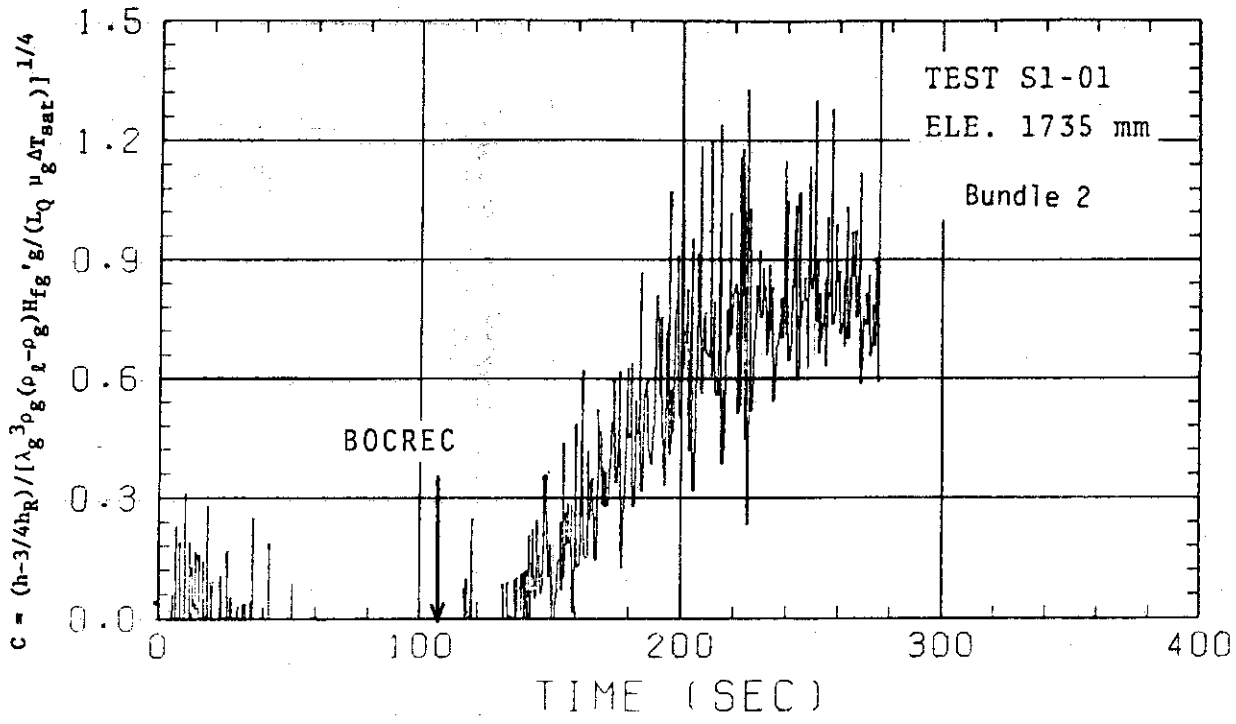

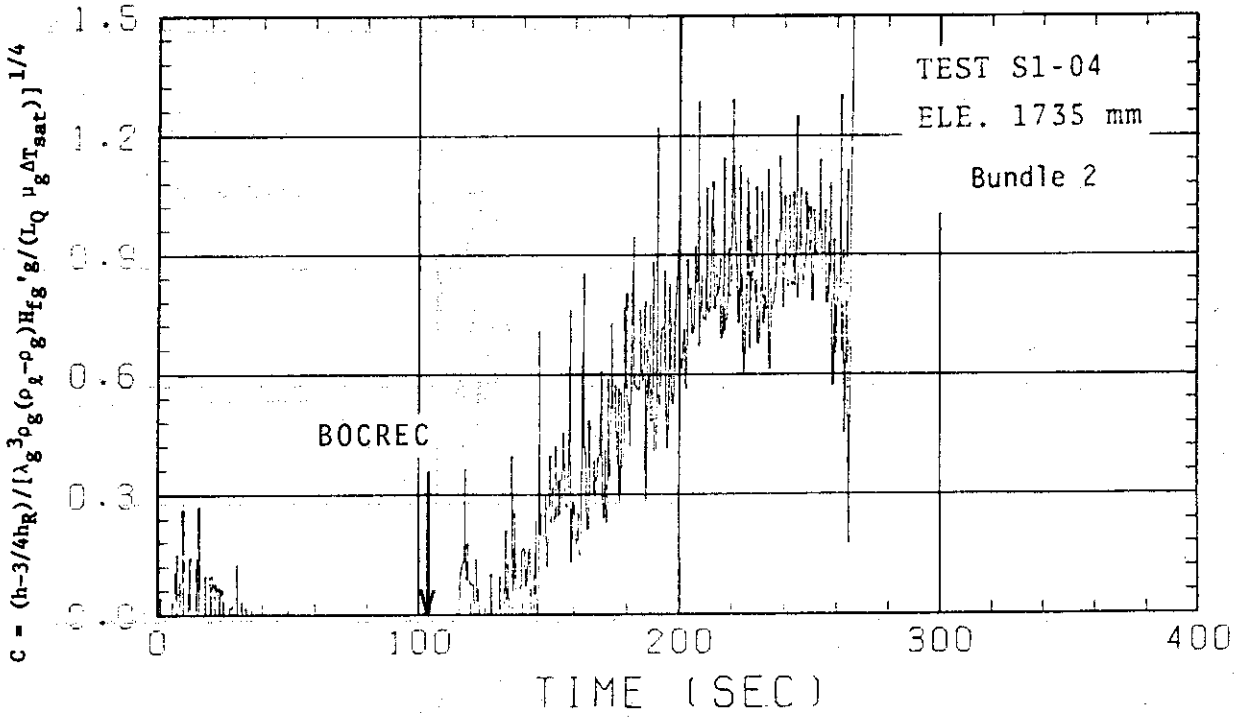

Fig. 3-7 Value of "C" in Bromley's correlation vs. time (elevation 1.735 m)

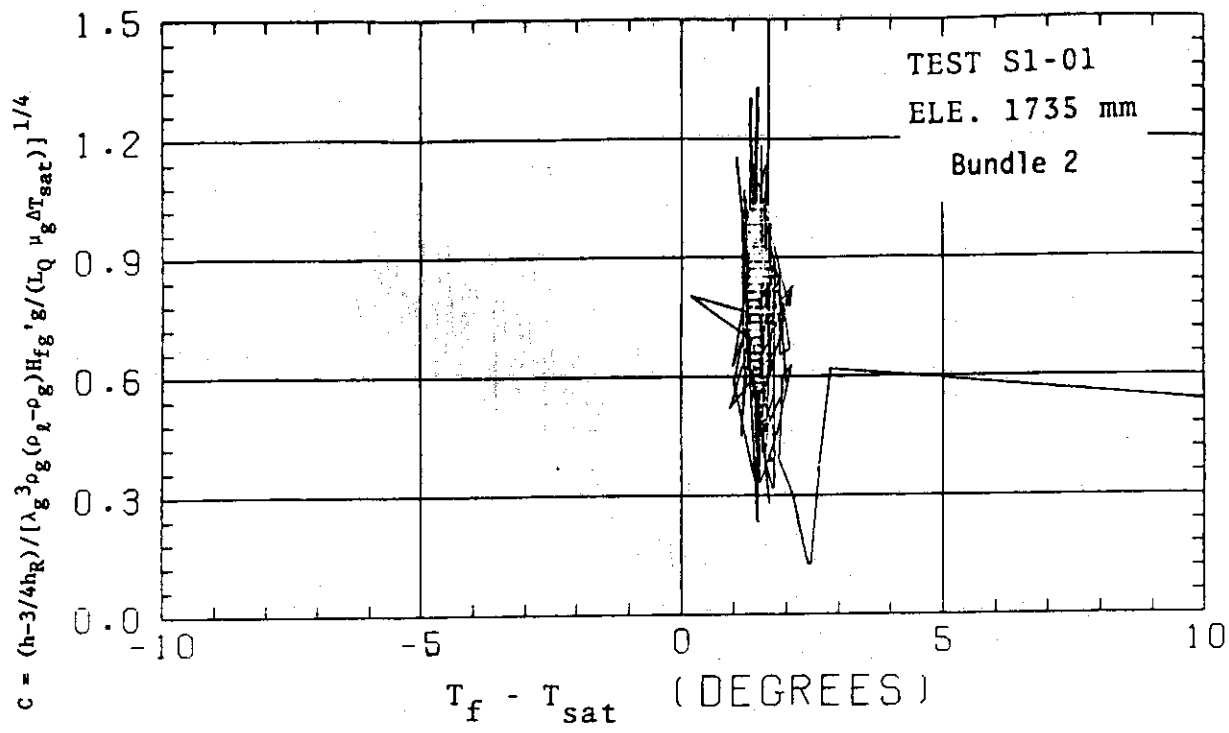

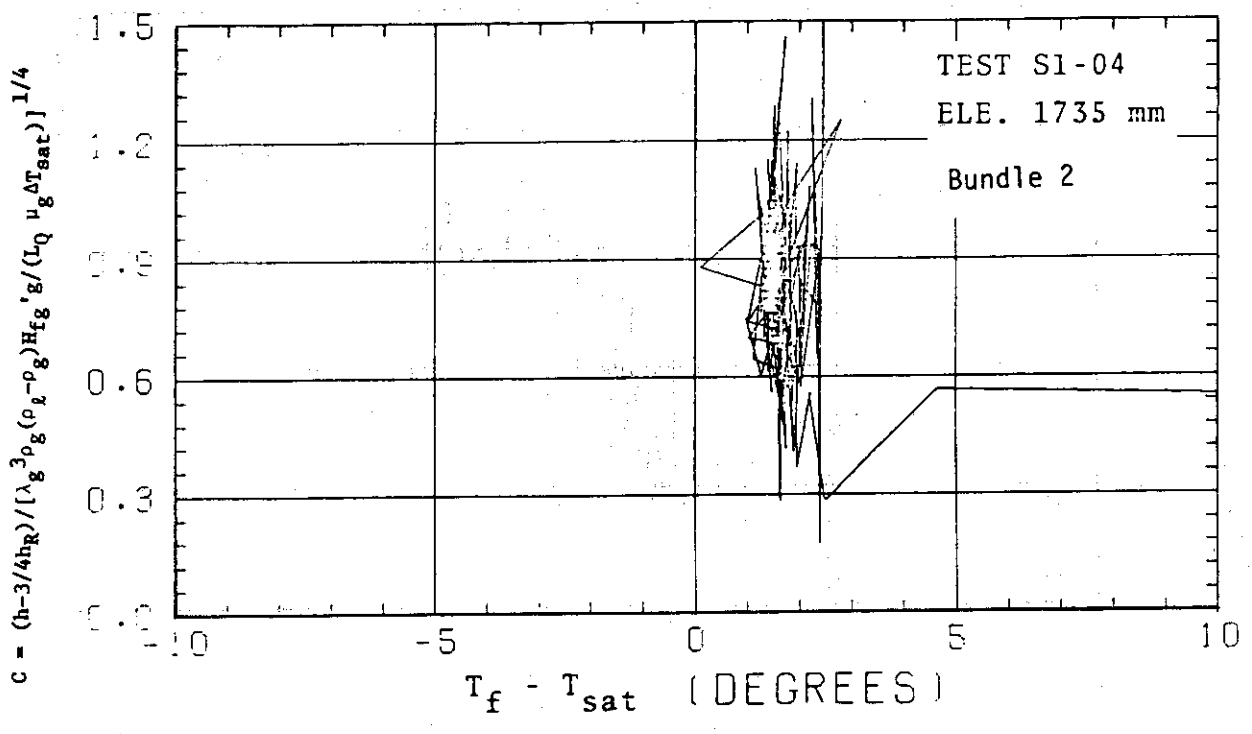

Fig. 3-8 Value of "C" in Bromley's correlation vs. local sobcooling (elevation 1.735 m)

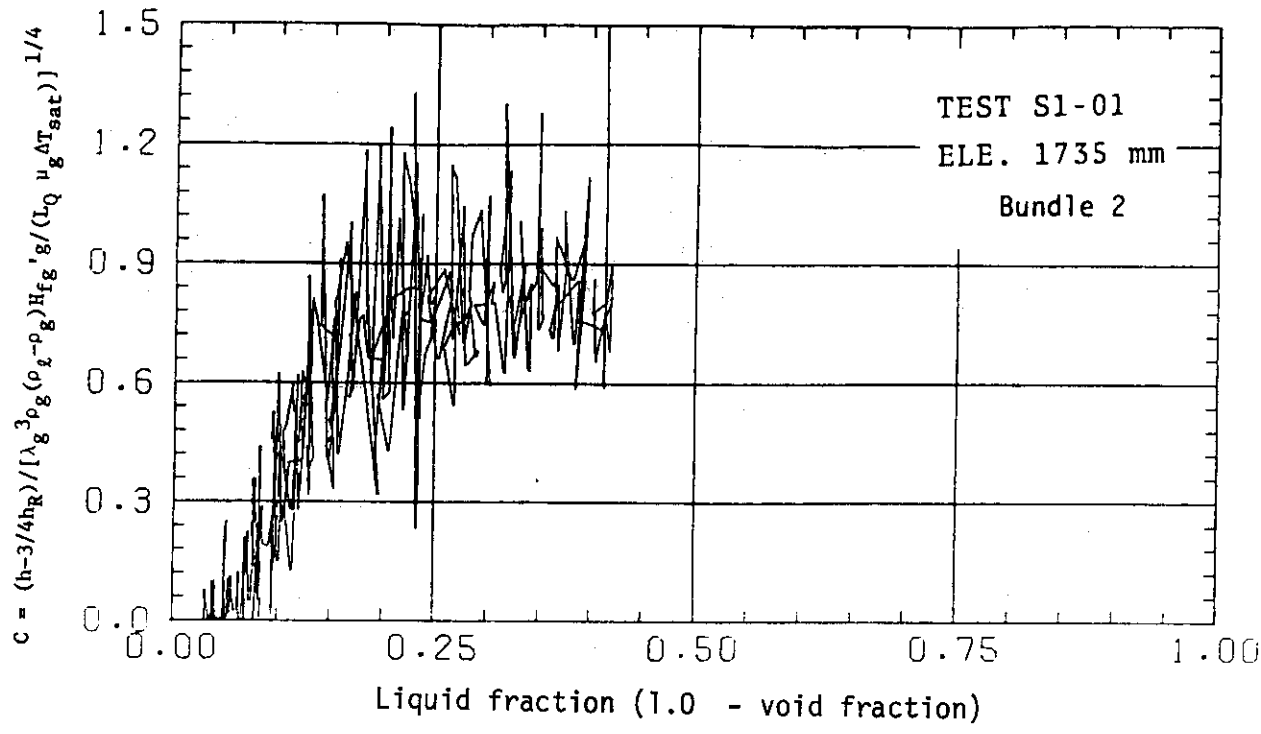

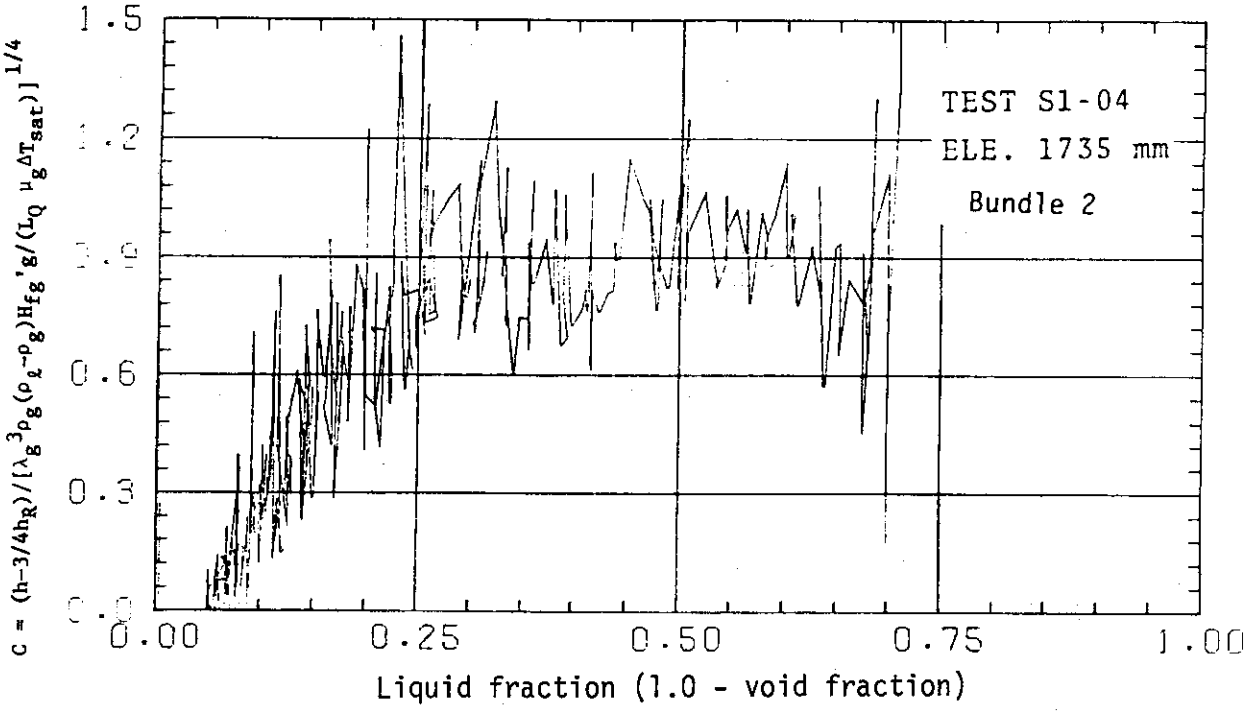

Fig. 3-9 Value of "C" in Bromley's correlation vs. liquid fraction (elevation 1.735 m)

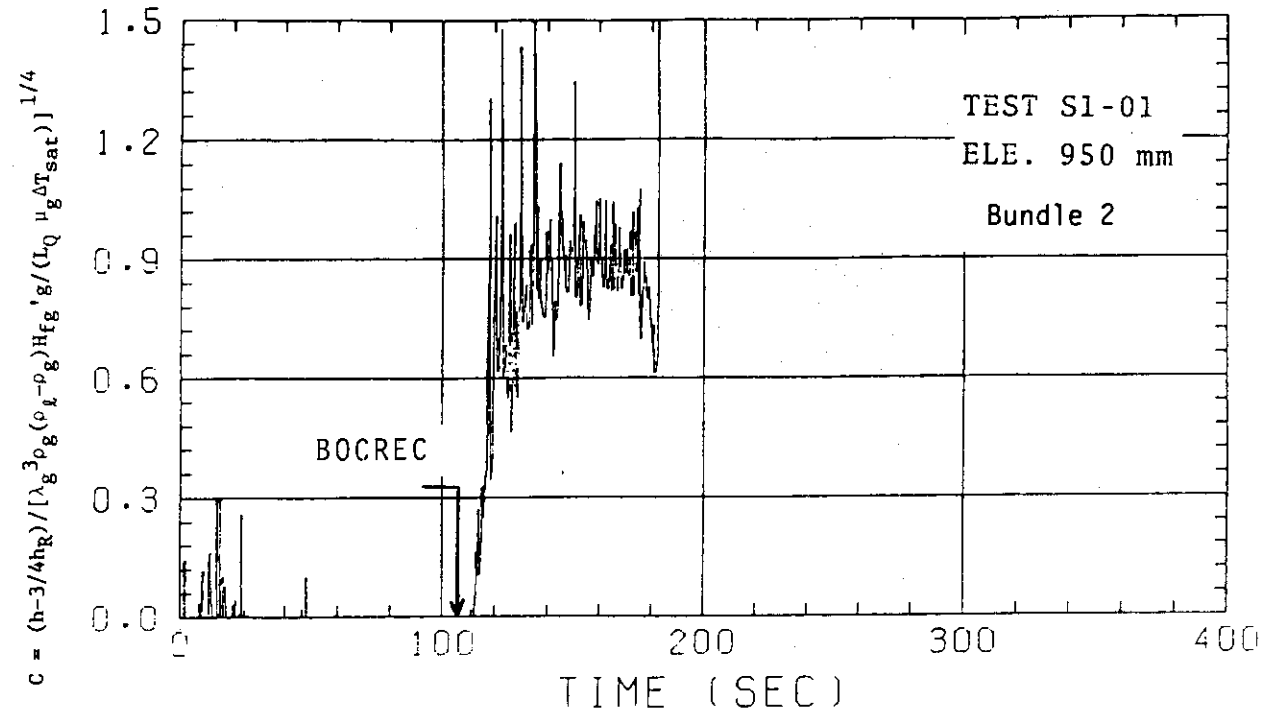

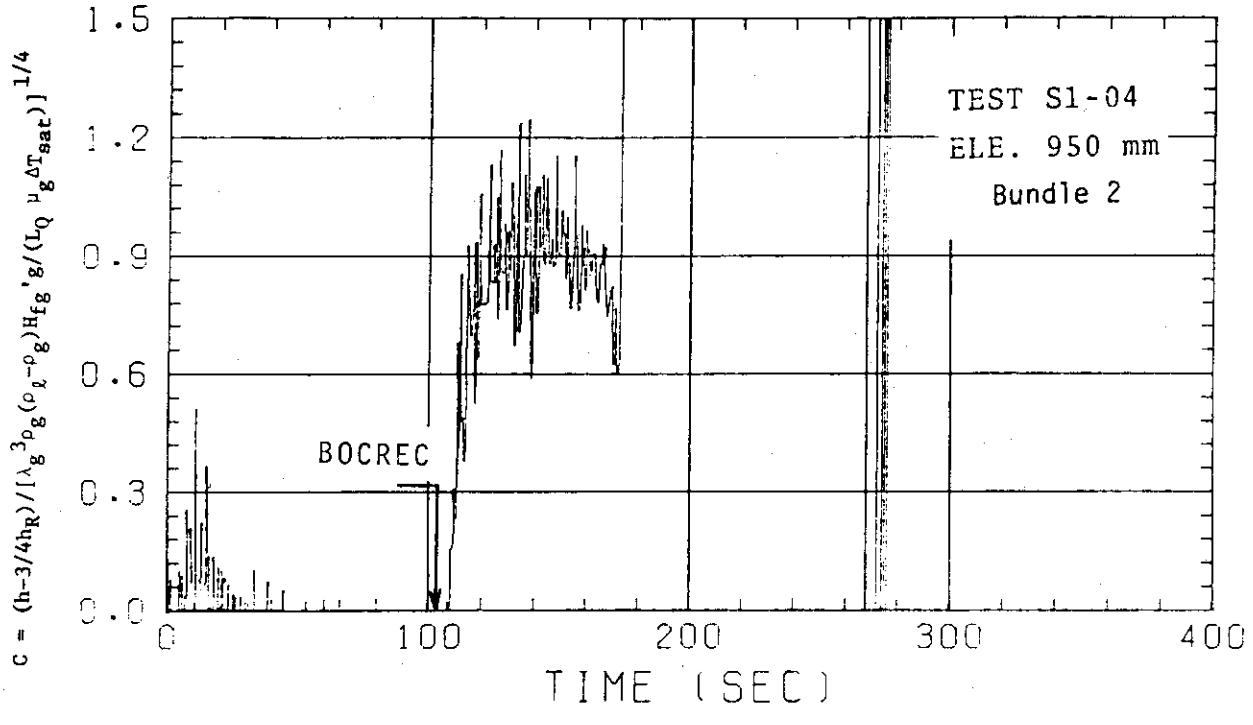

Fig. 3-10 Value of "C" in Bromley's correlation vs. time (elevation 0.95 m)

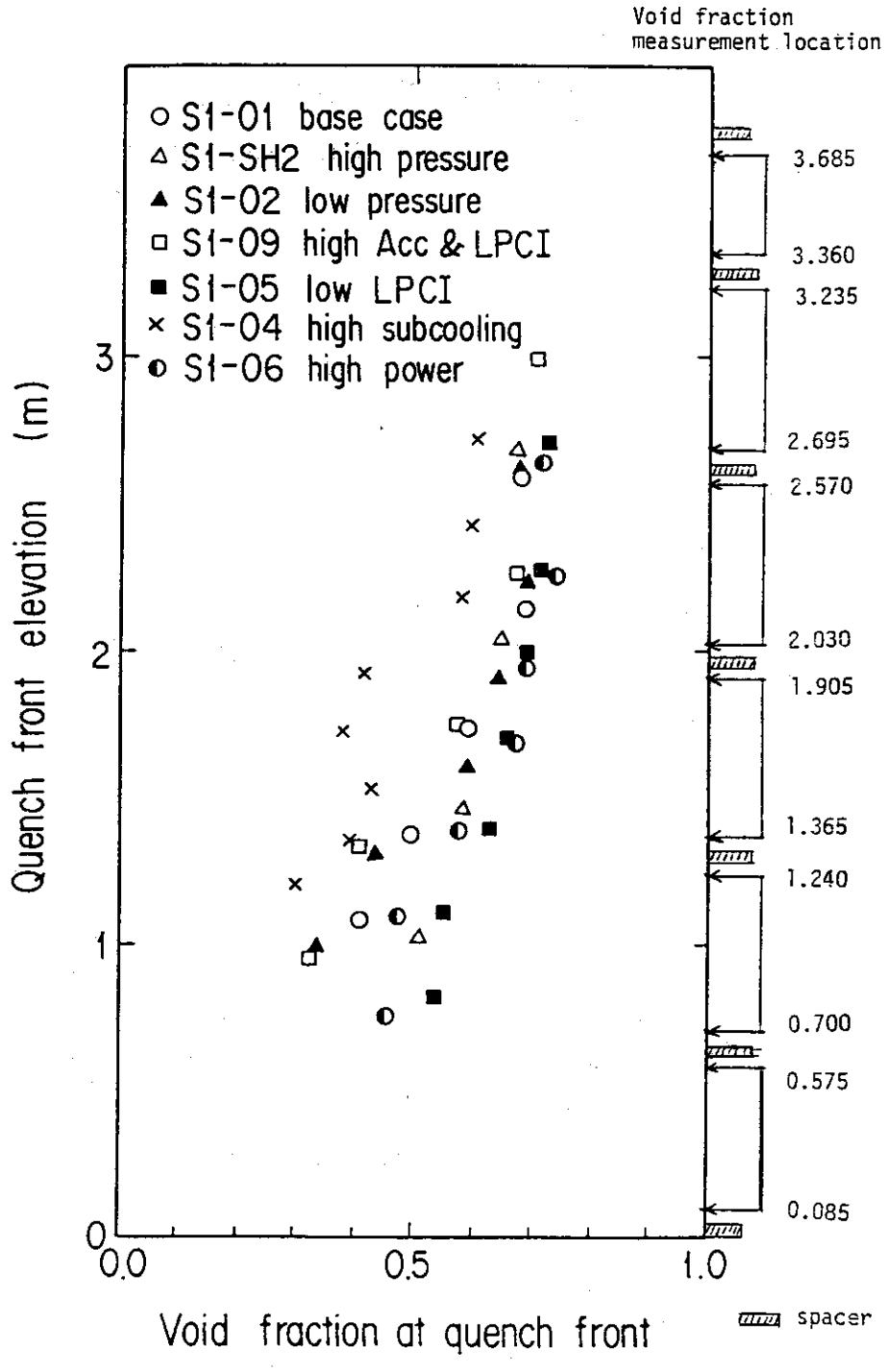

Fig.3-11 Quench front elevation vs. void fraction at quench front

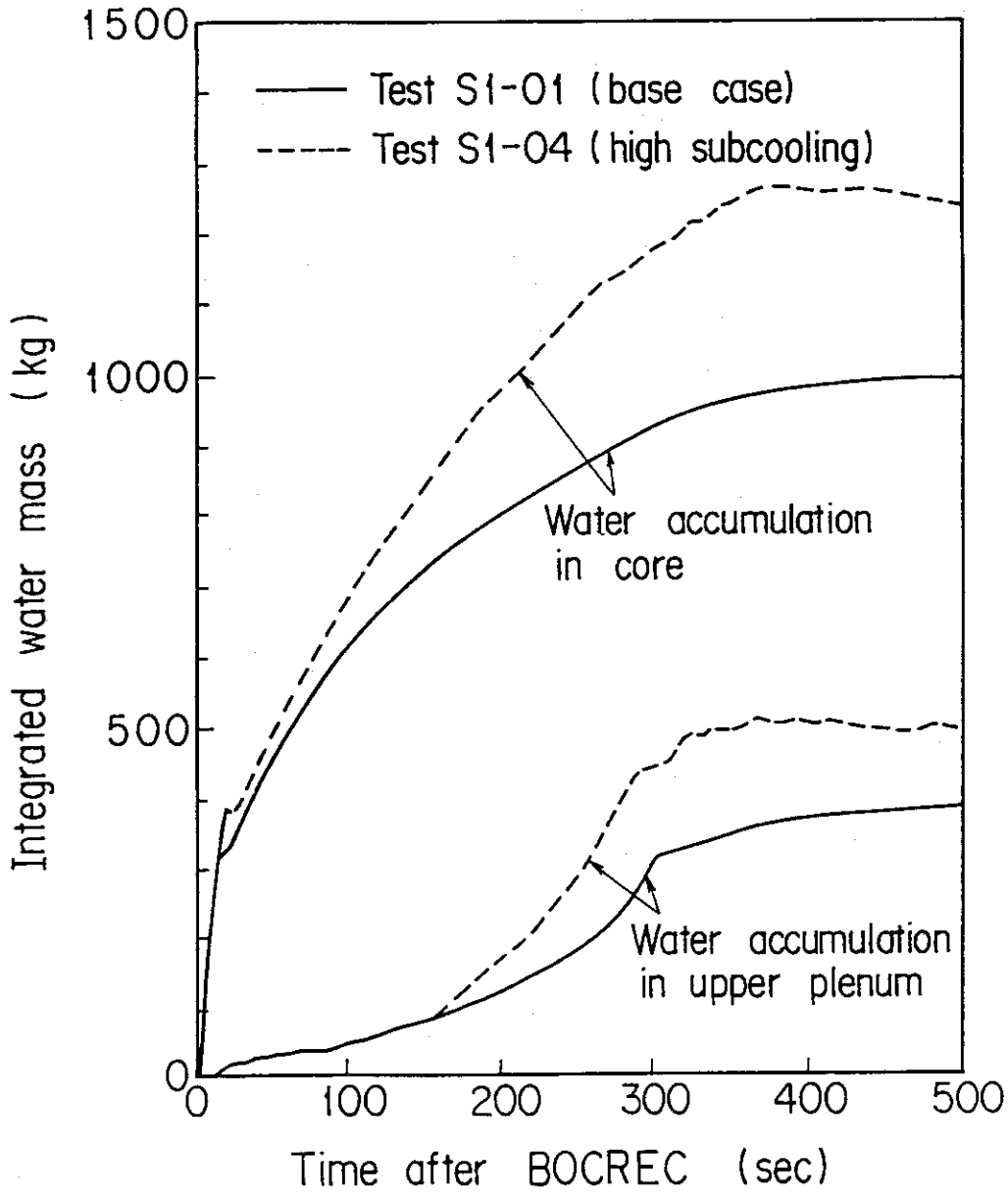

Fig.3-12 Water accumulation in core and upper plenum for Tests S1-01 and S1-04

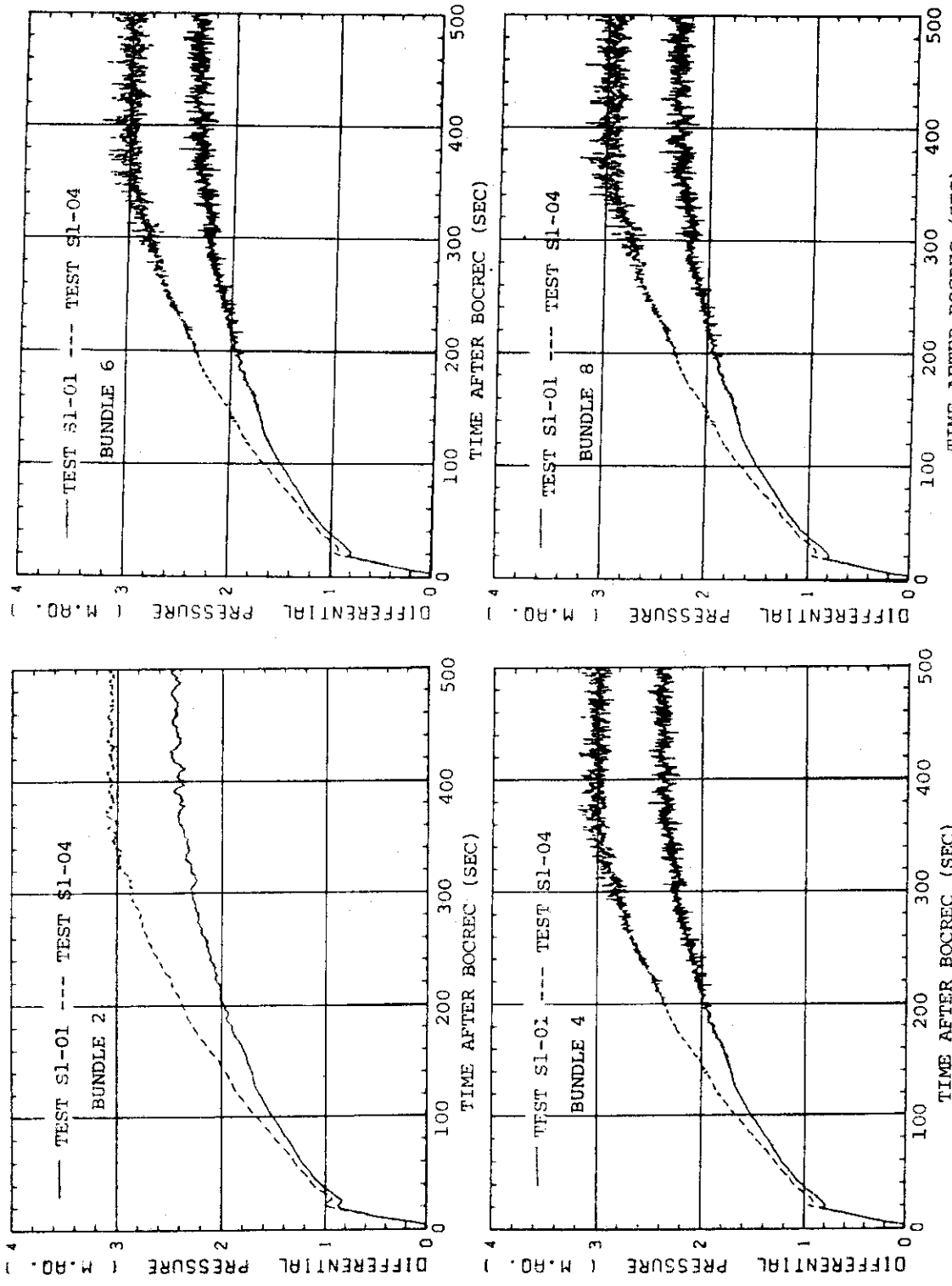

Fig. 3-13 Core full height differential pressures for Tests S1-01 and S1-04 (Bundles 2, 4, 6 and 8)

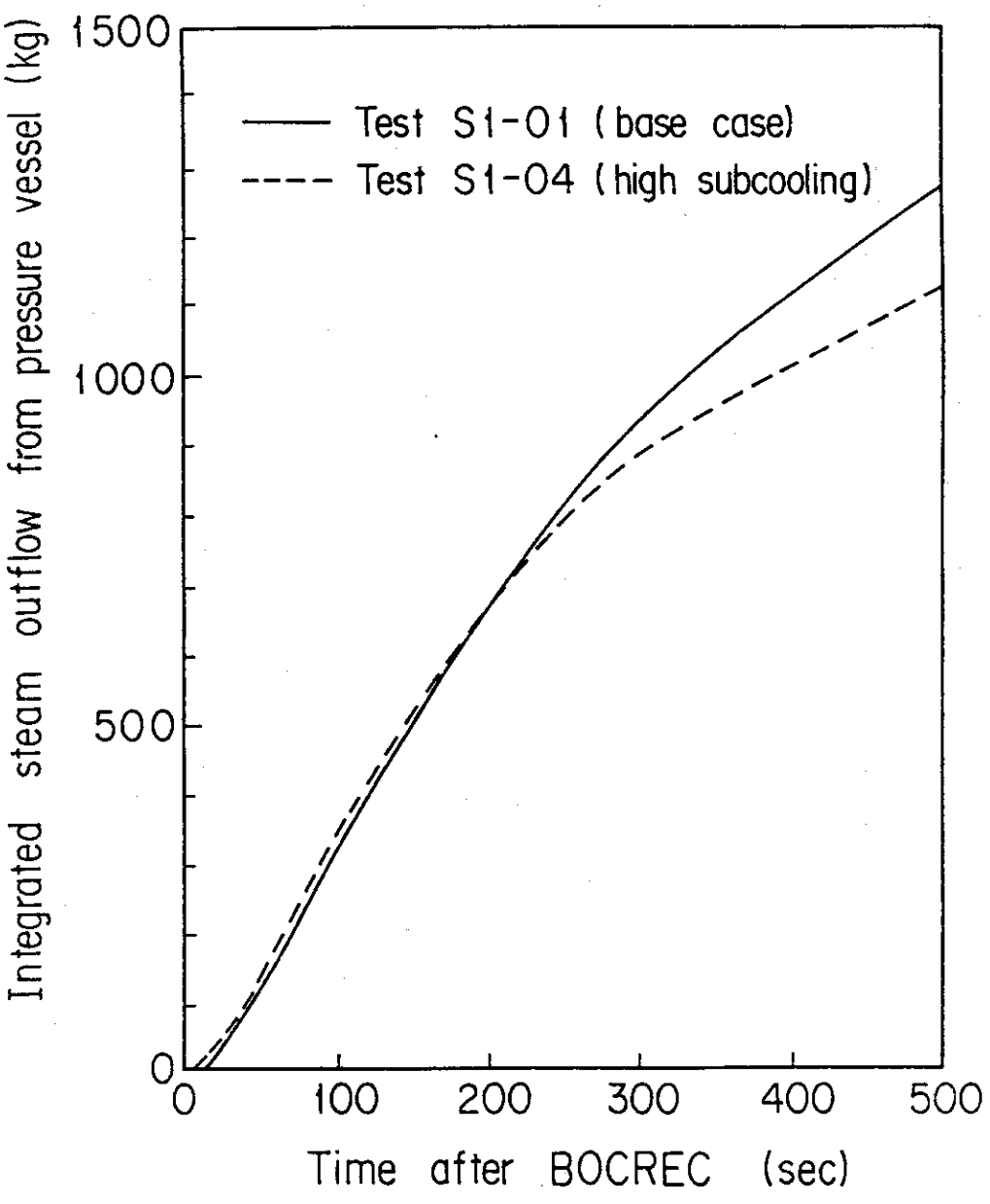

Fig.3-14 Integrated mass of steam outflow from pressure vessel for Tests S1-01 and S1-04

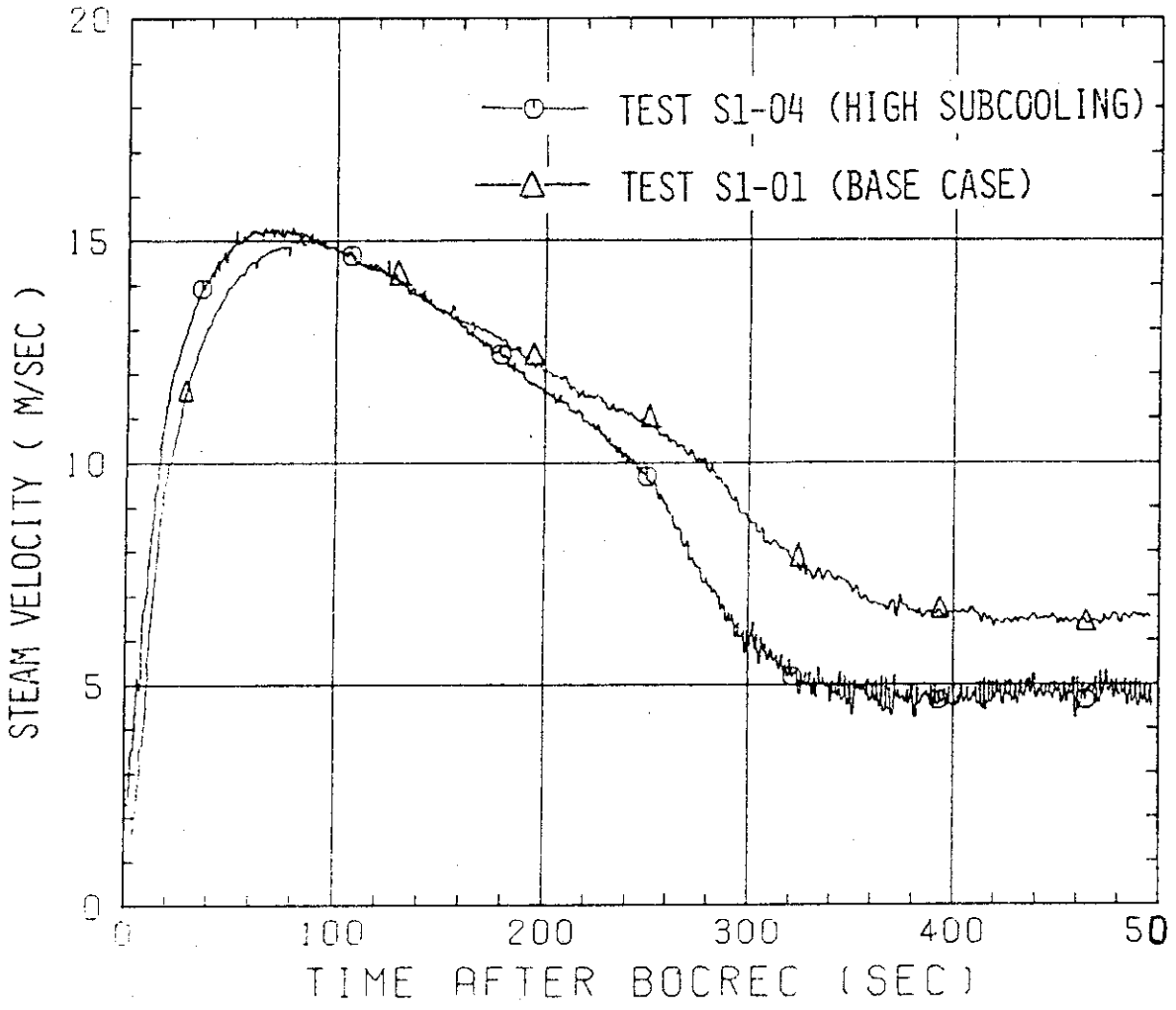

Fig. 3-15 Steam velocities at UCSP hole for Tests S1-01 and S1-04

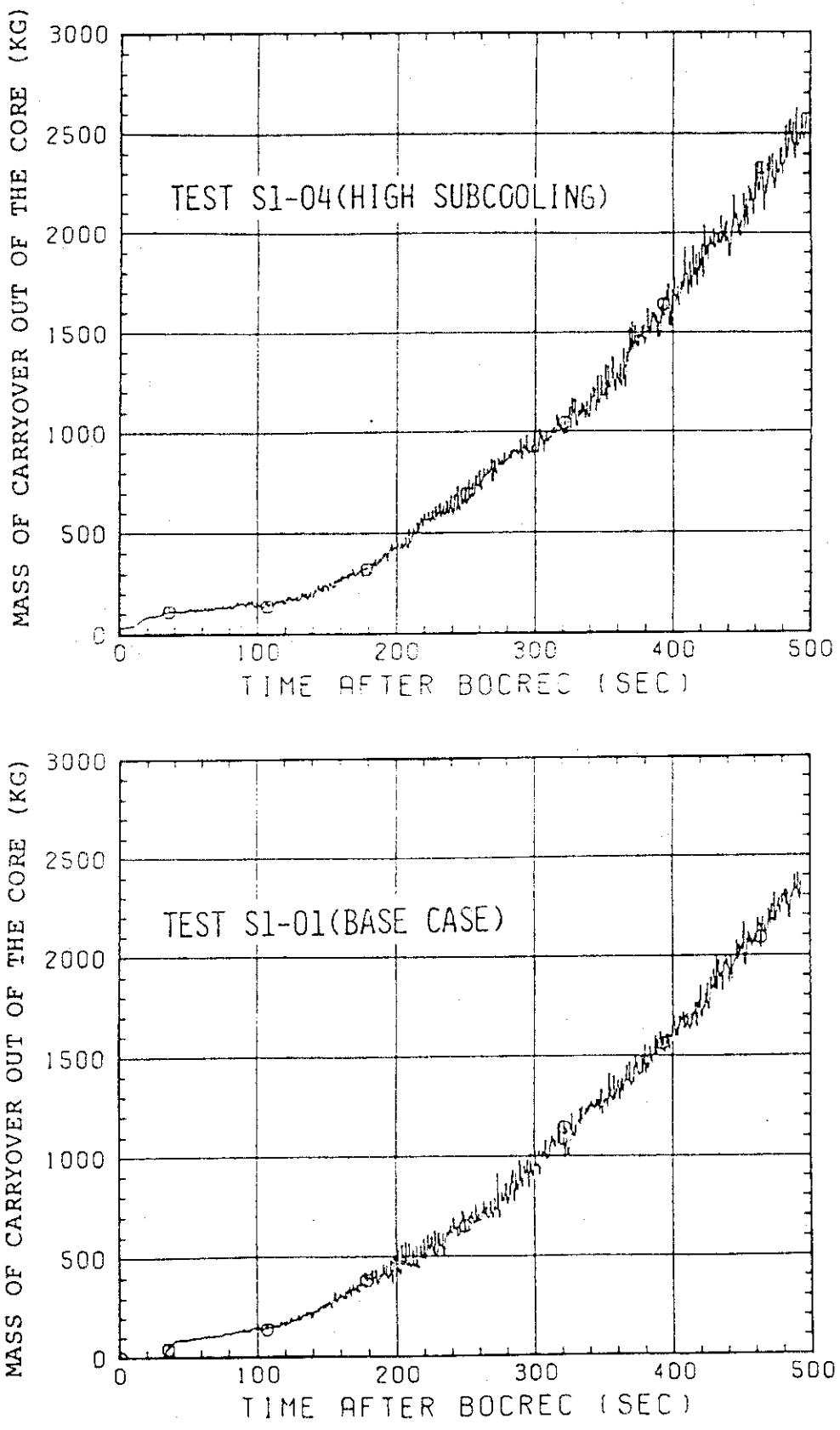

Fig. 3-16 Integrated mass of carryover water from core into upper plenum for Tests S1-01 and S1-04

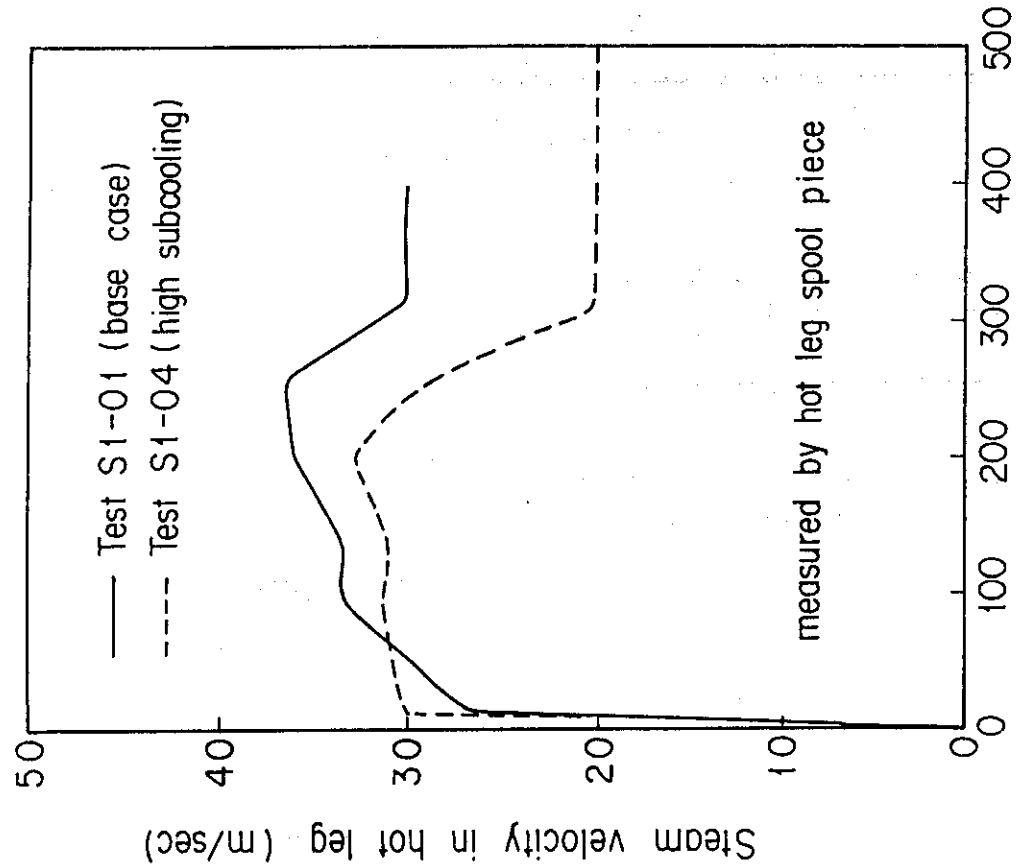

Fig.3-18 Steam velocities in hot leg for Tests S1-01 and S1-04

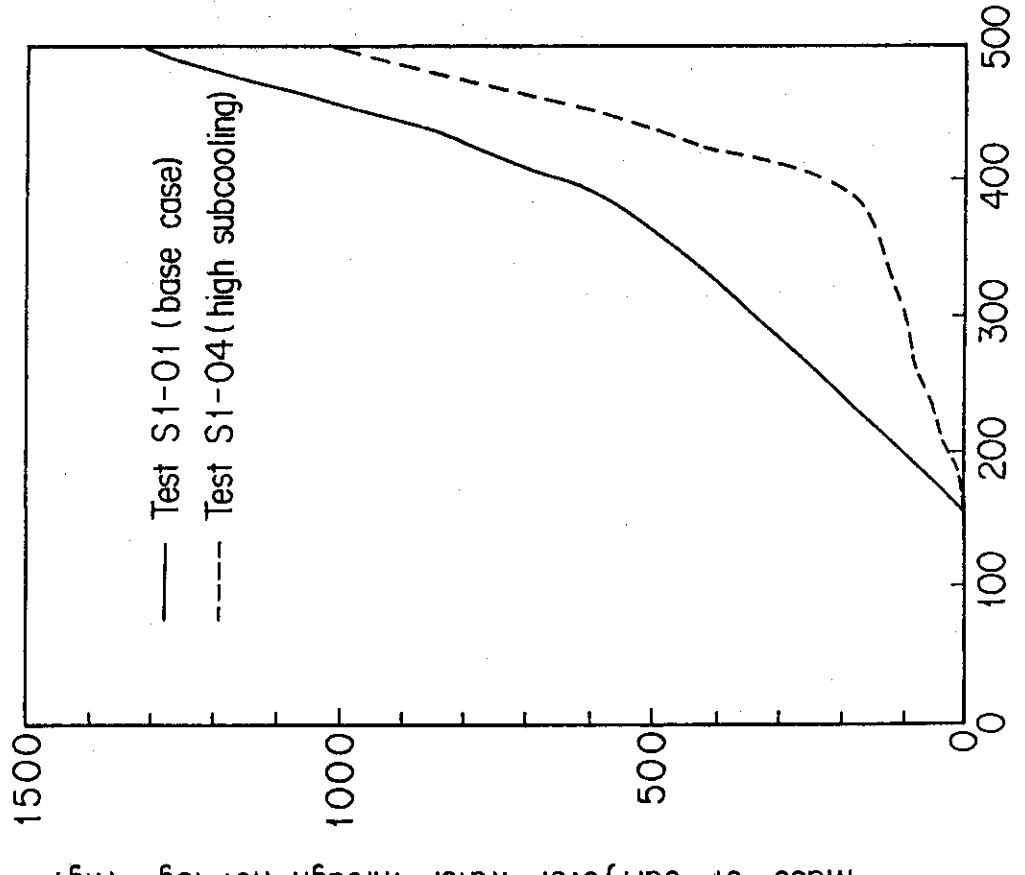

Fig.3-17 Integrated mass of carryover water through hot leg for Tests S1-01 and S1-04

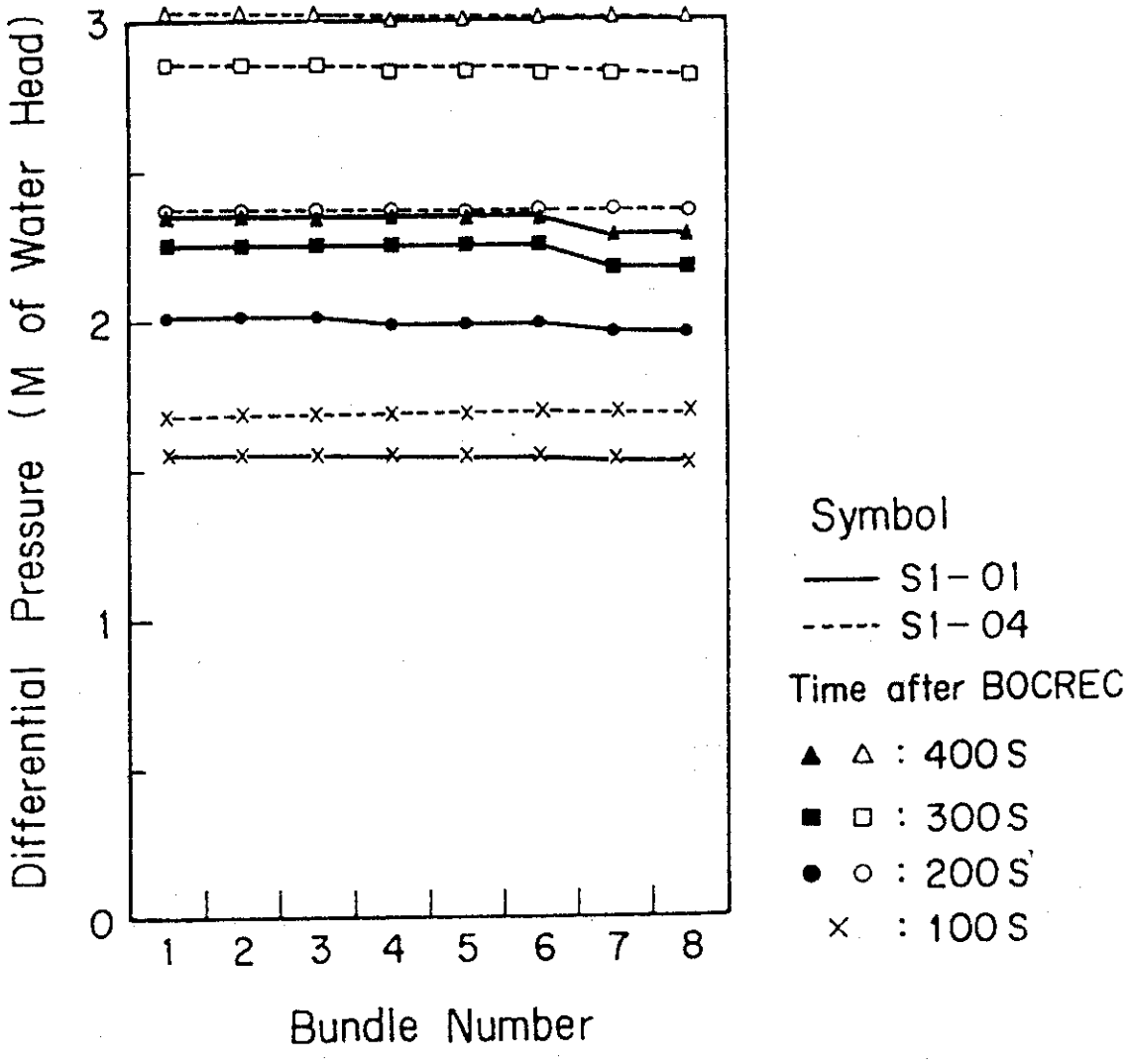

Fig. 3-19 Core full height differential pressure profile over 8 bundles for Tests S1-01 and S1-04

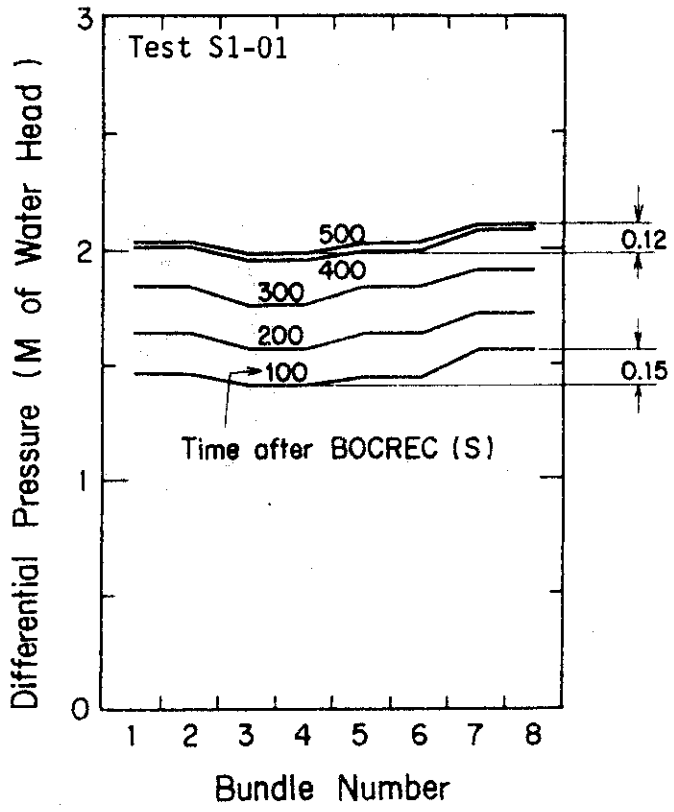

Fig. 3-20 Calculated core full height differential pressure profile over 8 bundles based on assumption of no fluid communication between bundles for test condition of Test S1-01

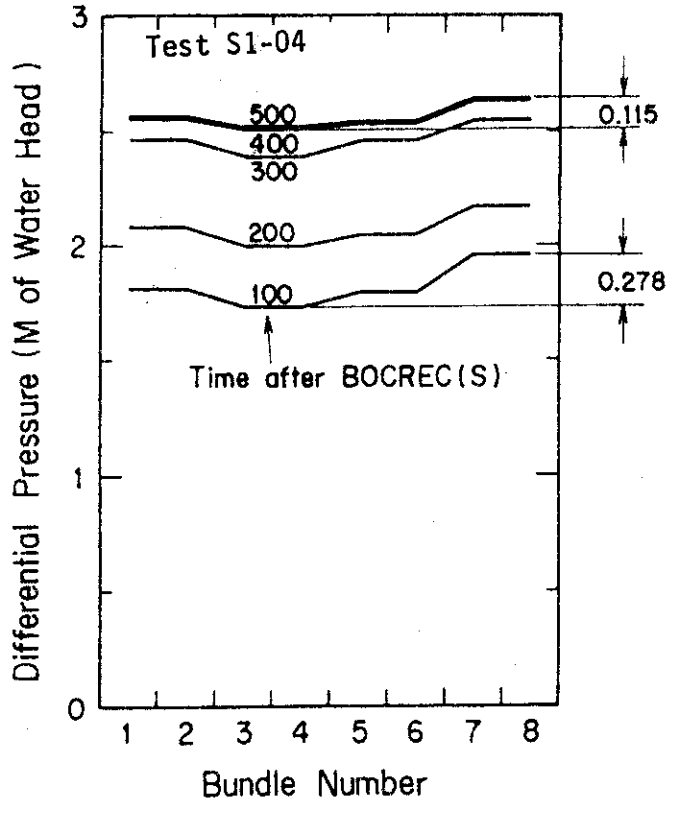

Fig. 3-21 Calculated core full height differential pressure profile over 8 bundles based on assumption of no fluid communication between bundles for test condition of Test S1-04

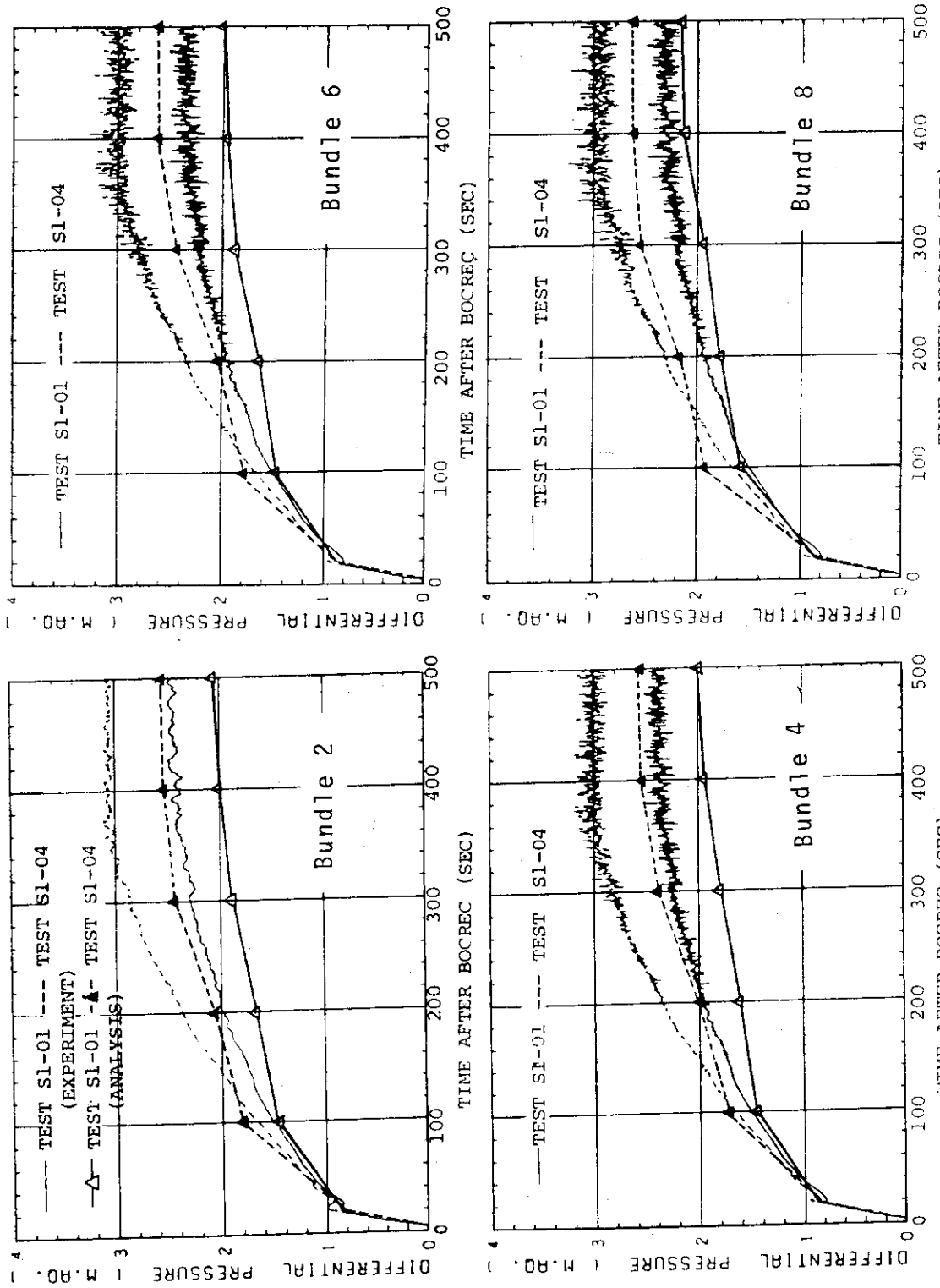

Fig. 3-22 Comparison of core full height differential pressure transients between measured and analytical results for Tests S1-01 and S1-04

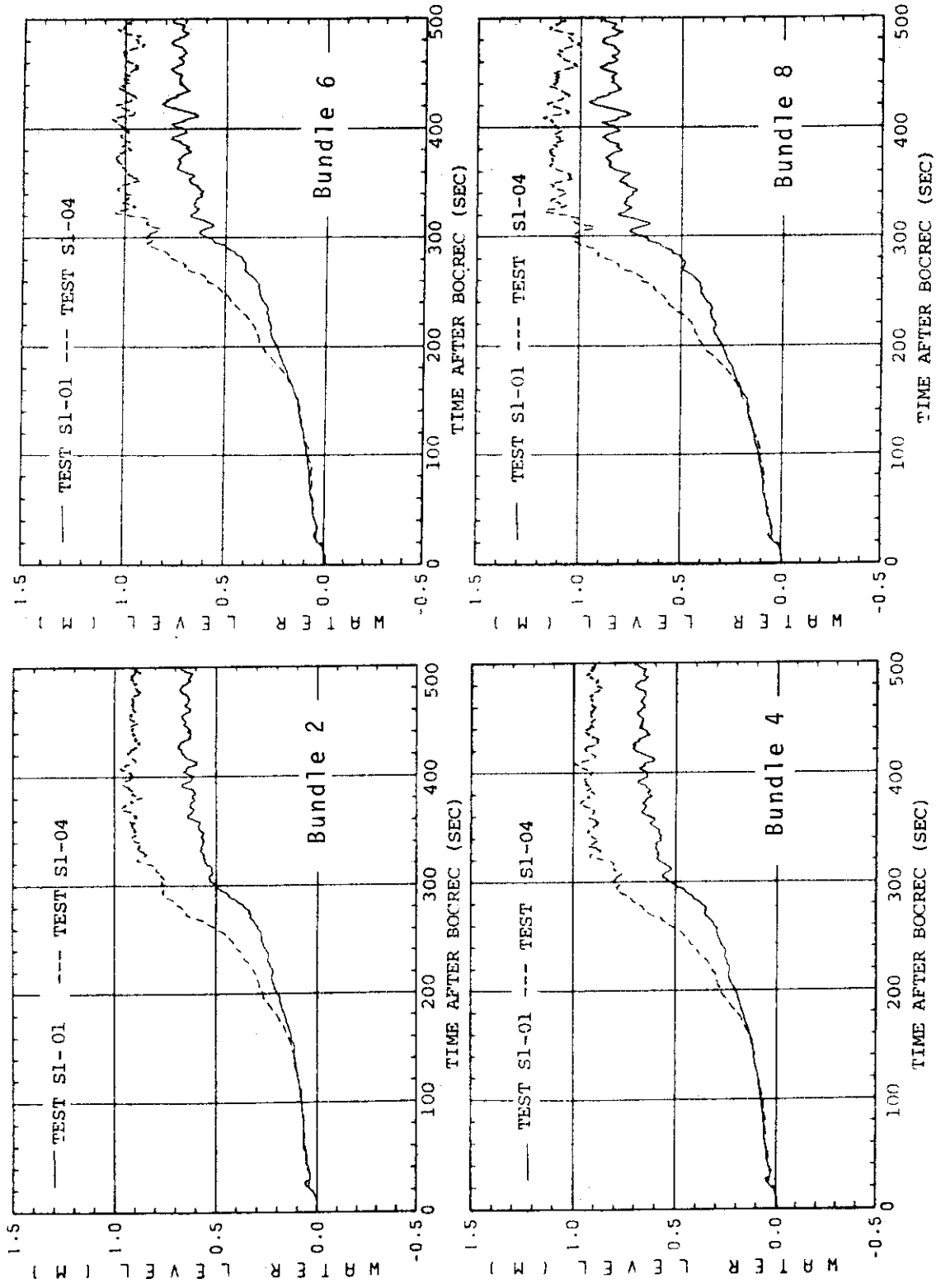

Fig. 3-23 Liquid level transients above UCSP for Tests S1-01 and S1-04

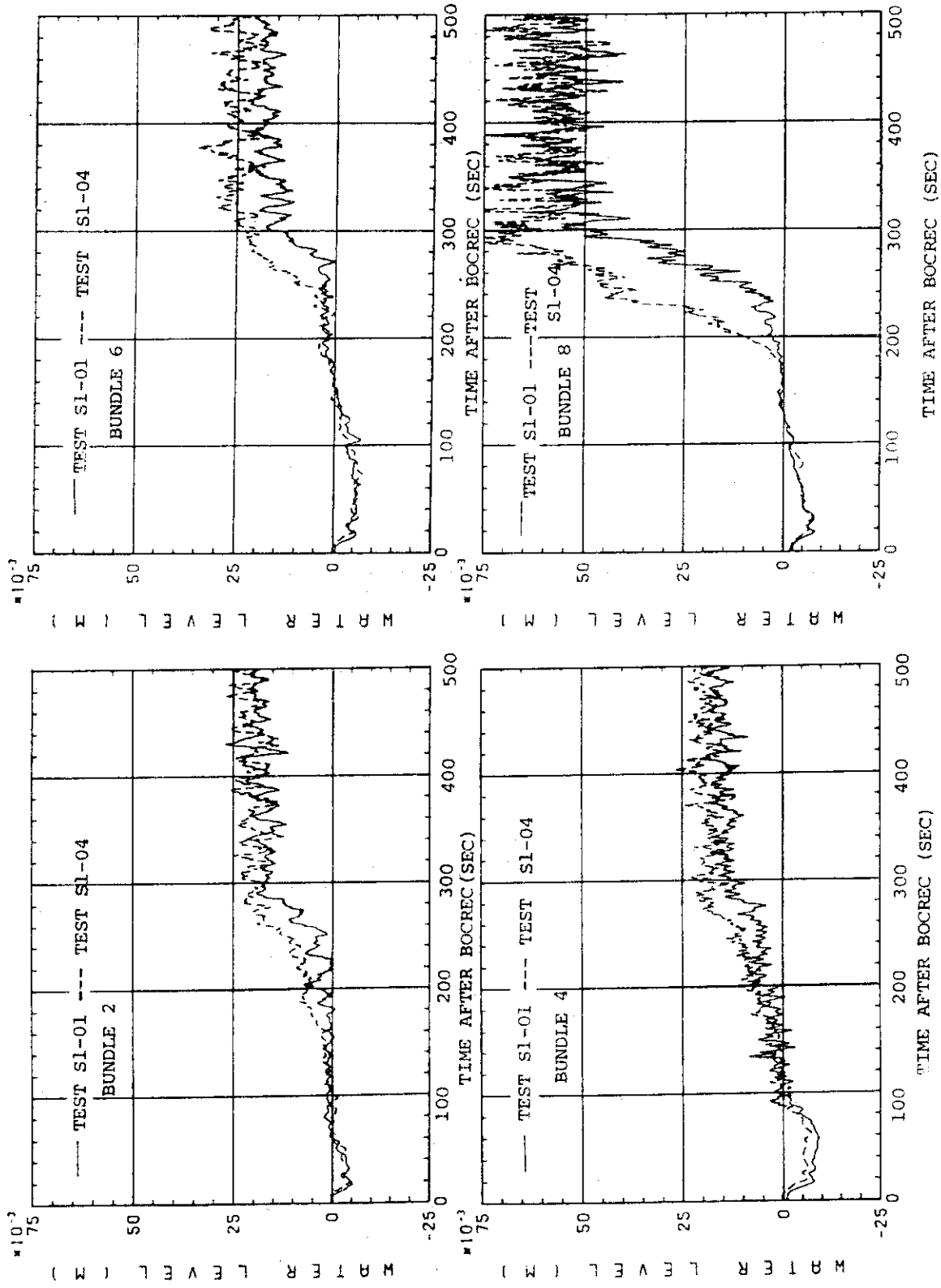

Fig. 3-24 Liquid level transients above end box tie plate for Tests S1-01 and S1-04

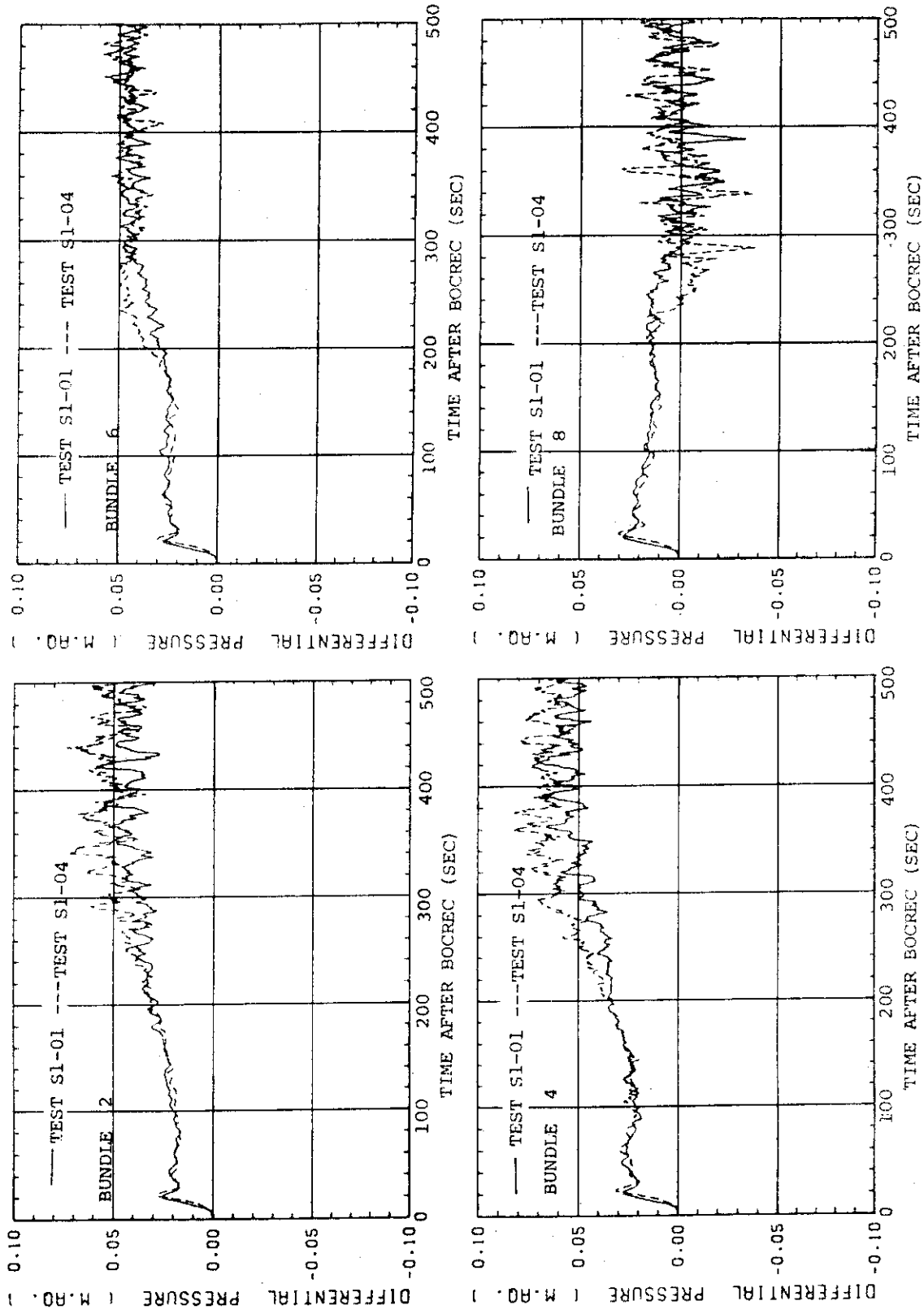

Fig. 3-25 Differential pressure transients across end box tie plate for Tests S1-01 and S1-04

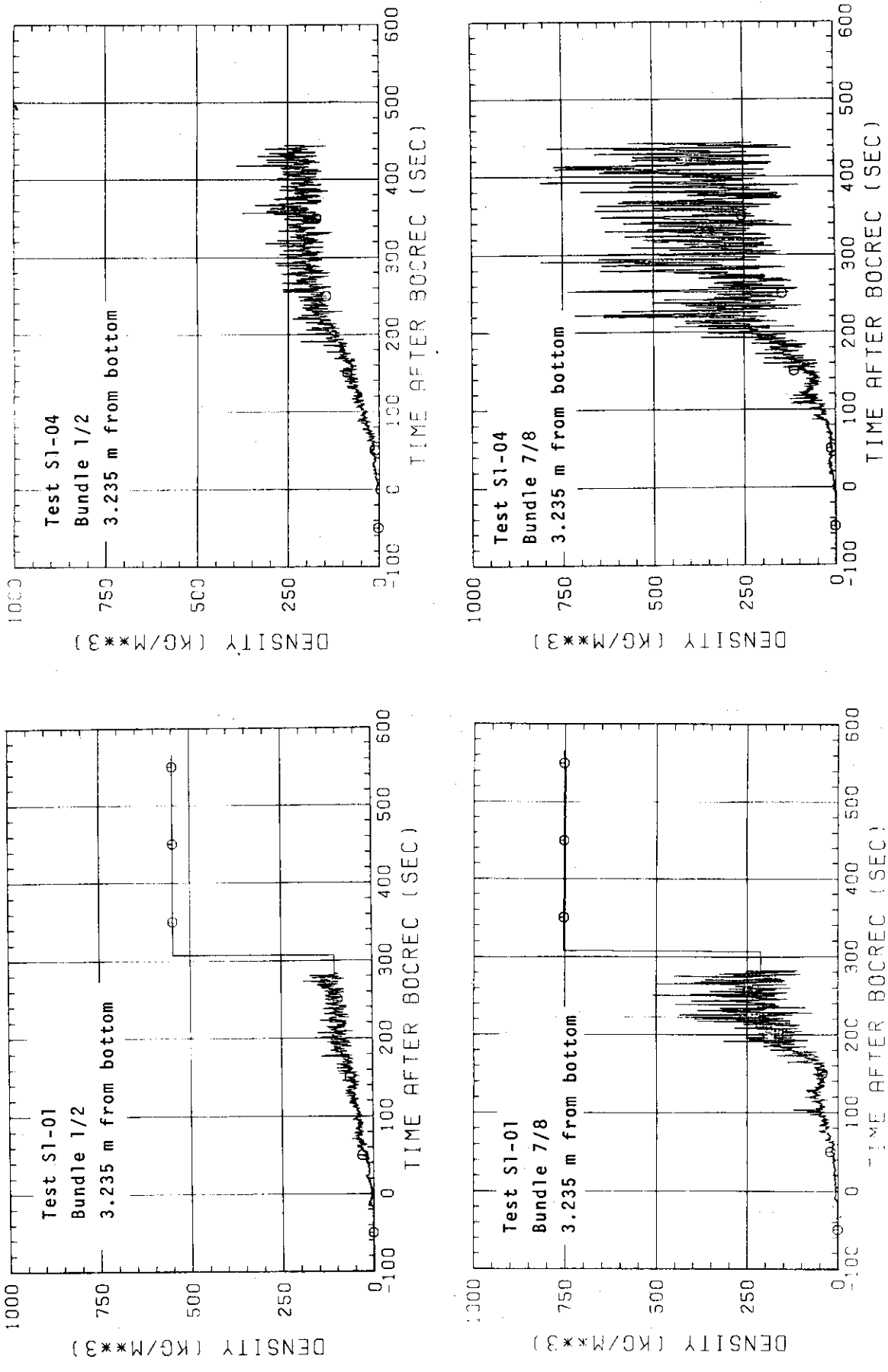

Fig. 3-26 Fluid density transients for Tests S1-01 and S1-04 at elevation 3.235 m

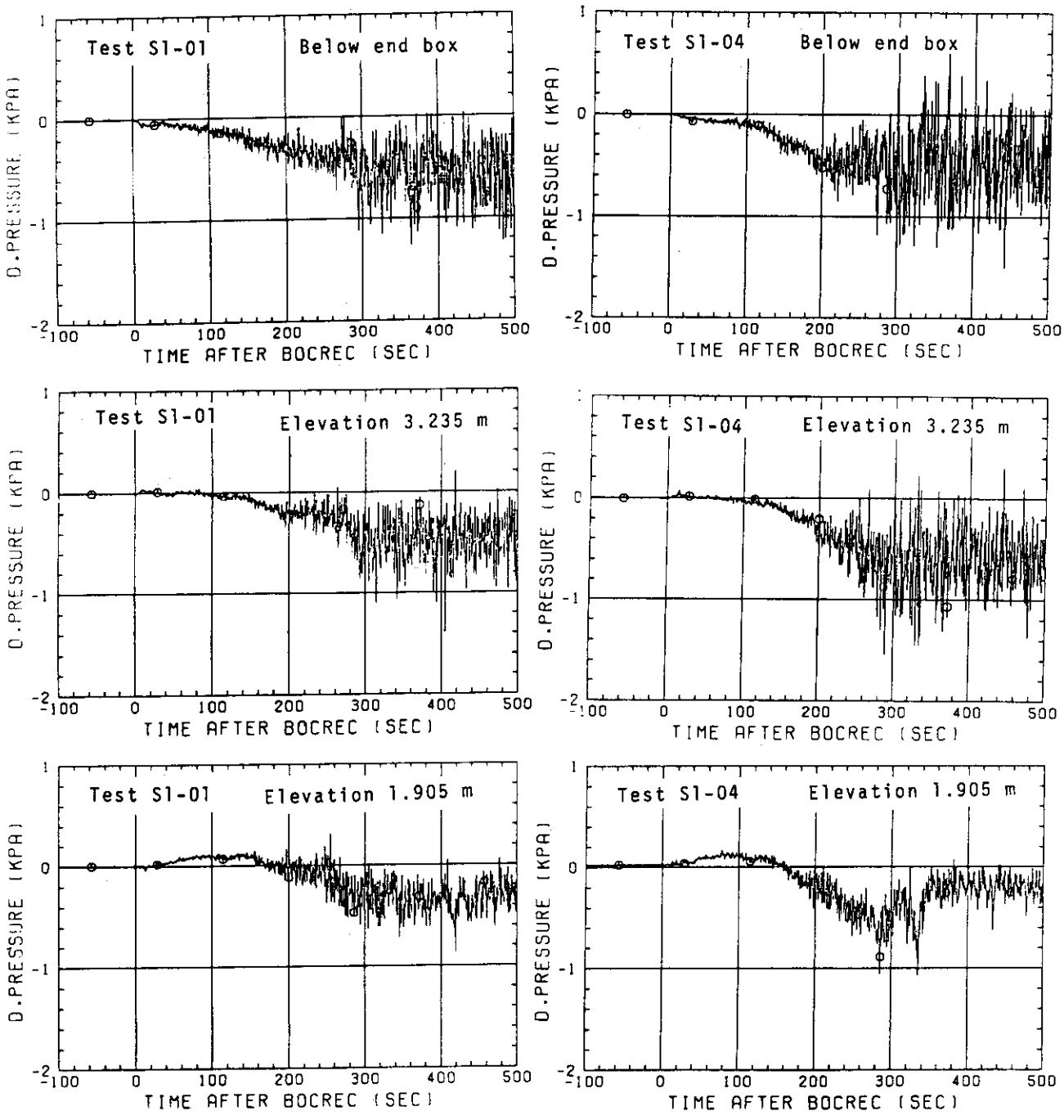

Fig. 3-27 Horizontal differential pressures between Bundles 5 and 8 for Tests S1-01 and S1-04 at elevations of 1.905, 3.235, and 3.821 m

4. Conclusions

(1) The higher core inlet water subcooling results in the shorter quench time, the higher quench velocity and the lower quench temperature for the upward propagated quench.

(2) The higher heat transfer coefficient just above the quench front observed in the higher core inlet water subcooling test can be attributed to the lower void fraction near the quench front.

(3) The Dittus-Boelter's correlation can be applied to the heat transfer coefficient far above the quench front both in the higher core inlet subcooling test and the base case test, suggesting the dispersed flow in this period.

(4) The higher core inlet water subcooling gives the larger water accumulation in the core and upper plenum and the smaller water carryover through the hot leg.

(5) The larger water accumulation in the upper plenum and the smaller water carryover through the hot leg from about 160 seconds after the beginning of reflood in the higher subcooling test can be attributted to the slower steam velocity through the UCSP.

(6) Difference in the integrated steam outflow from the core to the upper plenum before the quench of the whole core is relatively small between the two tests because the smaller steam generation rate below the quench front due to the higher core inlet water subcooling is almost canceled by the larger steam generation rate near the quench front due to the higher heat transfer coefficient and the rapider quench propagation.

(7) The higher core inlet water subcooling results in not only the larger differential pressure across the core full height but also the more uniform radial distribution of the differential pressure.

(8) One-dimensional analysis using the Cunningham-Yeh correlation for void fraction suggests that the intensity of cross flow in the core is much greater in the higher core inlet water subcooling test.

(9) Stronger and earlier water fall back into the peripheral rod bundles of the core can be seen in the higher core inlet water subcooling test.

Acknowledgement

The authors are much indebted to Dr. M. Nozawa, Deputy Director General of Tokai Research Establishment, JAERI, Dr. S. Katsuragi, Center Director of Reactor Safety Research Center, Dr. K. Hirano, Deputy Head of Div. of Reactor Safety, and Dr. Y. Murao, Chief of Reactor Safety Laboratory II, for their guidance and encouragement for this program.

They would like to express their appreciation to Mr. T. Iguchi, Mr. J. Sugimoto, Dr. H. Akimoto and Mr. T. Okubo of CCTF analysis group for their usefull discussions.

References

(1) N. Lee, et al., PWR FLECHT SEASET Unblocked Bundle, Forced and Gravity Reflood Task Data Evaluation and Analysis Report, NUREG/CR-2256 (1981).

(2) H. Adachi, et al., Design of Slab Core Test Facility (SCTF) in Large Scale Reflood Test Program, Part 1: Core-1, JAERI-M 83-080 (1983)

(3) M. Osakabe and Y. Sudo, Computer Codes HEATT and HEATQ for Heat Transfer Analysis in SCTF, Private Communication

(4) L.A. Bromley, et al., Chem. Eng. Progr., 46, 5, 221 (1950)

(5) J.P. Cuningham and H.C. Yeh, Trans. ANS, 17, 369-370 (1973)

Acknowledgement

The authors are much indebted to Dr. M. Nozawa, Deputy Director General of Tokai Research Establishment, JAERI, Dr. S. Katsuragi, Center Director of Reactor Safety Research Center, Dr. K. Hirano, Deputy Head of Div. of Reactor Safety, and Dr. Y. Murao, Chief of Reactor Safety Laboratory II, for their guidance and encouragement for this program.

They would like to express their appreciation to Mr. T. Iguchi, Mr. J. Sugimoto, Dr. H. Akimoto and Mr. T. Okubo of CCTF analysis group for their usefull discussions.

References

(1) N. Lee, et al., PWR FLECHT SEASET Unblocked Bundle, Forced and Gravity Reflood Task Data Evaluation and Analysis Report, NUREG/CR-2256 (1981).

(2) H. Adachi, et al., Design of Slab Core Test Facility (SCTF) in Large Scale Reflood Test Program, Part 1: Core-1, JAERI-M 83-080 (1983)

(3) M. Osakabe and Y. Sudo, Computer Codes HEATT and HEATQ for Heat Transfer Analysis in SCTF, Private Communication

(4) L.A. Bromley, et al., Chem. Eng. Progr., 46, 5, 221 (1950)

(5) J.P. Cuningham and H.C. Yeh, Trans. ANS, 17, 369-370 (1973)

Appendix A Measurement Locations

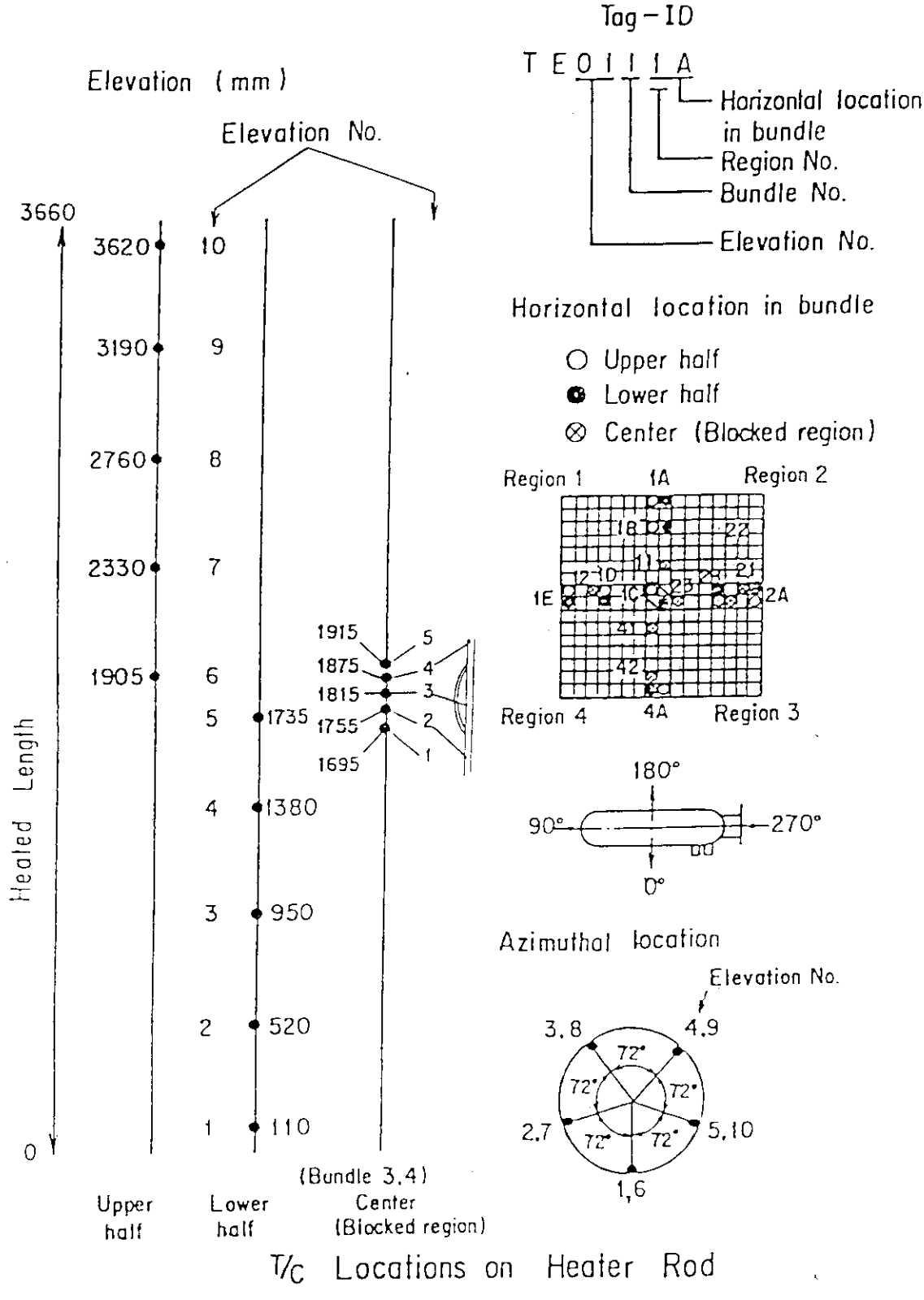

Fig. A-1 Thermocouple Locations of Heater Rod Surface Temperature Measurements

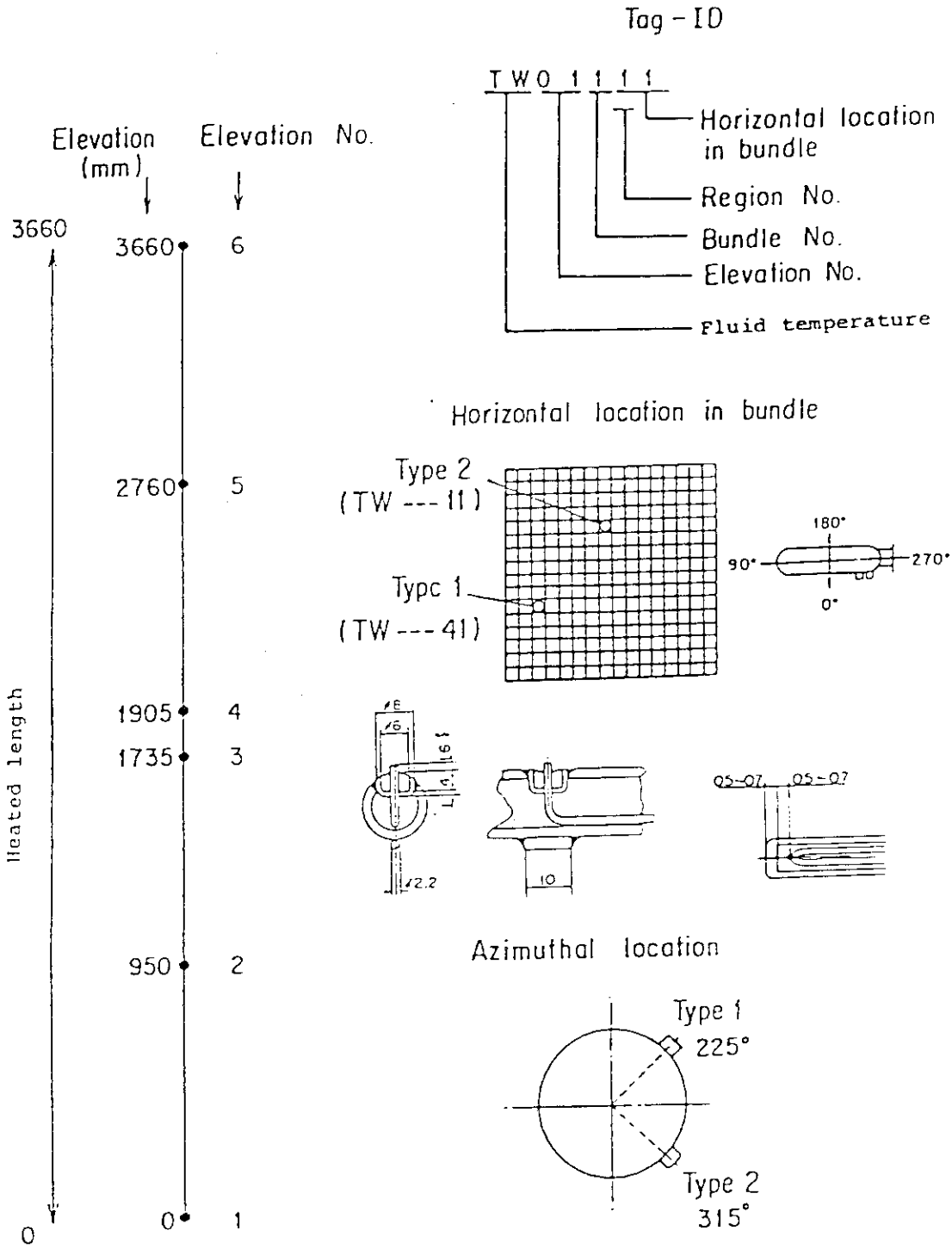

Fig. A-2 Thermocouple Locations of Fluid Temperature Measurements in Core

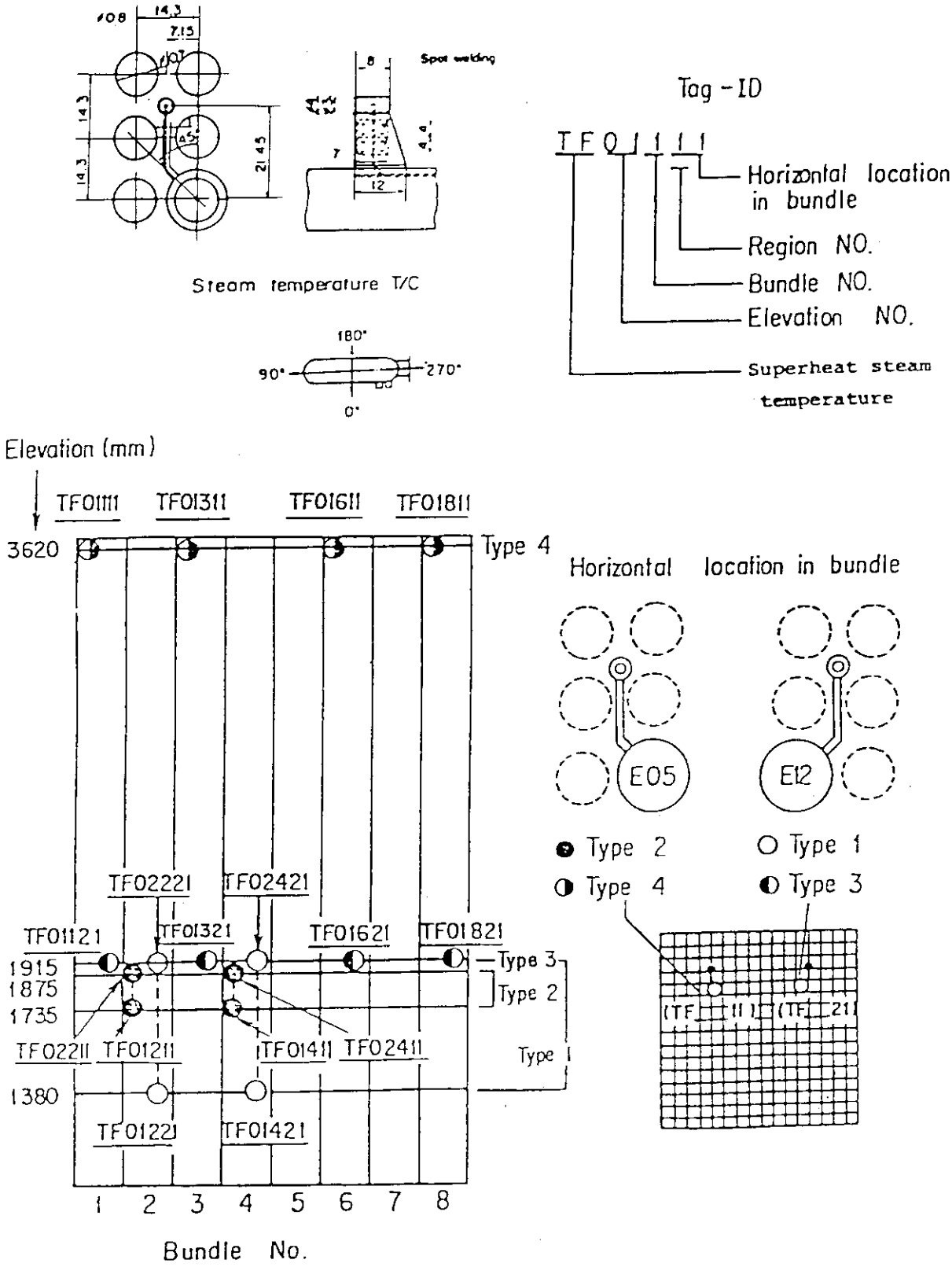

Fig. A-3 Thermocouple Locations of Steam Temperature Measurements in Core

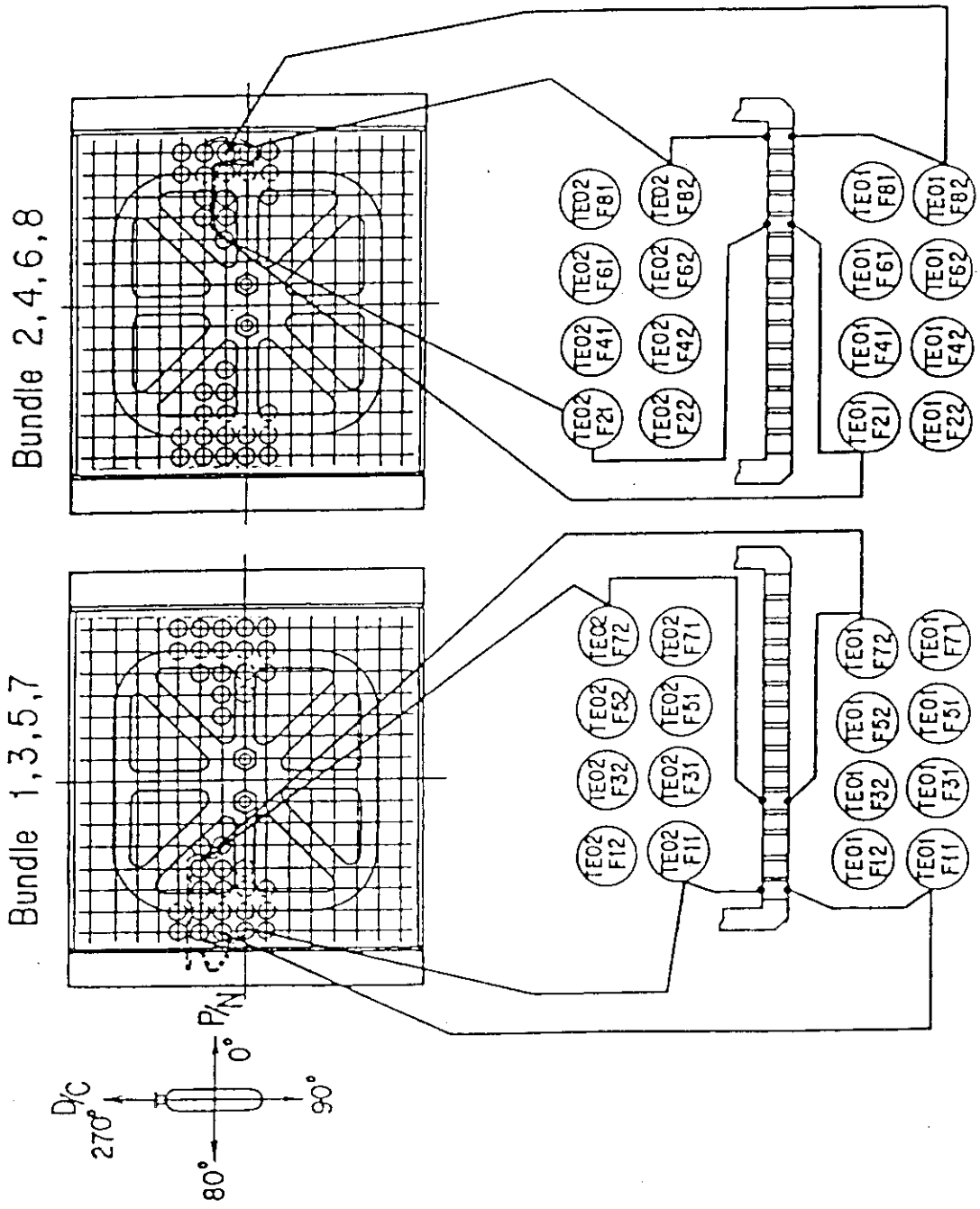

Fig. A-4 Thermocouple Locations of Fluid Temperature Measurements Just above and below End Box Tie Plate

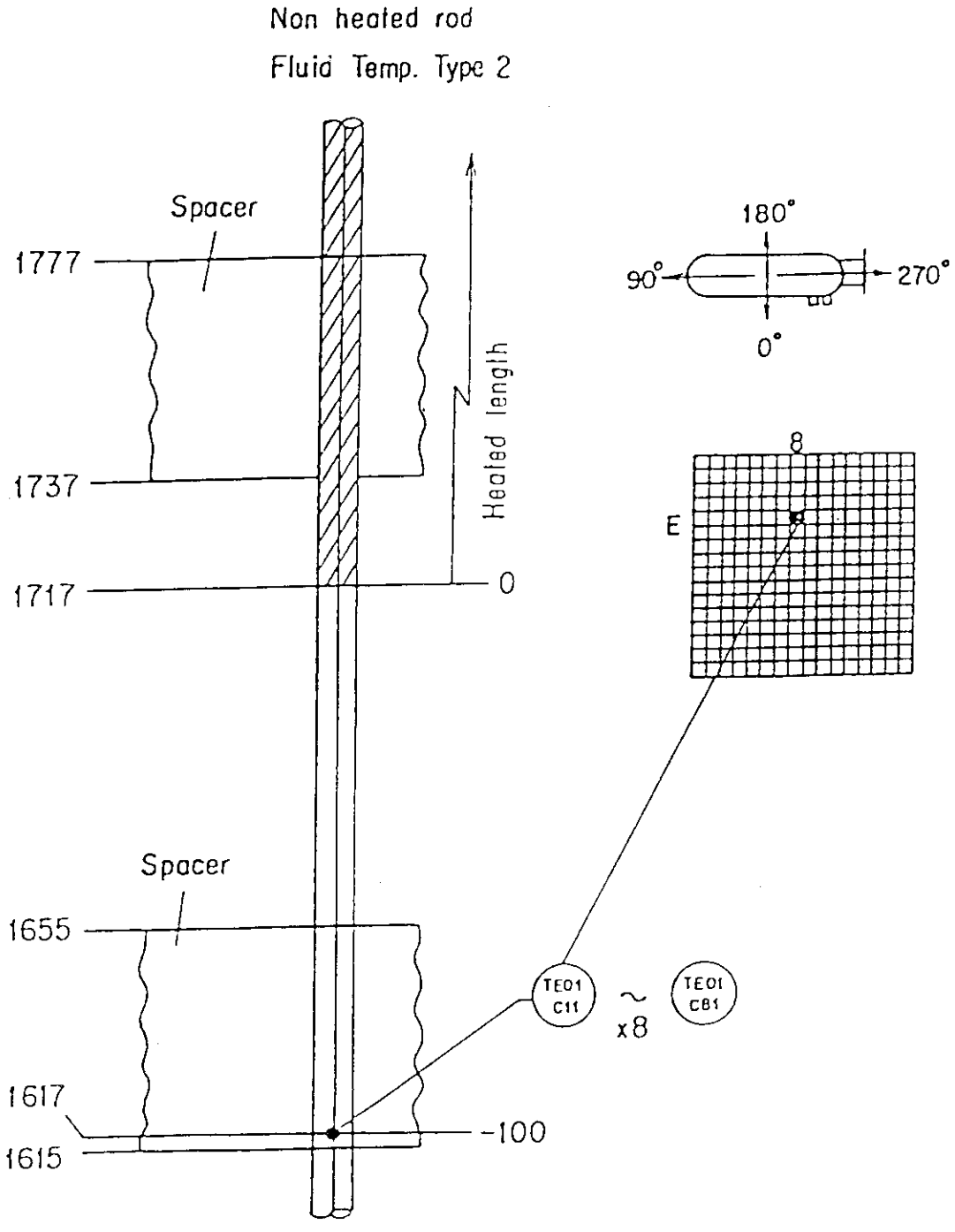

Fig. A-5 Thermocouple Locations of Fluid Temperature Measurements at Core Inlet

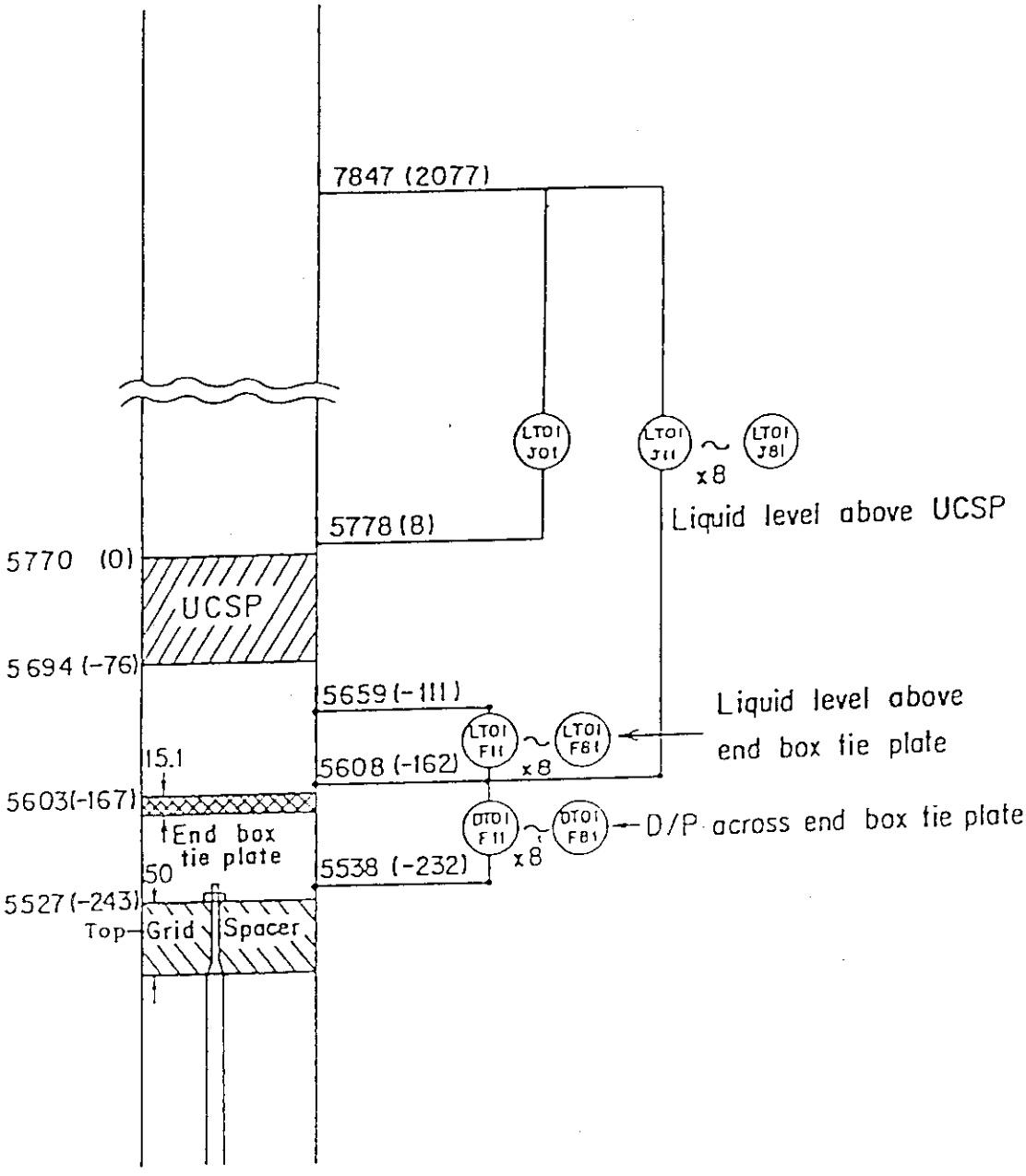

Fig. A-6 Locations of Differential Pressure Measurements across End Box Tie Plate and Liquid Level Measurements above UCSP and End Box Tie Plate

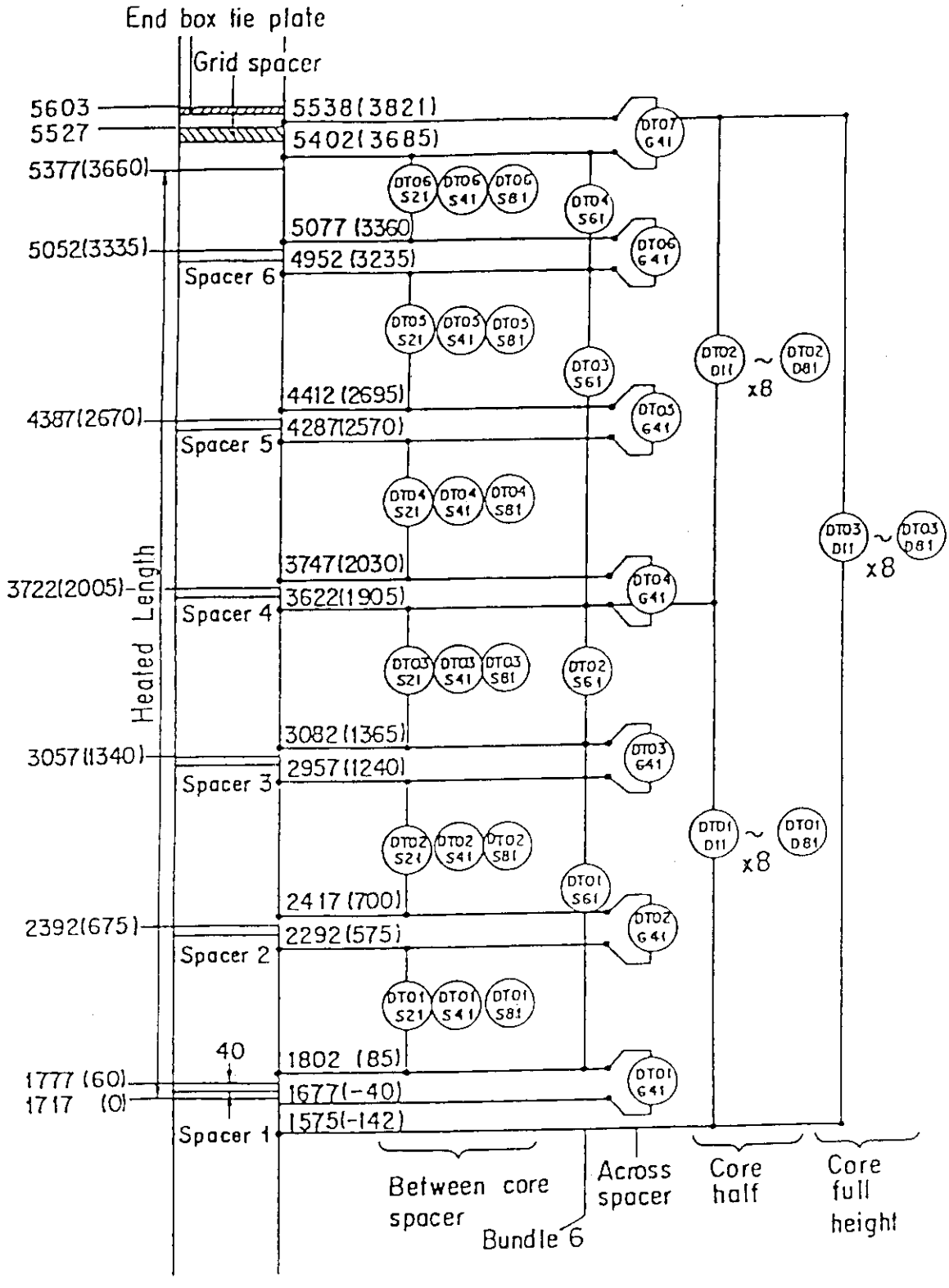

Fig. A-7 Locations of Vertical Differential Pressure Measurements in Core

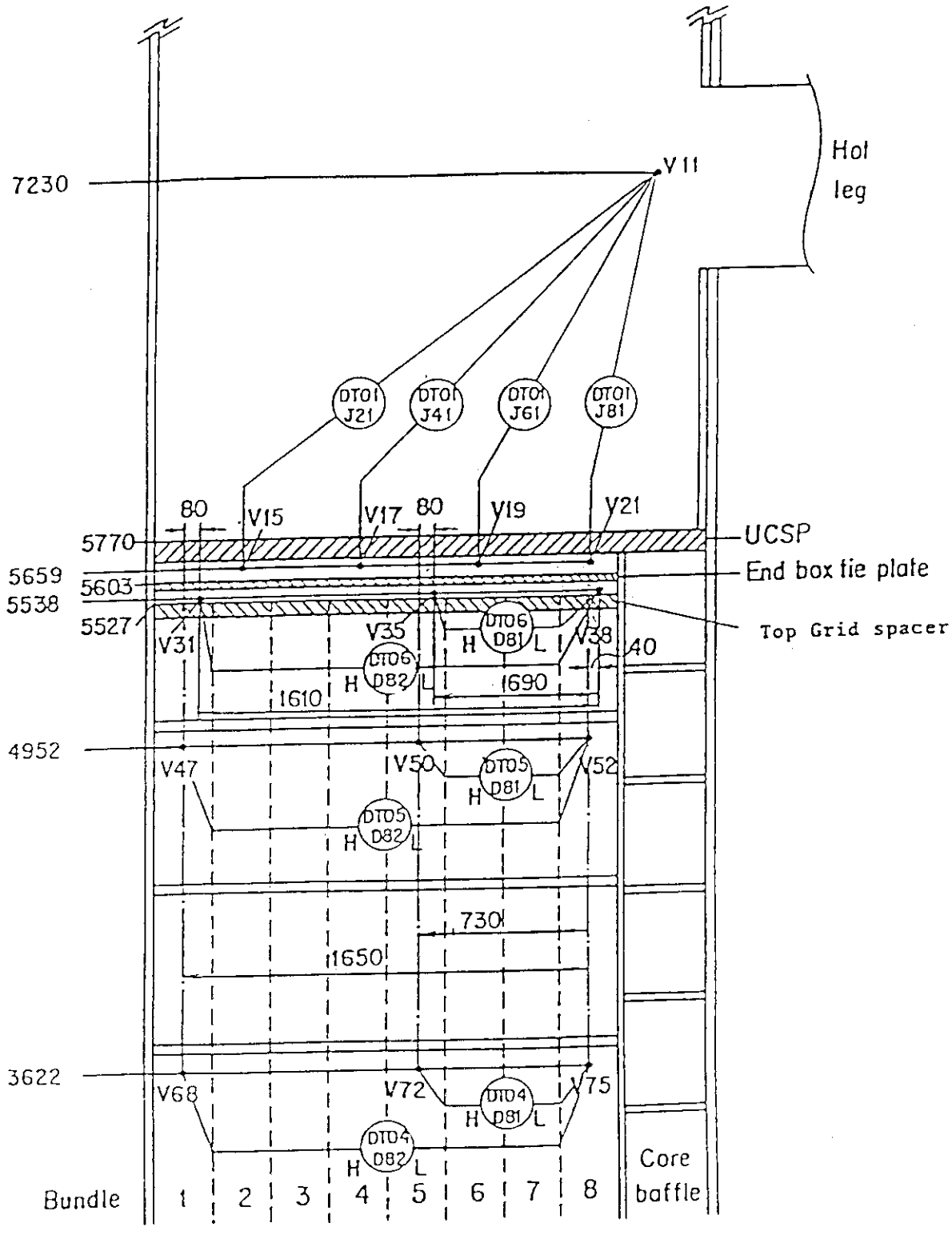

Fig. A-8 Locations of Horizontal Differential Pressure Measurements in Core and Differential Pressure Measurements between End Box and Inlet of Hot Leg

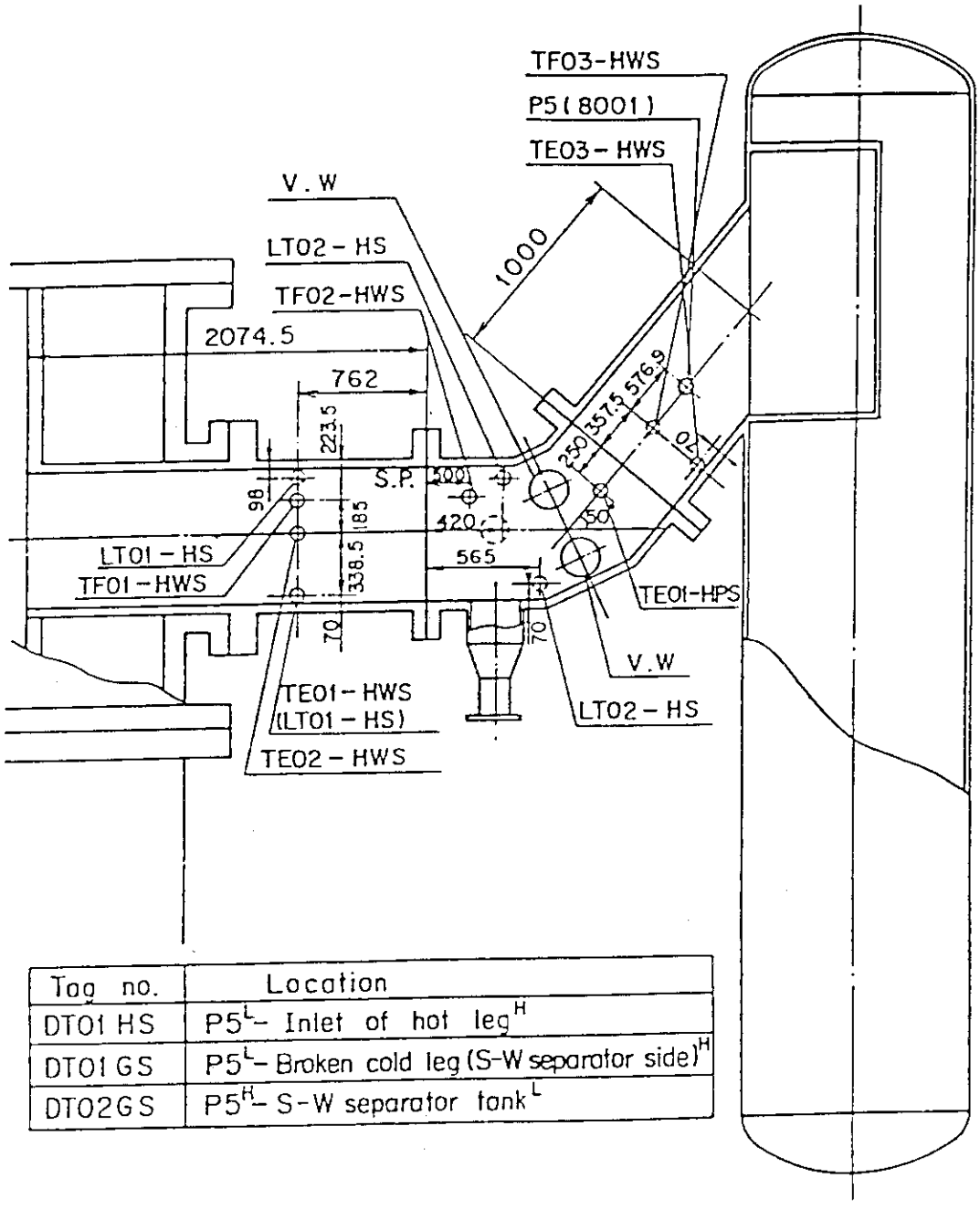

Tag no.	Location
DT01HS	$P5^{L}$ – Inlet of hot leg^{H}
DT01GS	$P5^{L}$ – Broken cold leg (S-W separator side)^{H}
DT02GS	$P5^{R}$ – S-W separator tank^{L}

Fig. A-9 Locations of Hot Leg Instrumentation

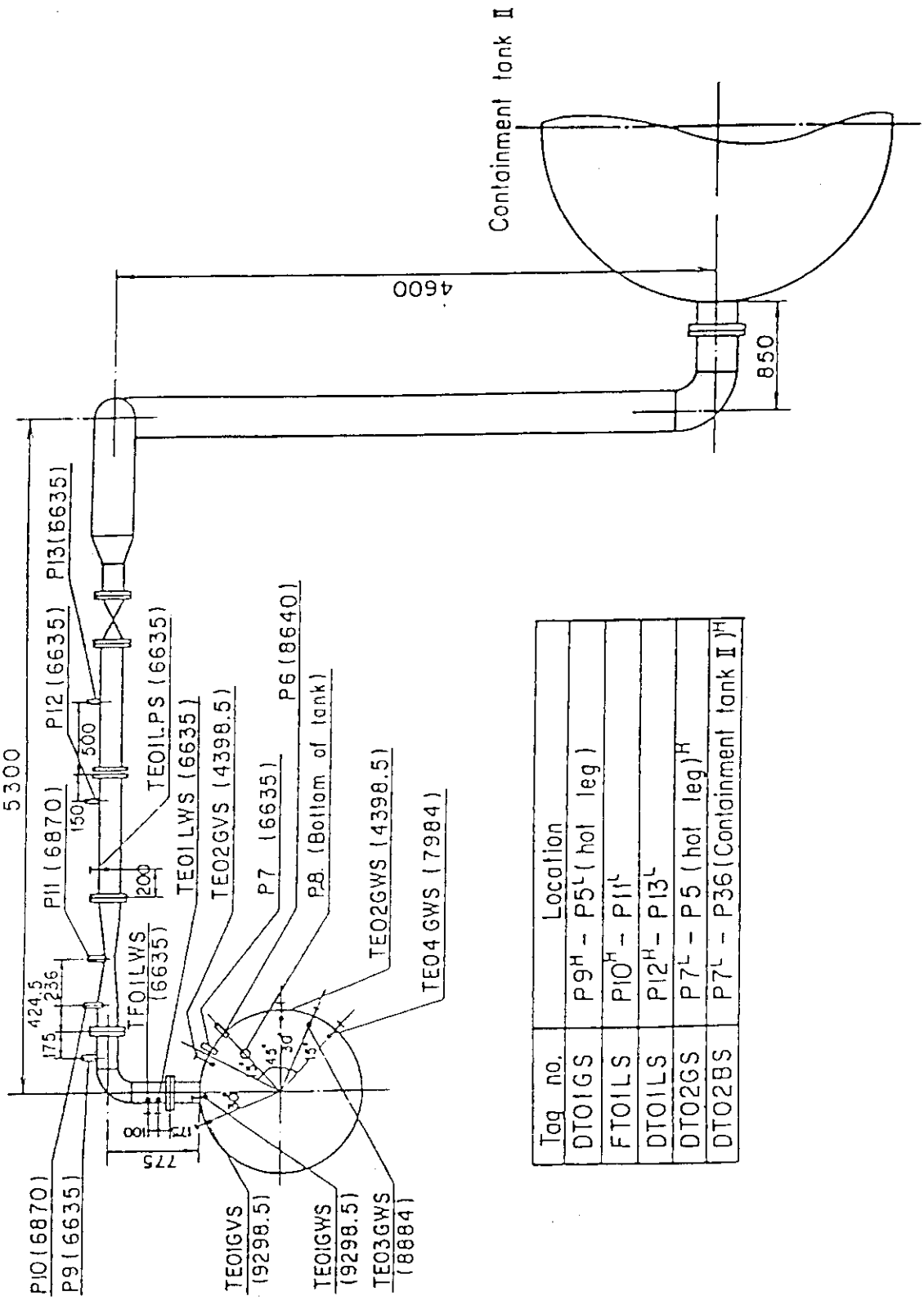

Tag no.	Location
DT01GS	$P9^H$ - $P5^L$ (hot leg)
FT01LS	$P10^H$ - $P11^L$
DT01LS	$P12^H$ - $P13^L$
DT02GS	$P7^L$ - P5 (hot leg)^H
DT02BS	$P7^L$ - P36 (Containment tank II)^H

Fig. A-10 Measurement Location of Steam/Water Separator Side Broken Cold Leg

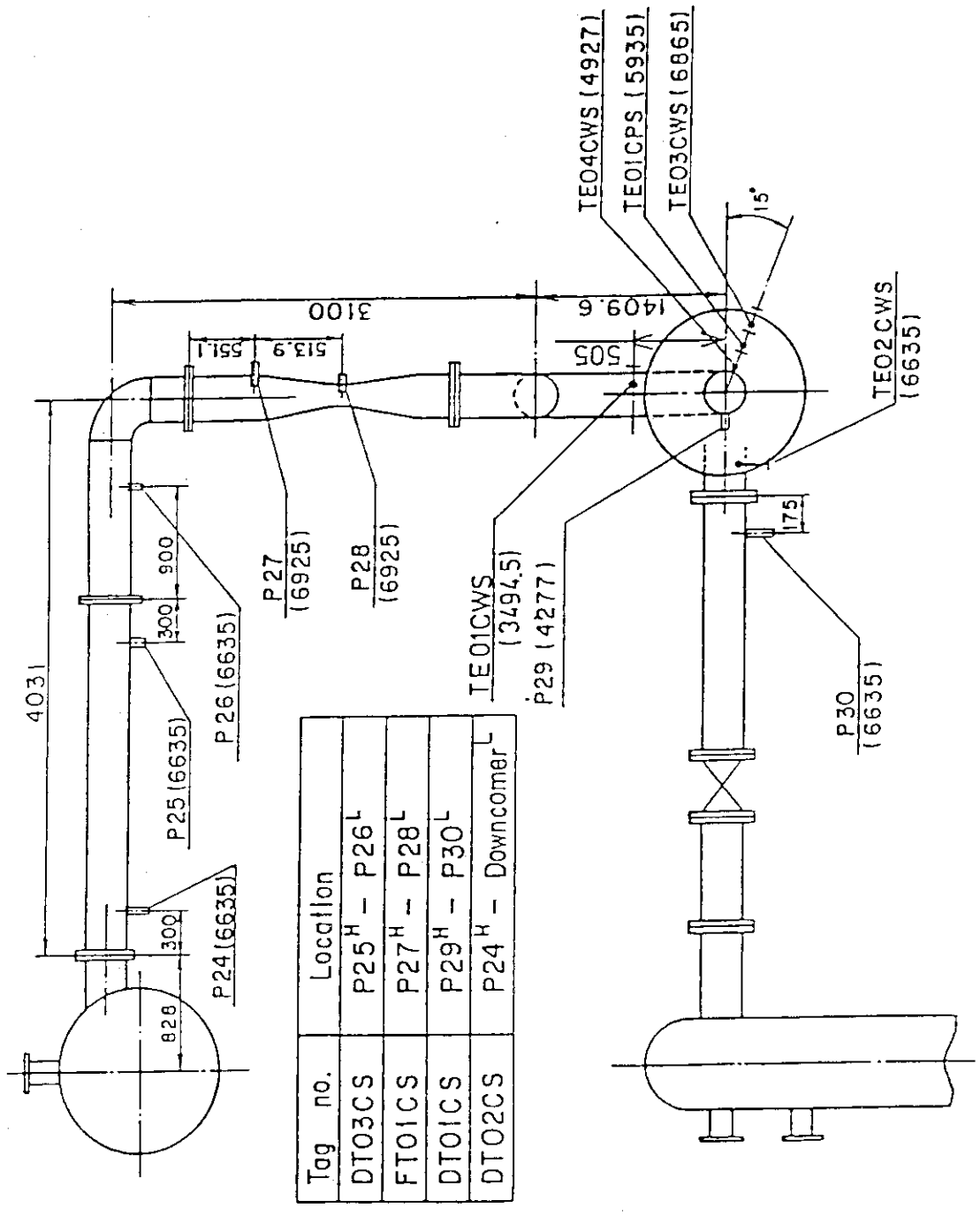

Fig. A-11 Locations of Intact Cold Leg Instrumentation

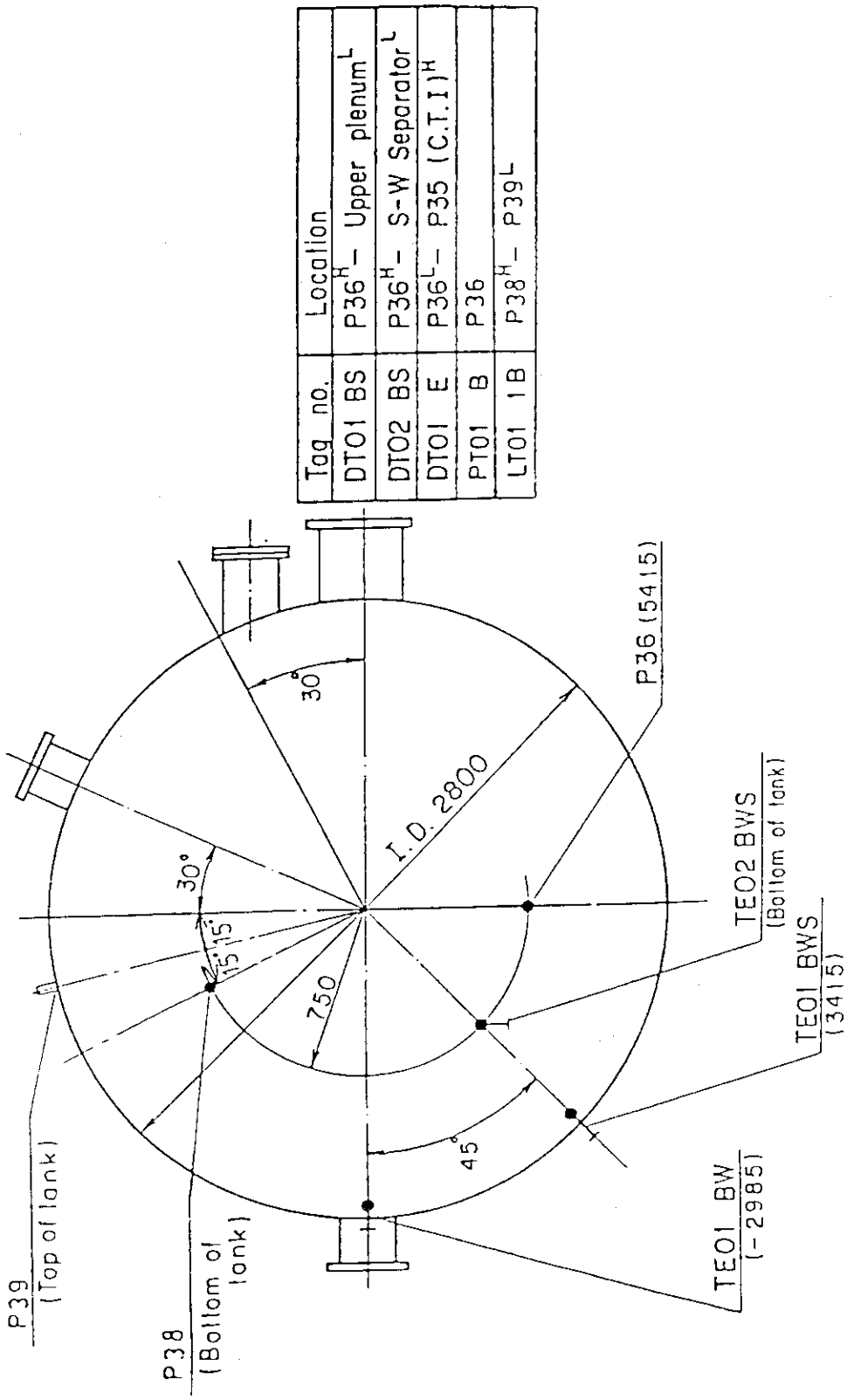

Fig. A-12 Locations of Containment Tank-II Instrumentation

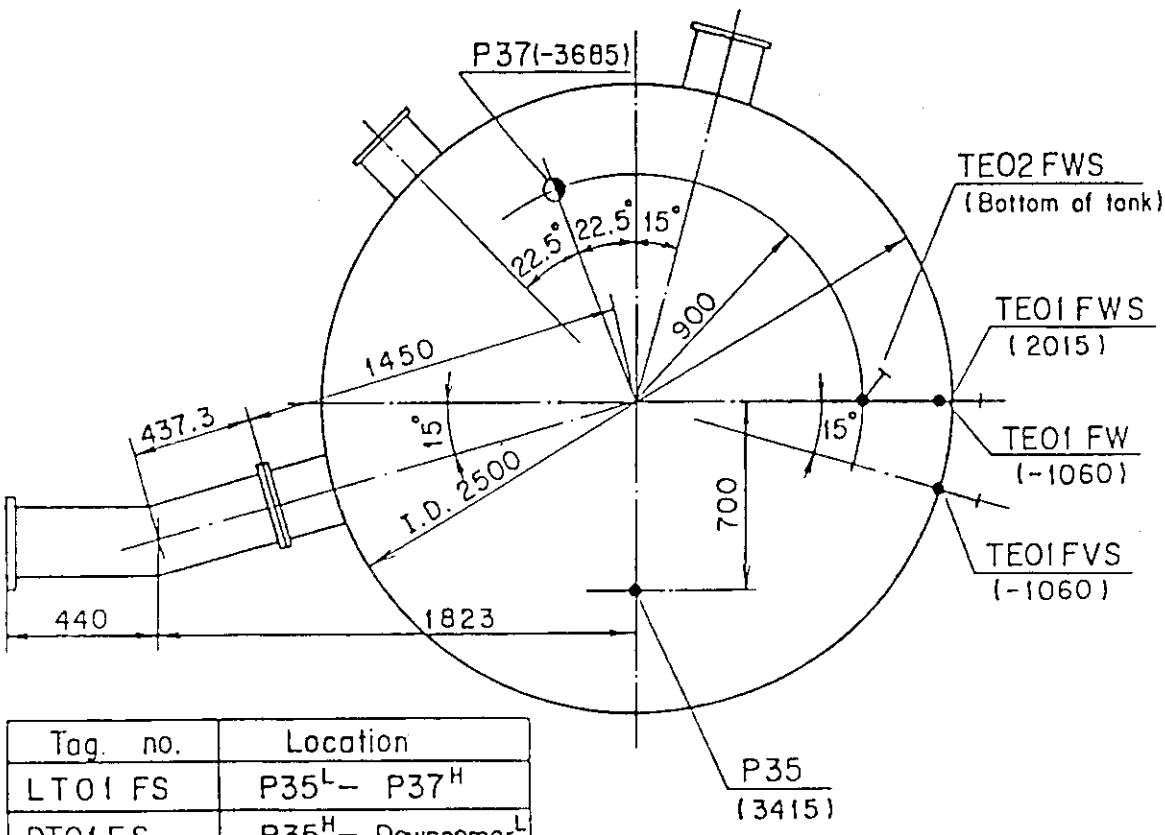

Tag. no.	Location
LT01 FS	$P35^{L}$ – $P37^{H}$
DT01 FS	$P35^{H}$ – $Downcomer^{L}$
DT01 E	$P35^{H}$ – P36 (C.T. II)
PT01 F	P35

Fig. A-13 Locations of Containment Tank-I Instrumentation

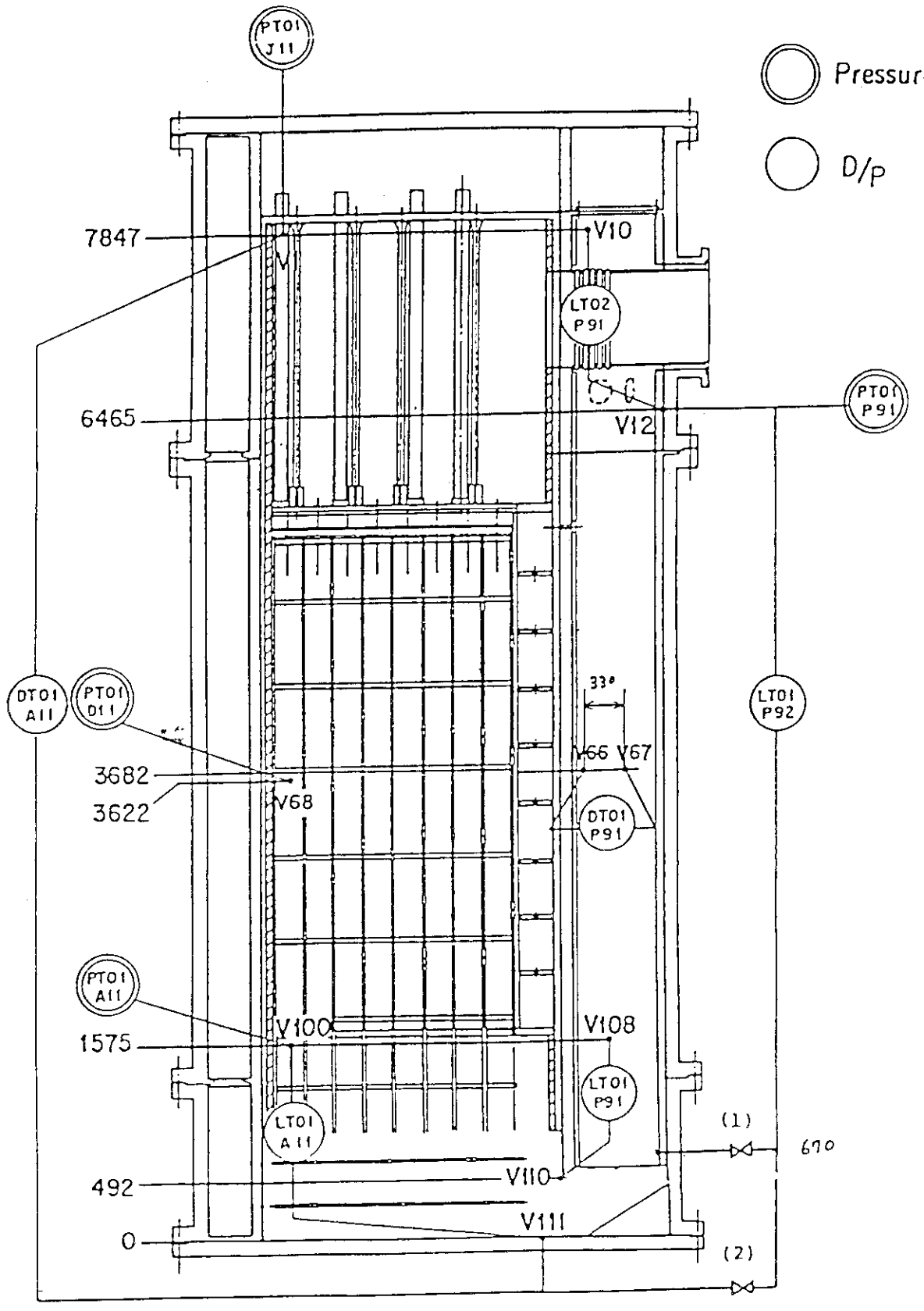

(1) used for lower plenum injection test
(the bottom of downcomer is blocked)
(2) used for the other tests

Fig. A-14 Location of Pressure Measurements in Pressure Vessel, Differential Pressure Measurements between Upper and Lower Plenums and Liquid Level Measurements in Downcomer and Lower Plenum

Appendix B Selected Data of Test S1-04 (Run 510)

Fig. No.	Measurement item	Fig. No. of measurement location
B- 1 ∿ B-16	Heater rod temperature	A-1
B-17 ∿ B-20	Fluid temperature in core	A-2
B-21 ∿ B-22	Steam temperature in core	A-3
B-23 ∿ B-24	Fluid temperature just above end box tie plate	A-4
B-25 ∿ B-26	Fluid temperature at core inlet	A-5
B-27 ∿ B-28	Liquid level above end box tie plate	A-6
B-29 ∿ B-30	Liquid level above UCSP	A-6
B-31 ∿ B-32	Differential pressure of core full height	A-7
B-33 ∿ B-34	Differential pressure across end box tie plate	A-6
B-35 ∿ B-36	Horizontal differential pressure in core	A-8
B-37	Differential pressure of hot leg	A-9
B-38	Differential pressure across steam/water separator	A-9, A-10
B-39	Differential pressure of intact cold leg	A-11
B-40	Differential pressure between steam water separator and containment tank-II	A-10
B-41	Differential pressure between top of upper plenum and containment tank-II	A-12
B-42	Differential pressure between containment tanks I and II	A-12
B-43	Differential pressure of broken cold leg	A-13
B-44	Pressures in pressure vessel	A-14
B-45, B-46	Bundle powers	
B-47	ECC water flow rate	

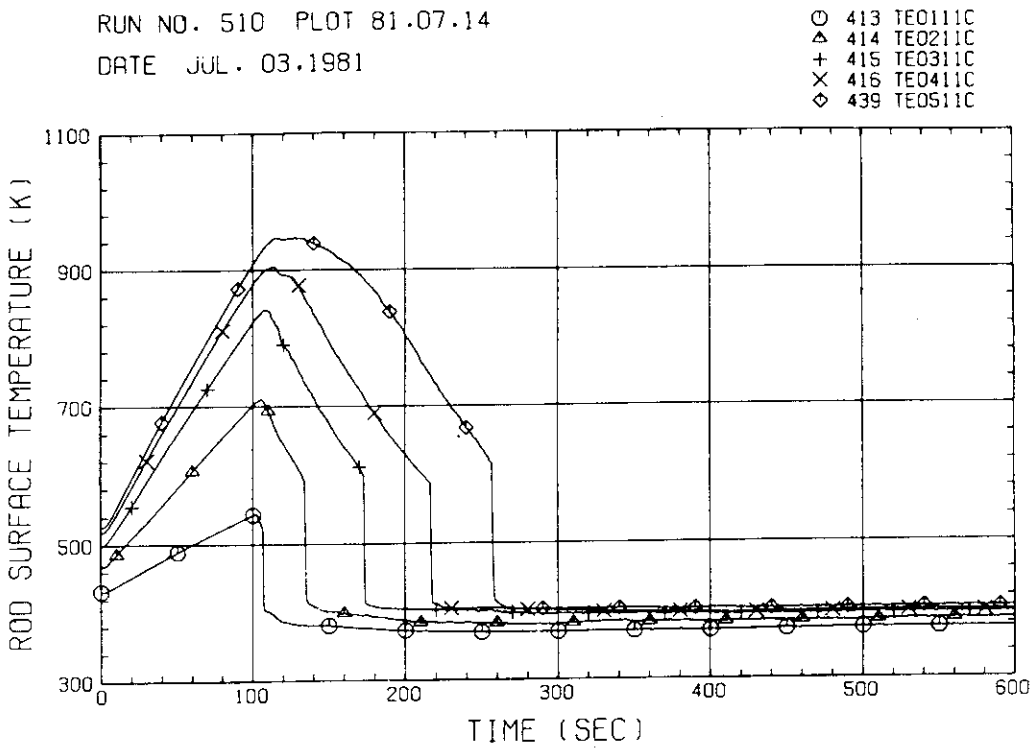

Fig.B-1 HEATER ROD TEMPERATURE (BUNDLE 1-1C, LOWER HALF)

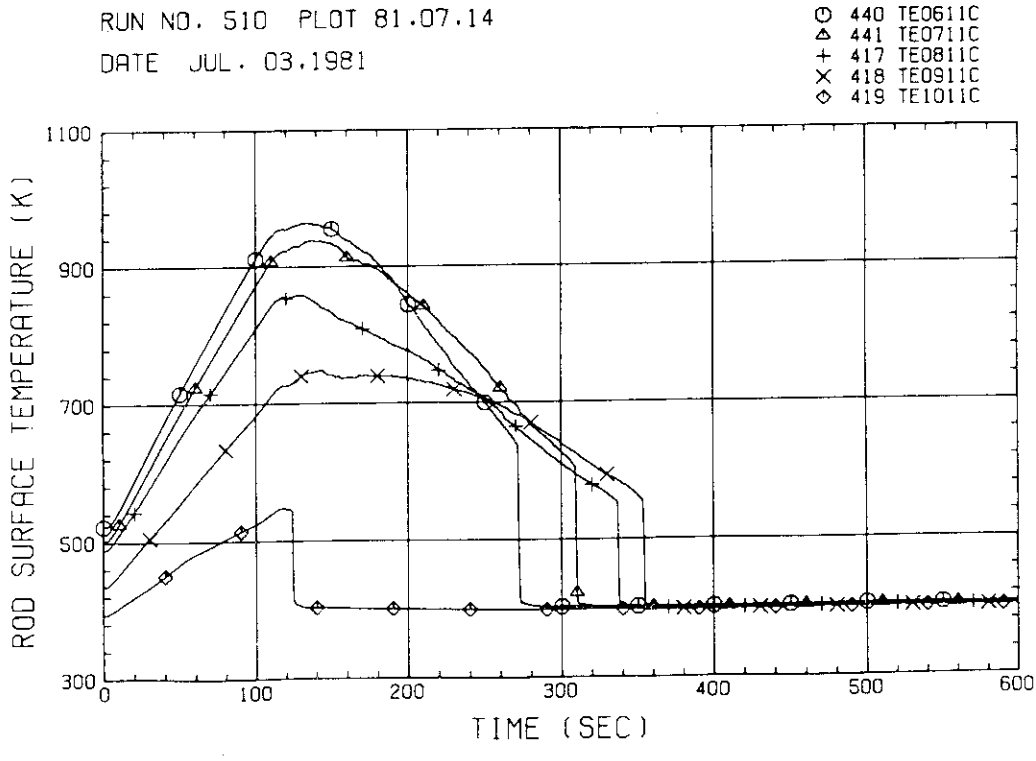

Fig.B-2 HEATER ROD TEMPERATURE (BUNDLE 1-1C, UPPER HALF)

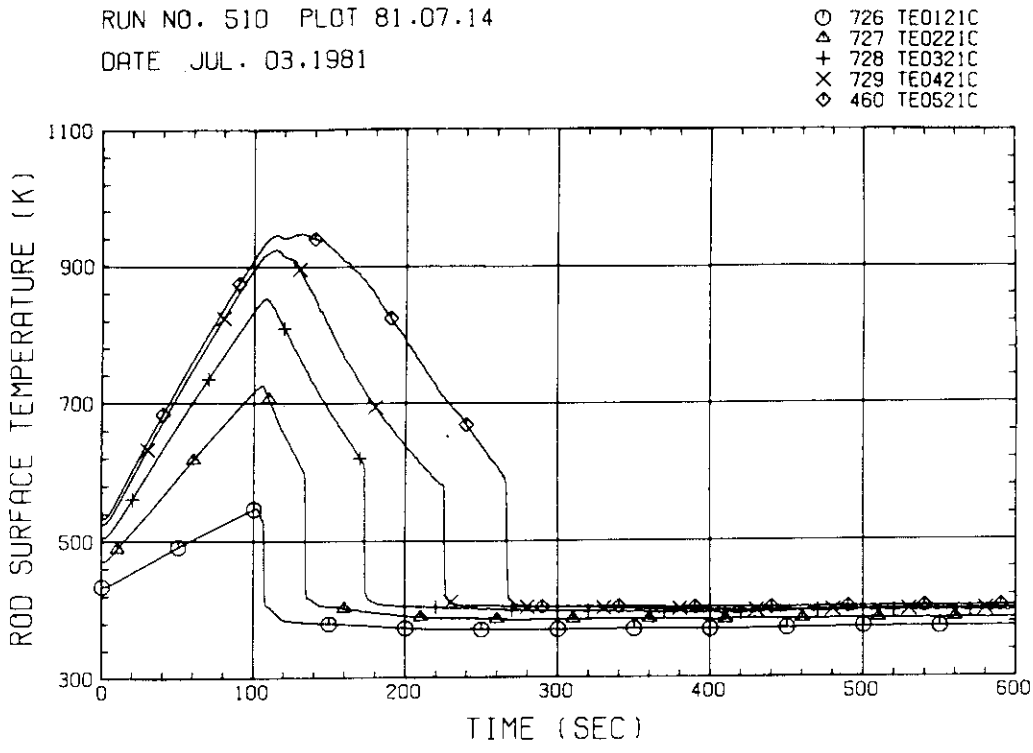

Fig.B-3 HEATER ROD TEMPERATURE (BUNDLE 2-1C, LOWER HALF)

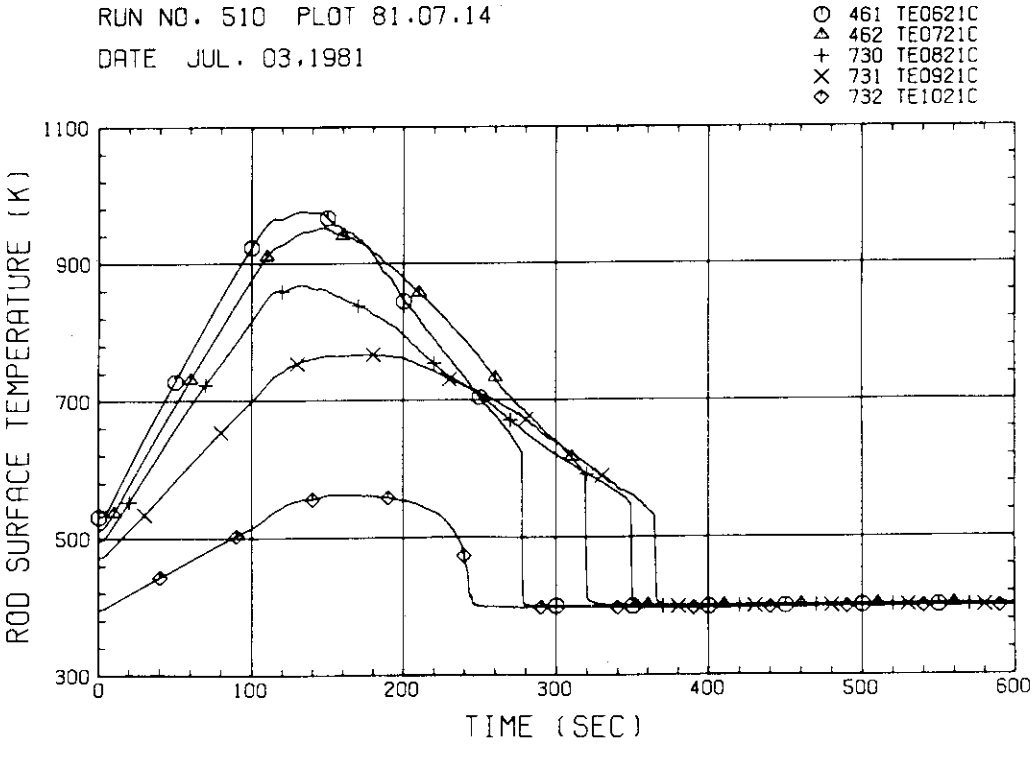

Fig.B-4 HEATER ROD TEMPERATURE (BUNDLE 2-1C, UPPER HALF)

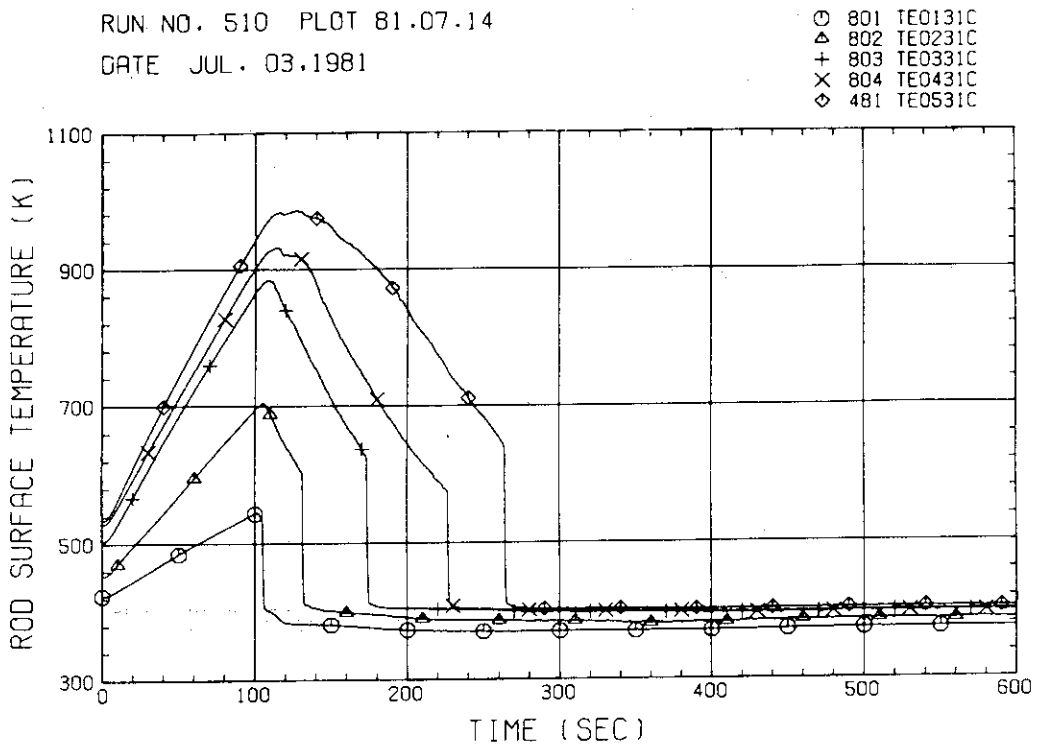

Fig.B-5 HEATER ROD TEMPERATURE (BUNDLE 3-1C, LOWER HALF)

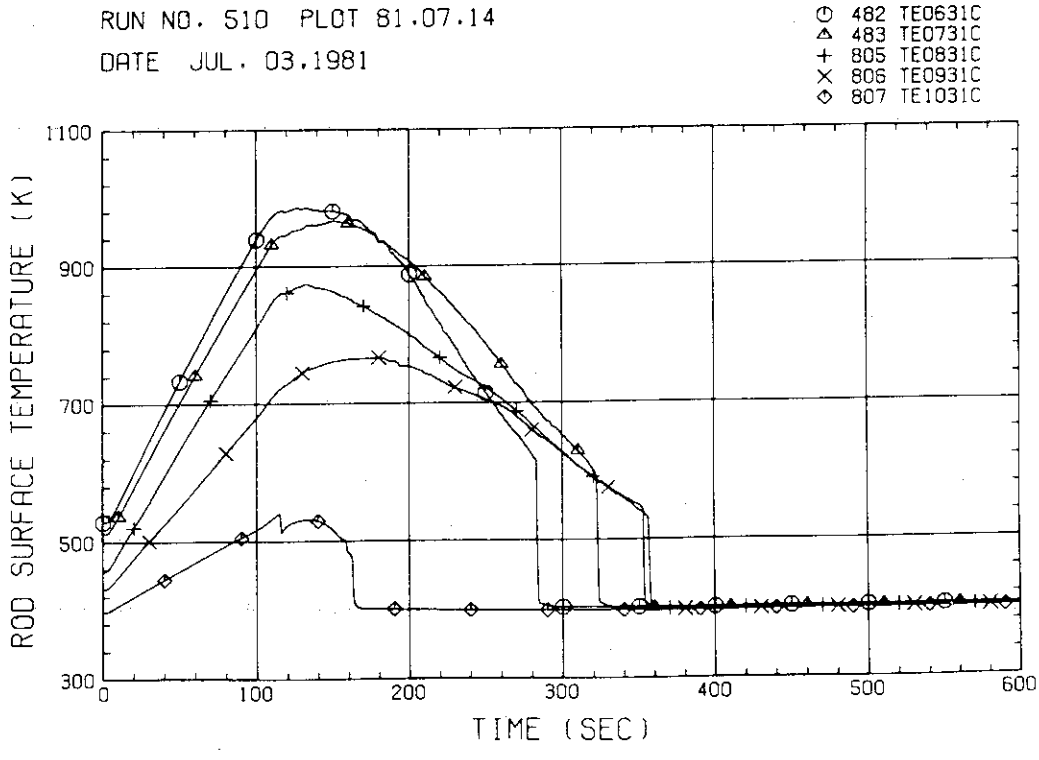

Fig.B-6 HEATER ROD TEMPERATURE (BUNDLE 3-1C, UPPER HALF)

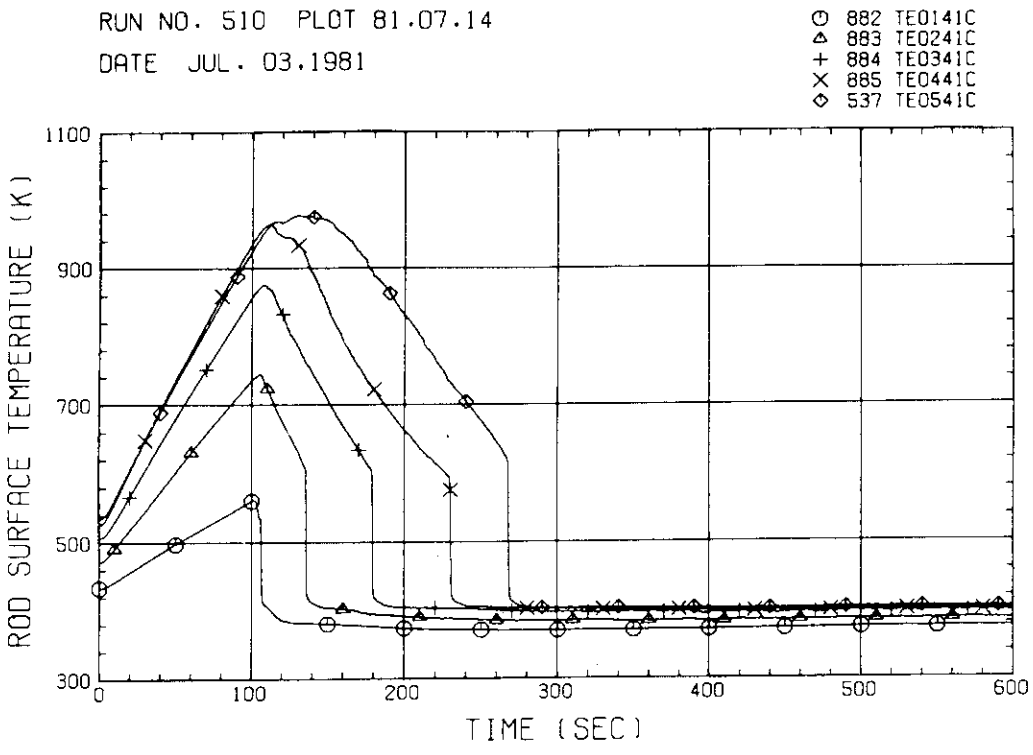

Fig.B-7 HEATER ROD TEMPERATURE (BUNDLE 4-1C, LOWER HALF)

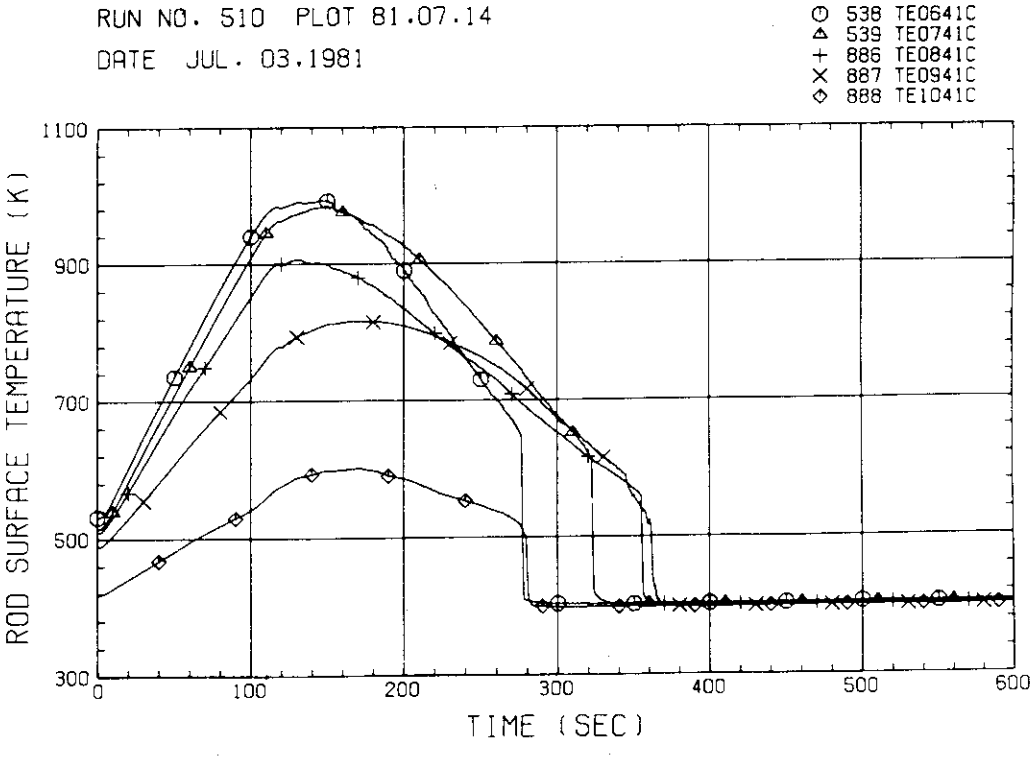

Fig.B-8 HEATER ROD TEMPERATURE (BUNDLE 4-1C, UPPER HALF)

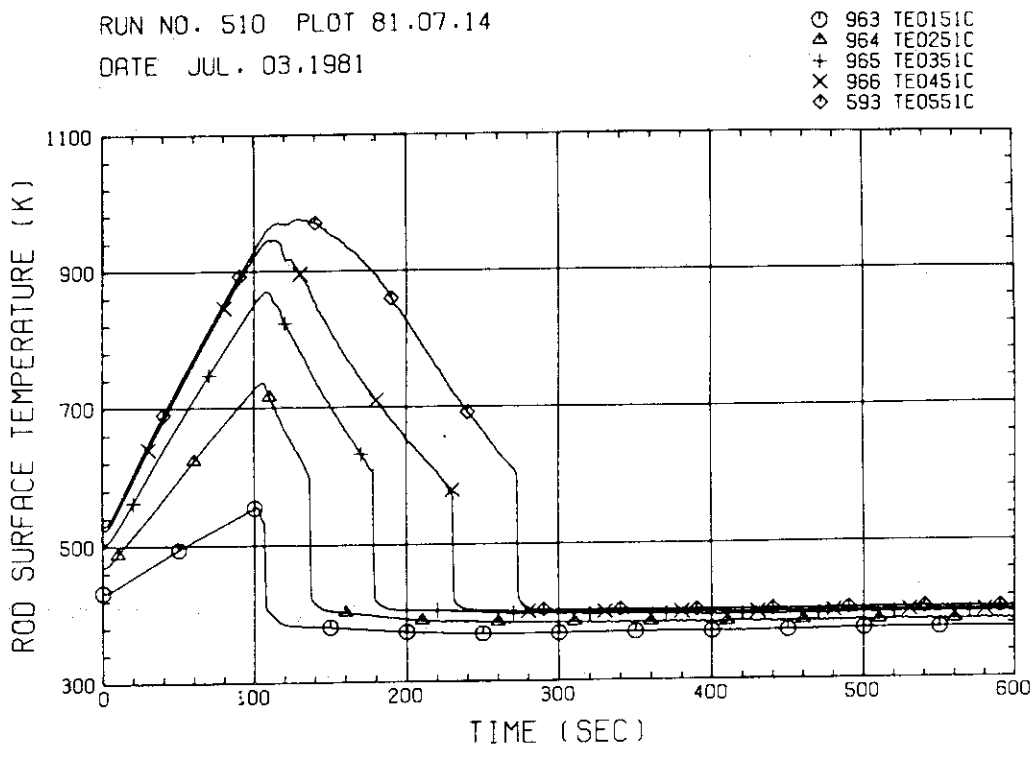

Fig.B-9 HEATER ROD TEMPERATURE (BUNDLE 5-1C, LOWER HALF)

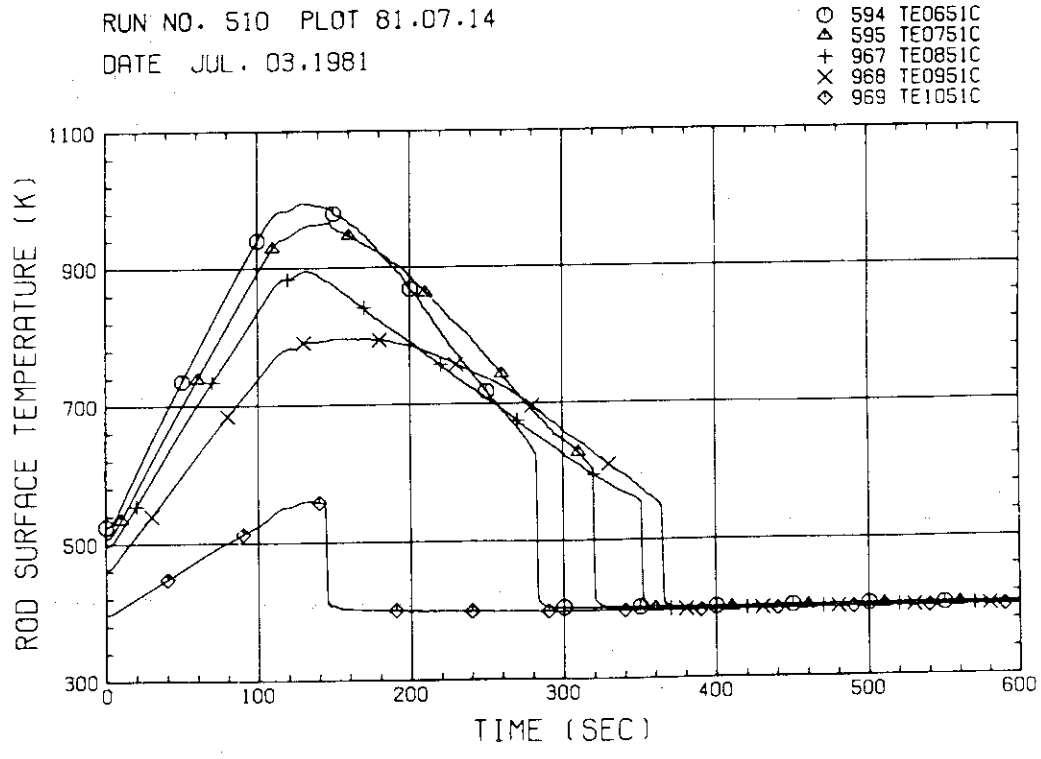

Fig.B-10 HEATER ROD TEMPERATURE (BUNDLE 5-1C, UPPER HALF)

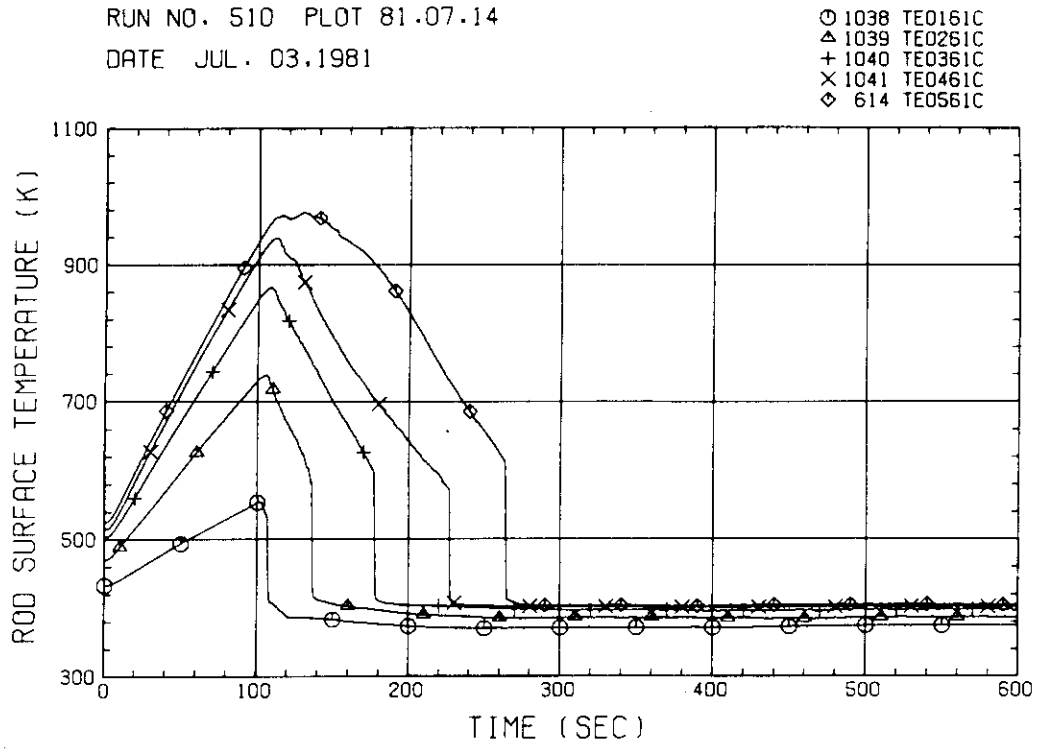

Fig.B-11 HEATER ROD TEMPERATURE (BUNDLE 6-1C, LOWER HALF)

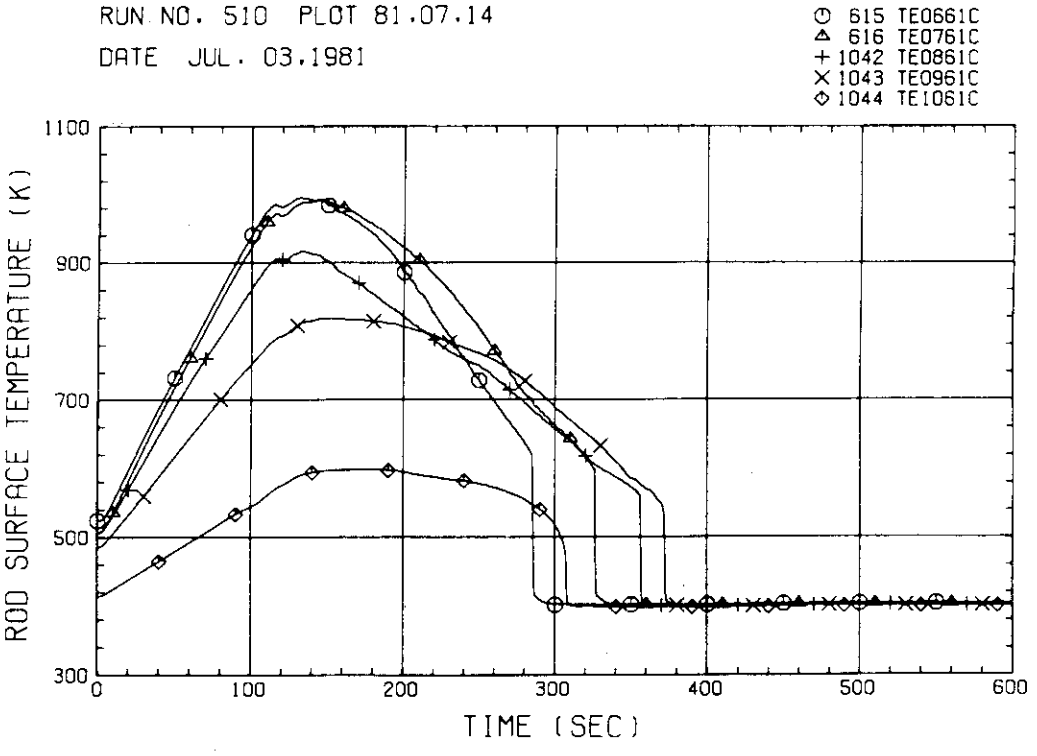

Fig.B-12 HEATER ROD TEMPERATURE (BUNDLE 6-1C, UPPER HALF)

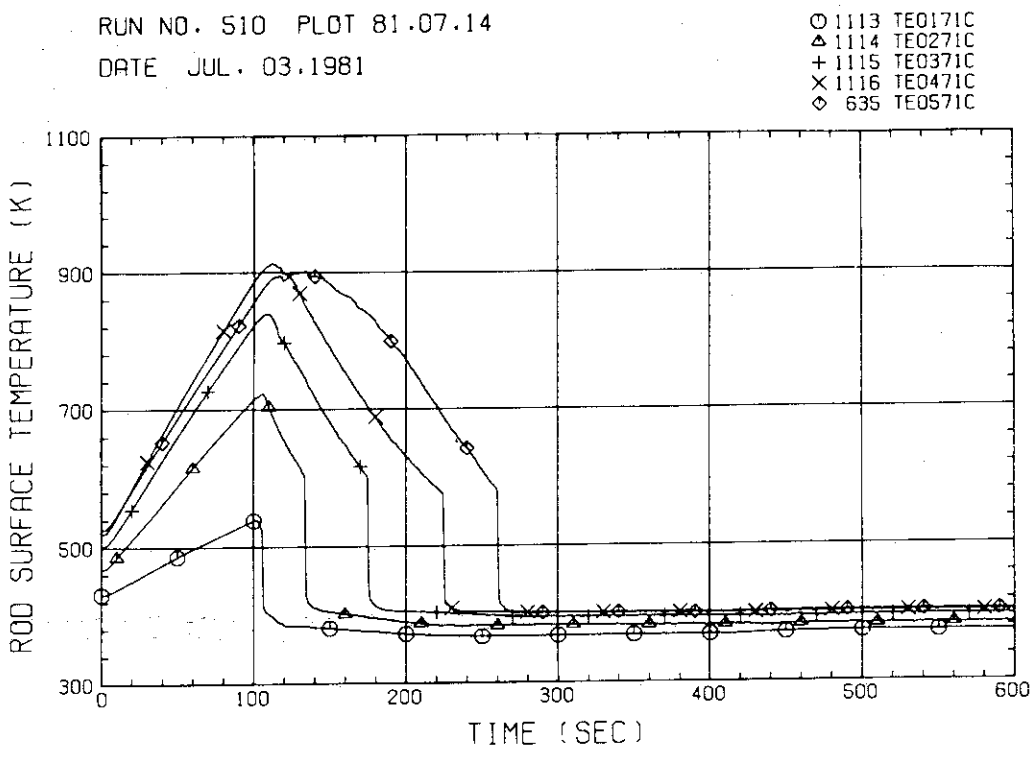

Fig.B-13 HEATER ROD TEMPERATURE (BUNDLE 7-1C, LOWER HALF)

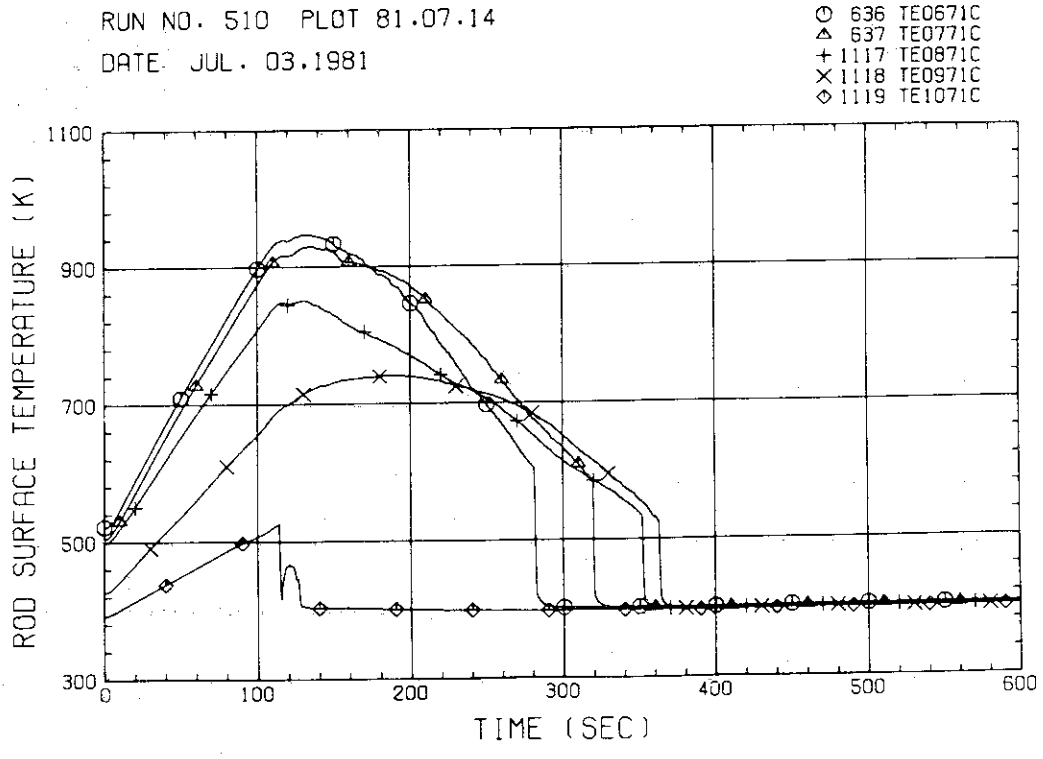

Fig.B-14 HEATER ROD TEMPERATURE (BUNDLE 7-1C, UPPER HALF)

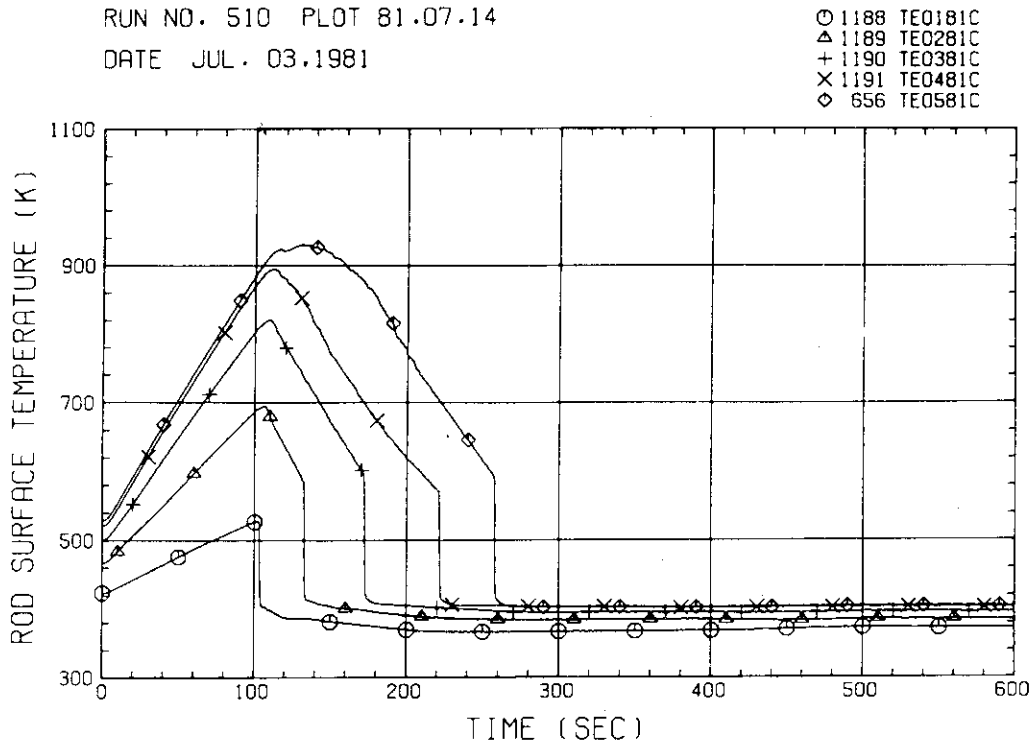

Fig.B-15 HEATER ROD TEMPERATURE (BUNDLE 8-1C, LOWER HALF)

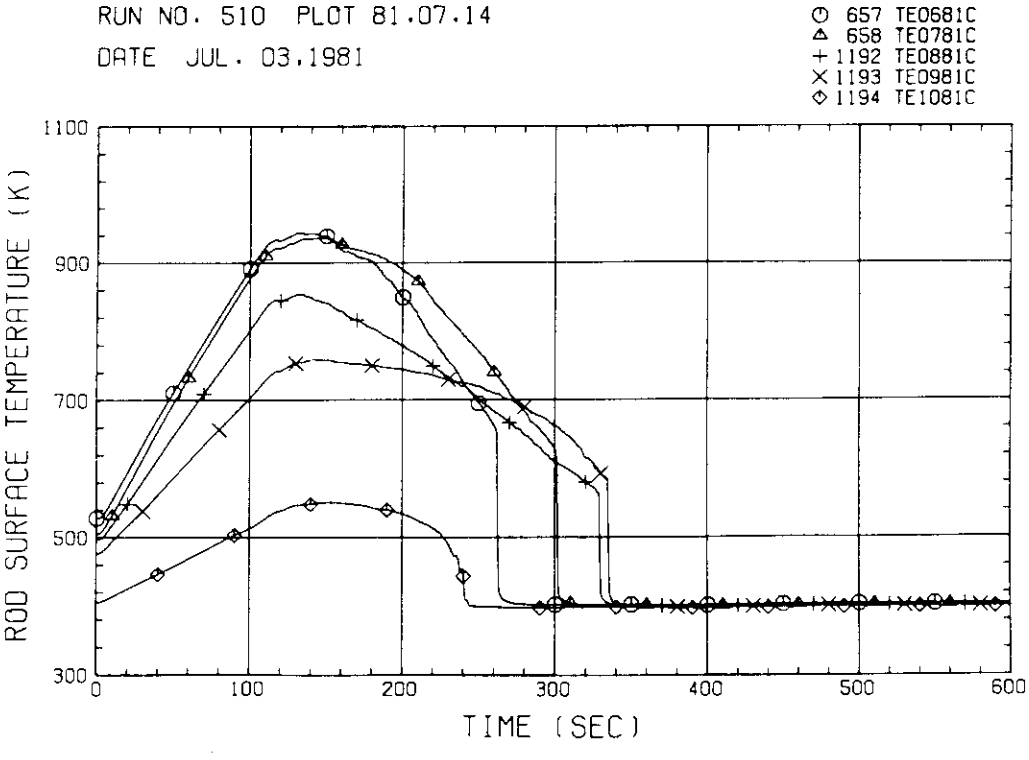

Fig.B-16 HEATER ROD TEMPERATURE (BUNDLE 8-1C, UPPER HALF)

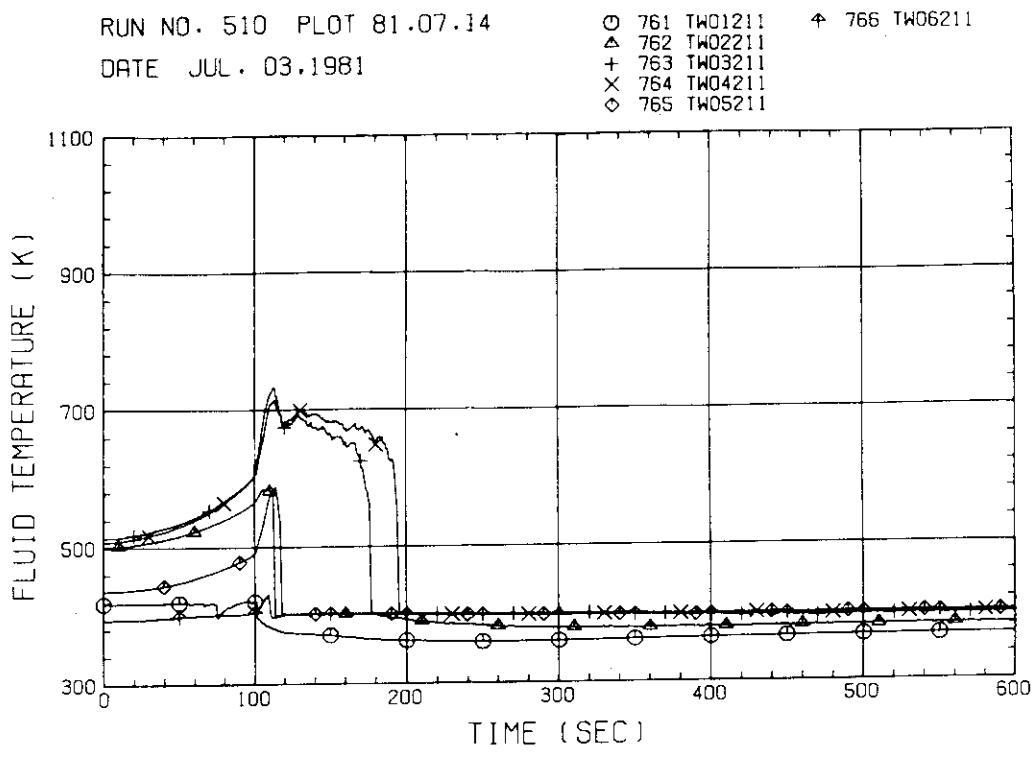

Fig.B-17 FLUID TEMPERATURE IN CORE (BUNDLE 2-1)

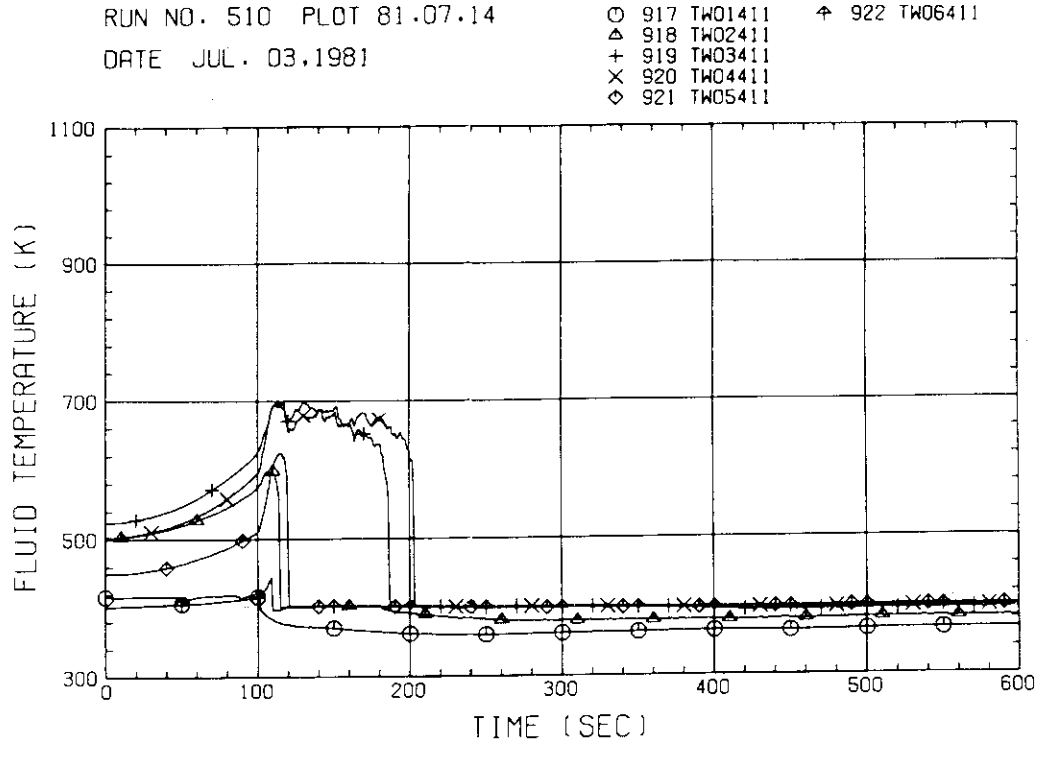

Fig.B-18 FLUID TEMPERATURE IN CORE (BUNDLE 4-1)

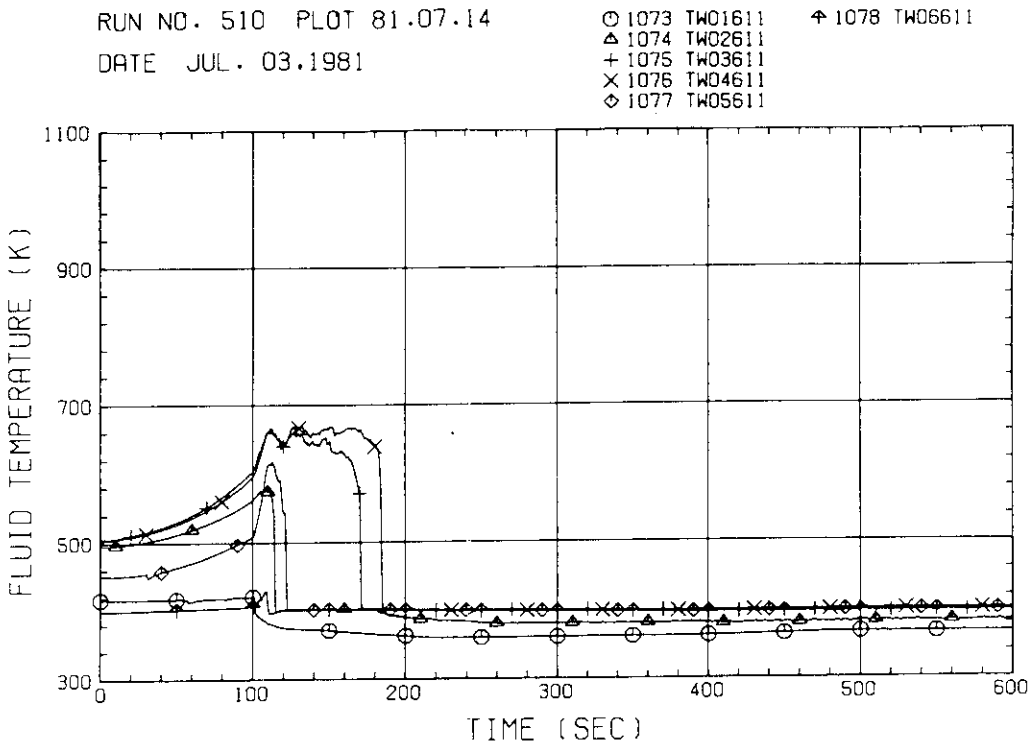

Fig.B-19 FLUID TEMPERATURE IN CORE (BUNDLE 6-1)

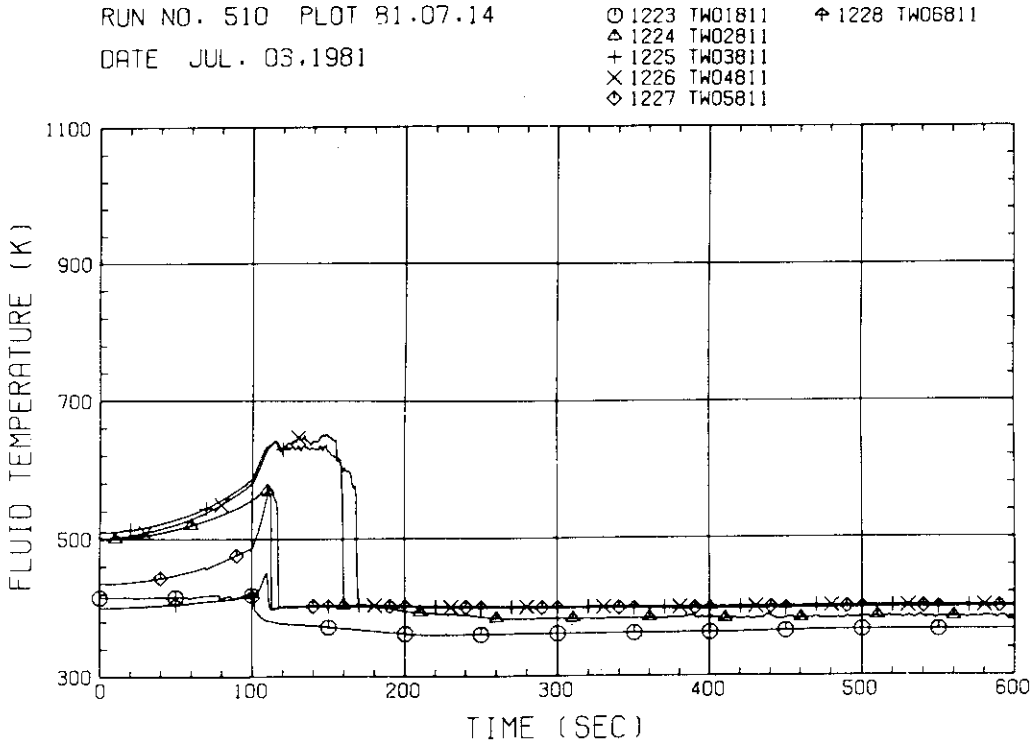

Fig.B-20 FLUID TEMPERATURE IN CORE (BUNDLE 8-1)

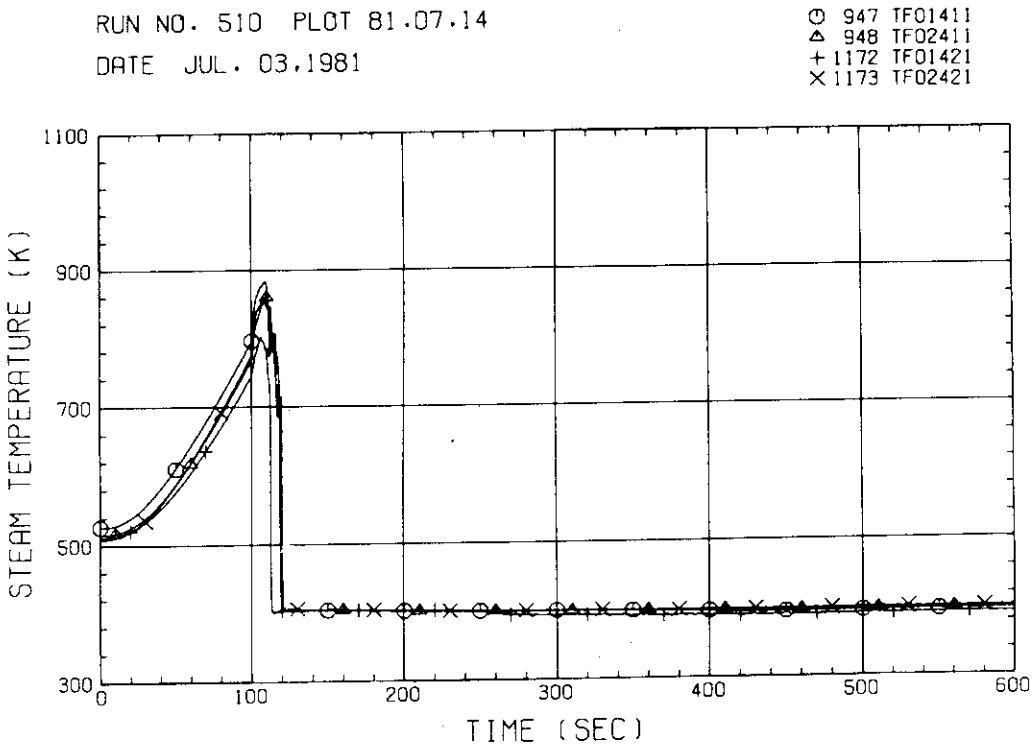

Fig.B-21 STEAM TEMPERATURE IN CORE, BUNDLE 4
(01411-1.735M, 02411-1.875M, 01421-1.38M, 02421-1.915M)

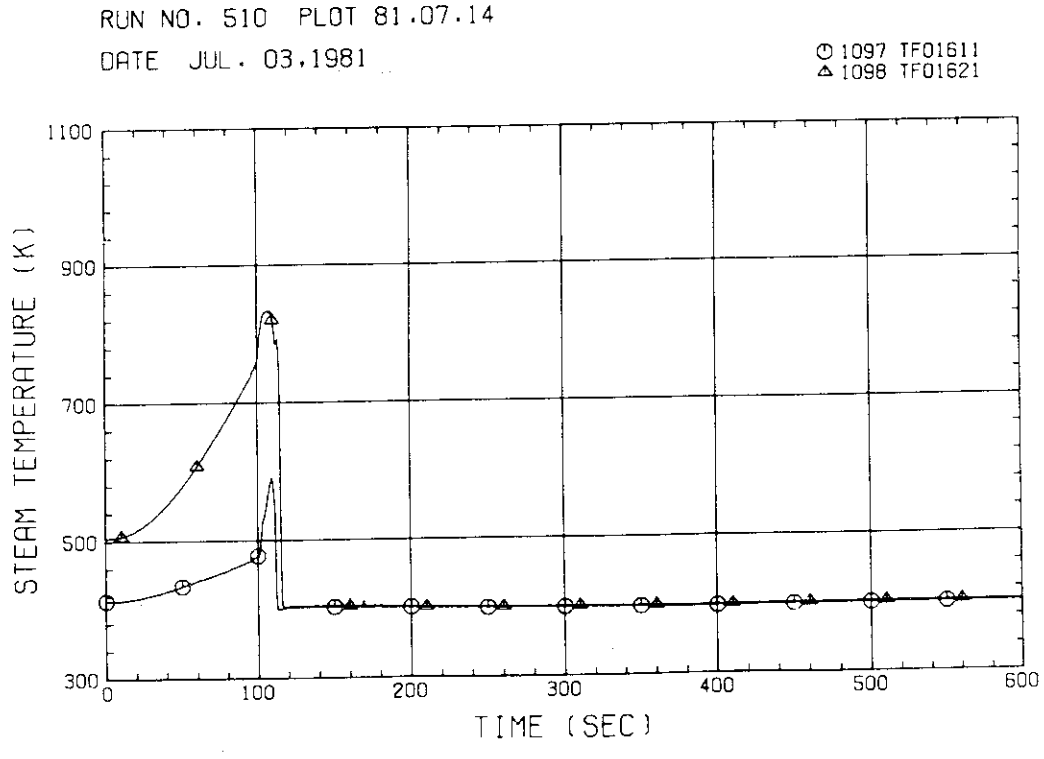

Fig.B-22 STEAM TEMPERATURE IN CORE, BUNDLE 6
(01611-3.62M, 01621-1.915M)

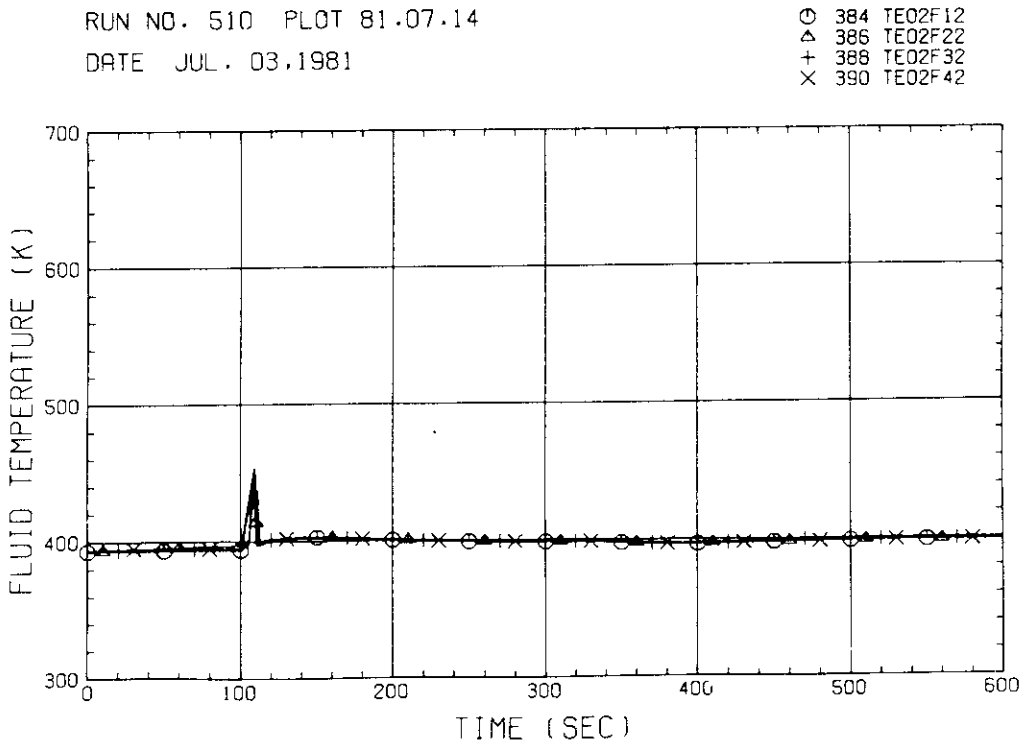

Fig.B-23 FLUID TEMPERATURE JUST ABOVE END BOX (BUNDLE 1.2.3.4. COLD LEG SIDE)

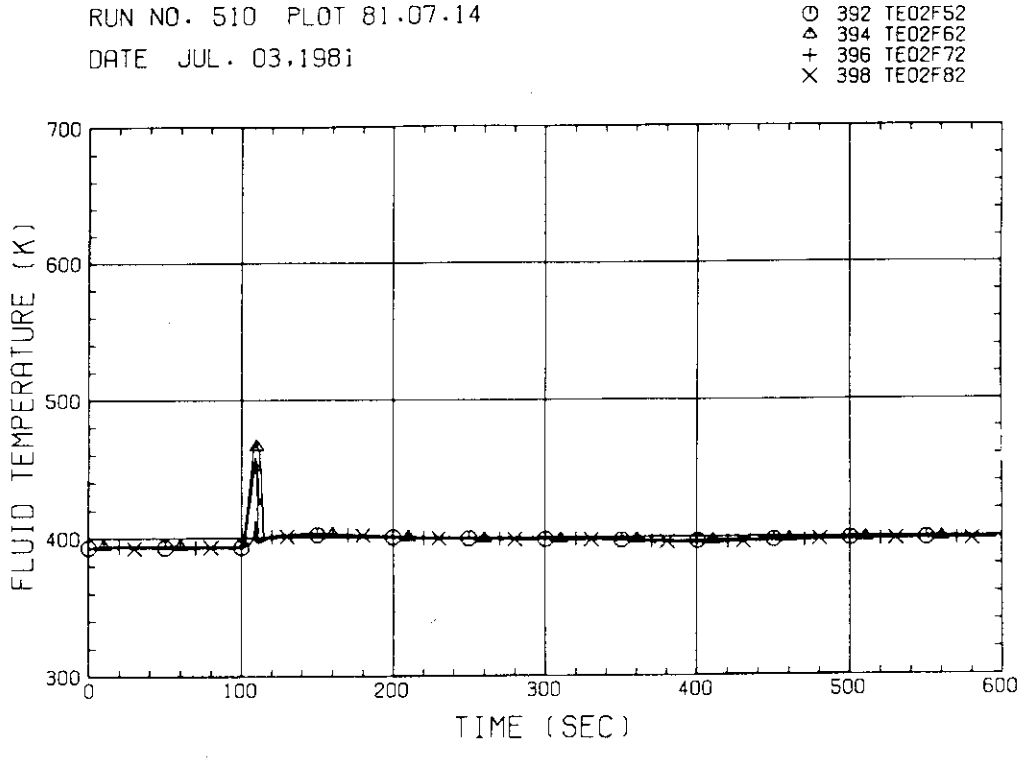

Fig.B-24 FLUID TEMPERATURE JUST ABOVE END BOX (BUNDLE 5.6.7.8. COLD LEG SIDE)

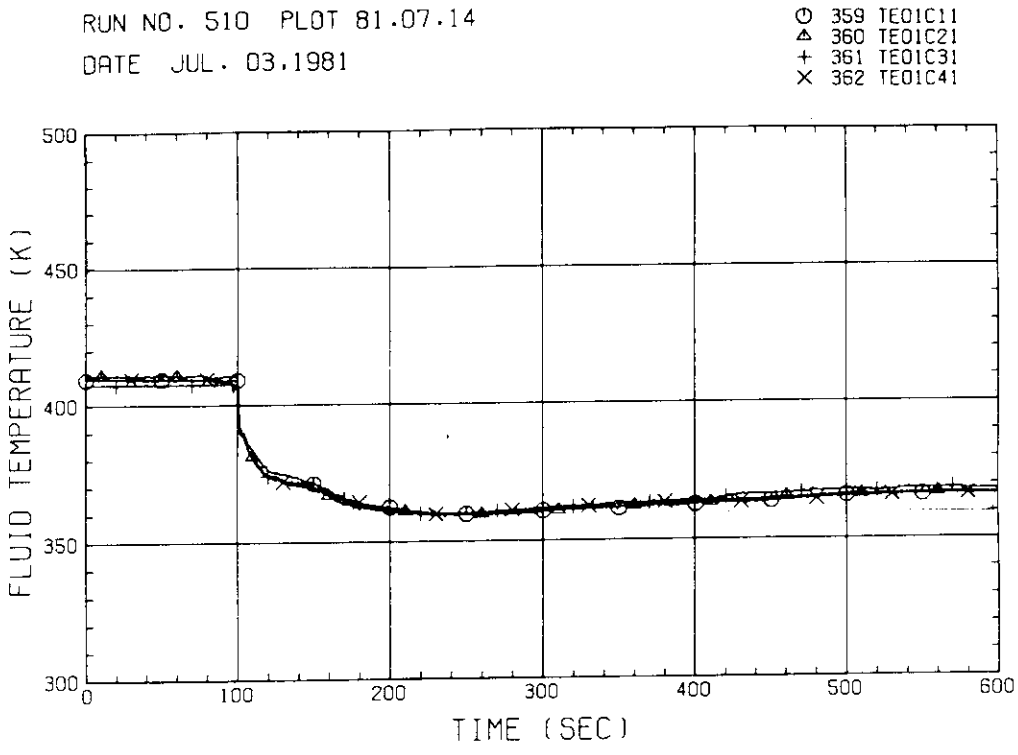

Fig.B-25 FLUID TEMPERATURE AT CORE INLET (BUNDLE 1.2.3.4. 100MM BELOW HEATED PART)

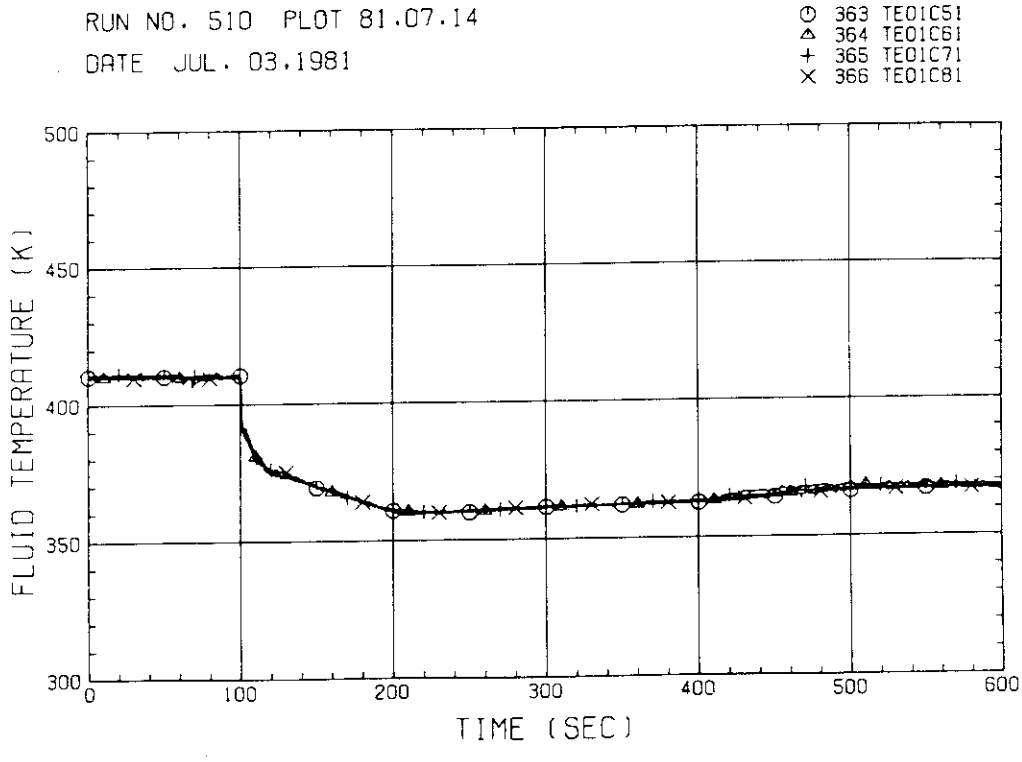

Fig.B-26 FLUID TEMPERATURE AT CORE INLET (BUNDLE 5.6.7.8. 100MM BELOW HEATED PART)

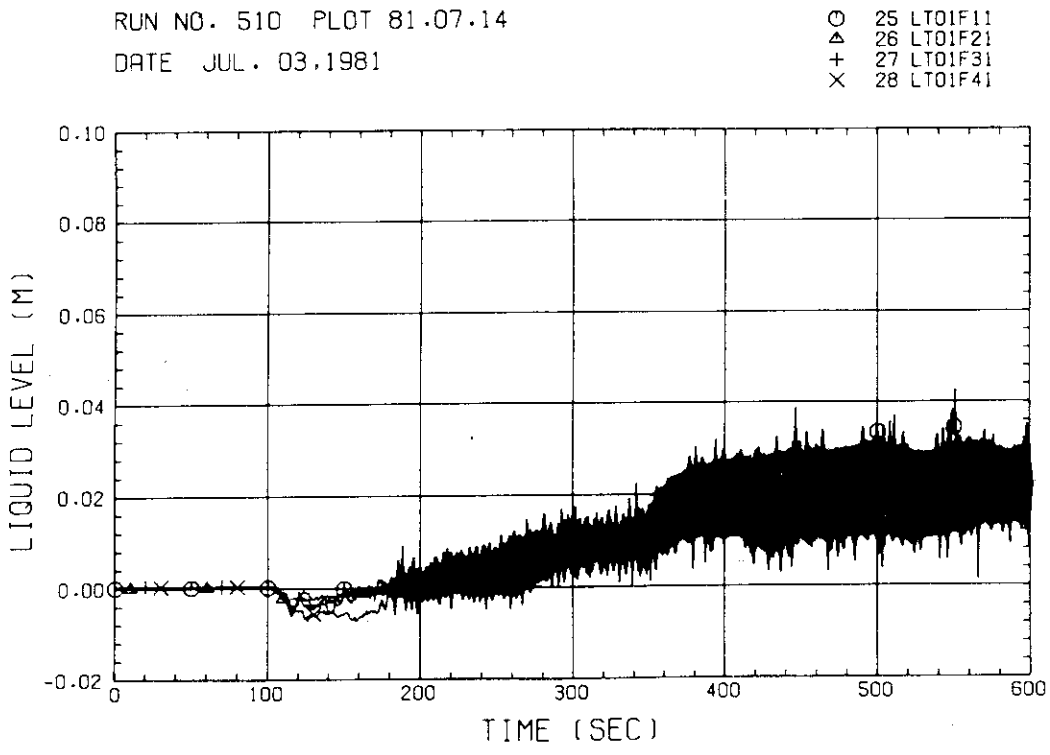

Fig.B-27 LIQUID LEVEL ABOVE END BOX TIE PLATE (BUNDLE 1,2,3,4)

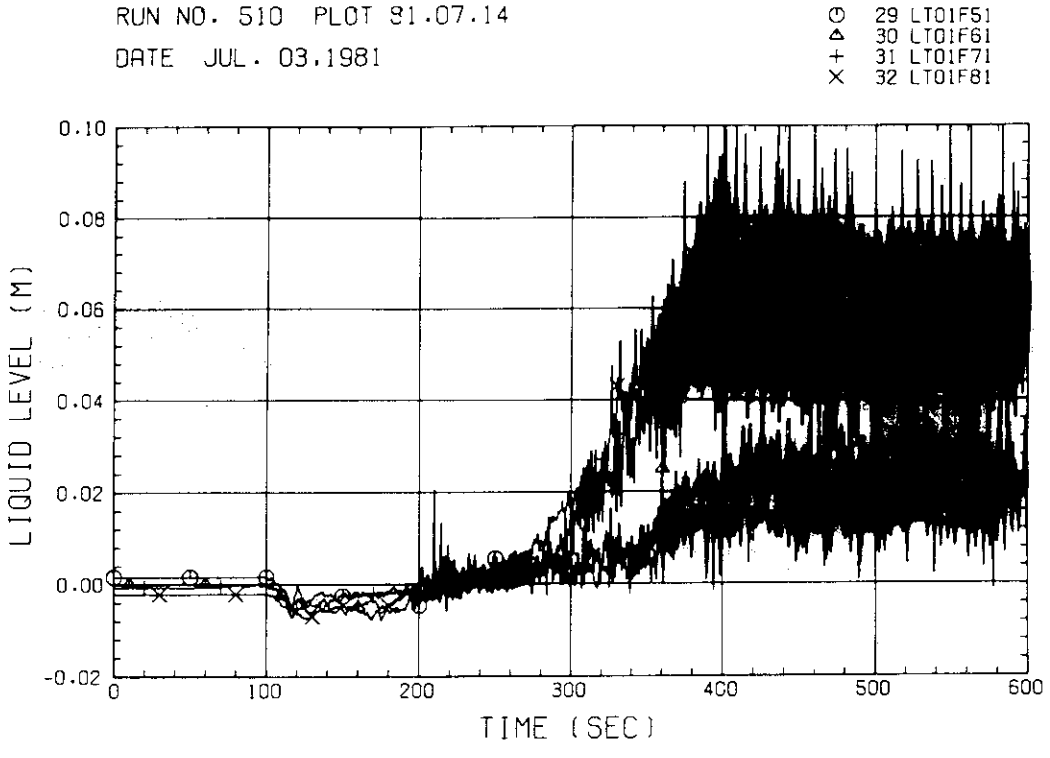

Fig.B-28 LIQUID LEVEL ABOVE END BOX TIE PLATE (BUNDLE 5,6,7,8)

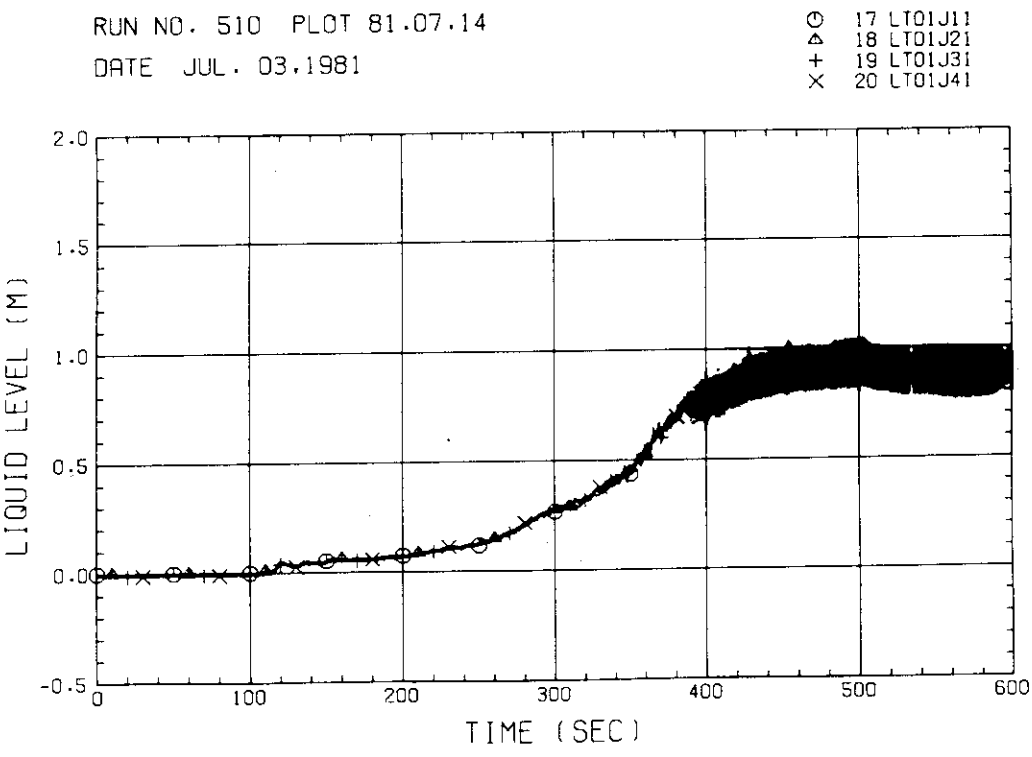

Fig.B-29 LIQUID LEVEL ABOVE UCSP (BUNDLE 1.2.3.4)

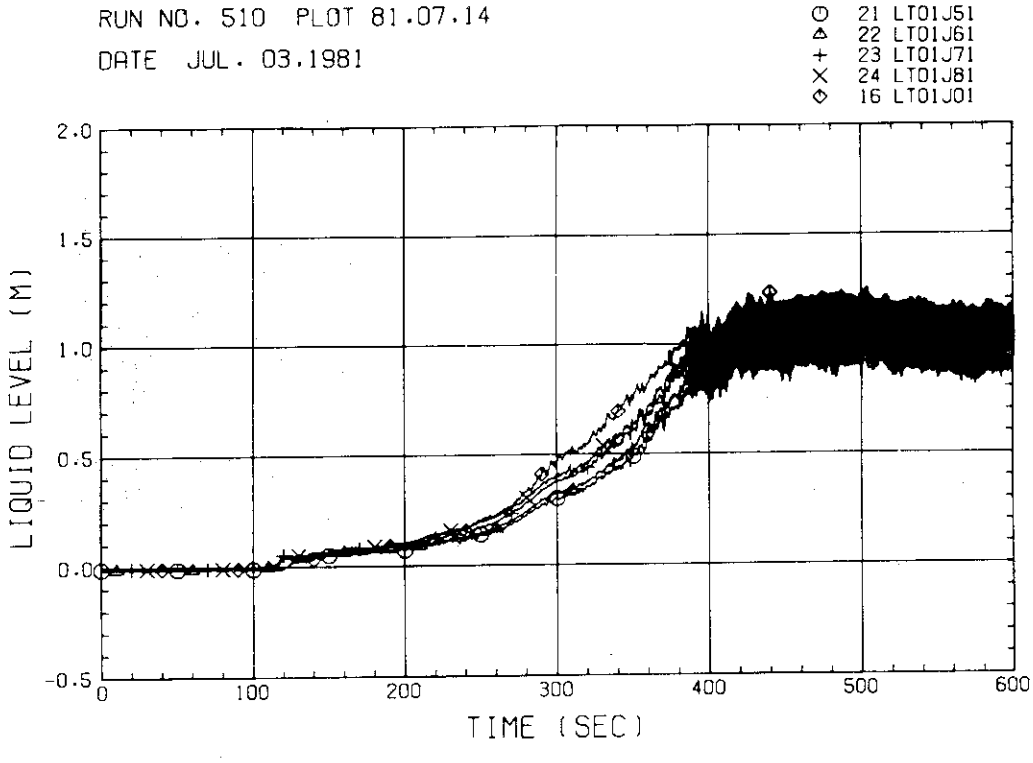

Fig.B-30 LIQUID LEVEL ABOVE UCSP (BUNDLE 5.6.7.8 AND CORE BAFFLE)

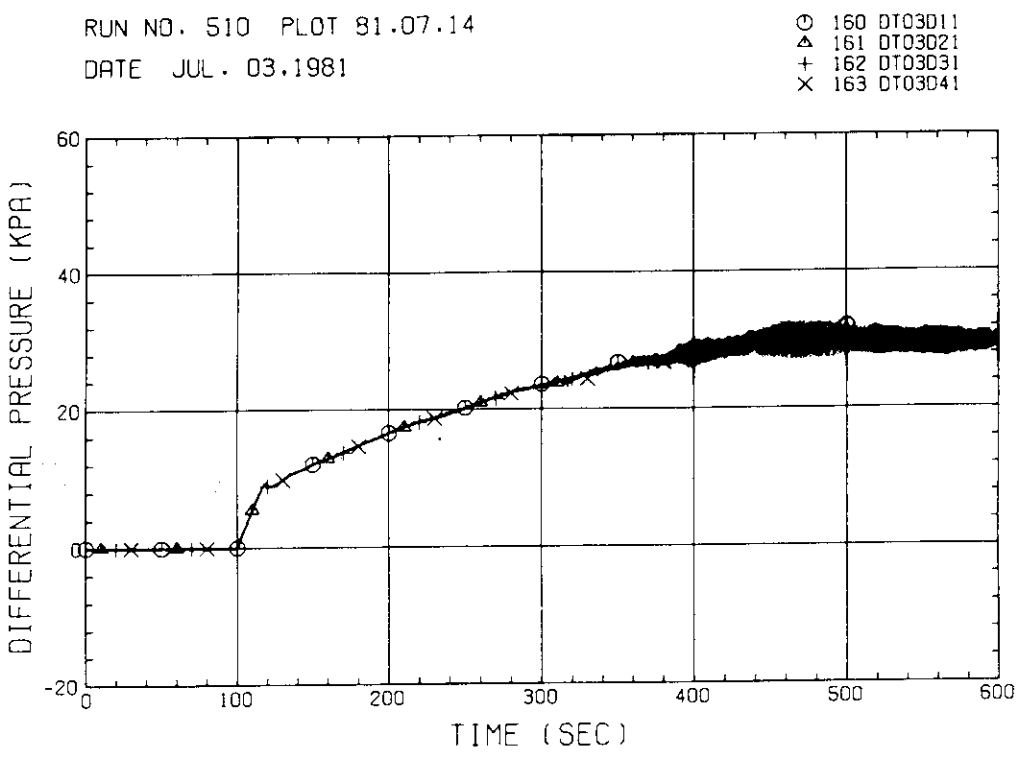

Fig.B-31 DIFFERENTIAL PRESSURE OF CORE FULL HEIGHT (BUNDLE 1.2.3.4)

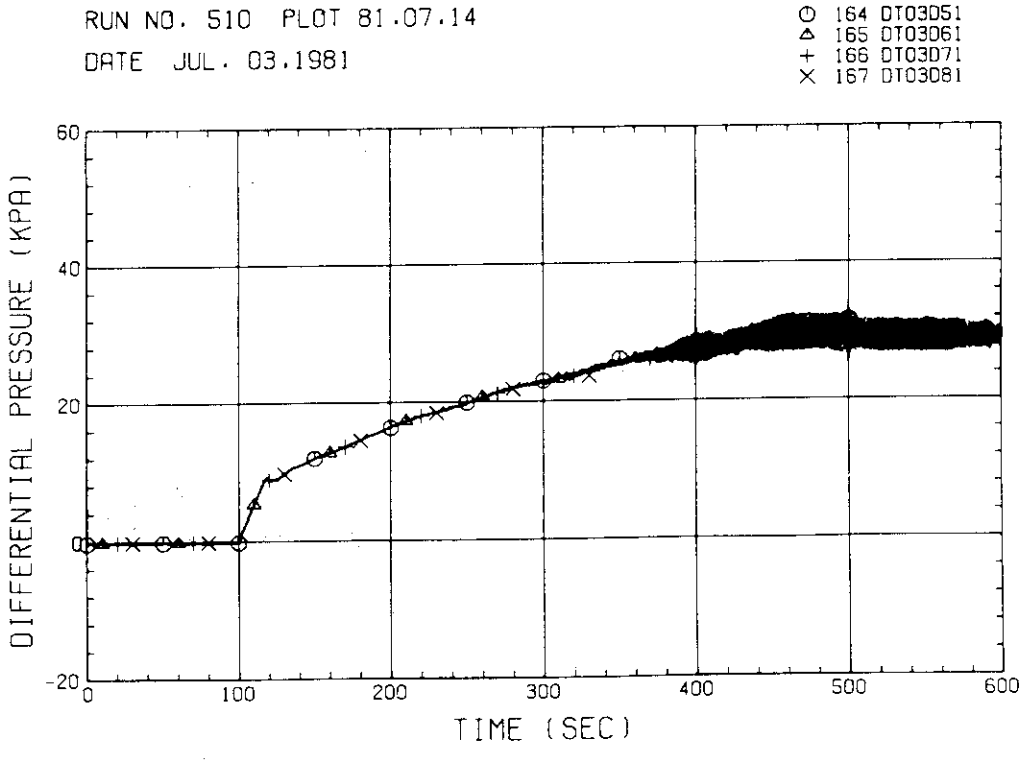

Fig.B-32 DIFFERENTIAL PRESSURE OF CORE FULL HEIGHT (BUNDLE 5.6.7.8)

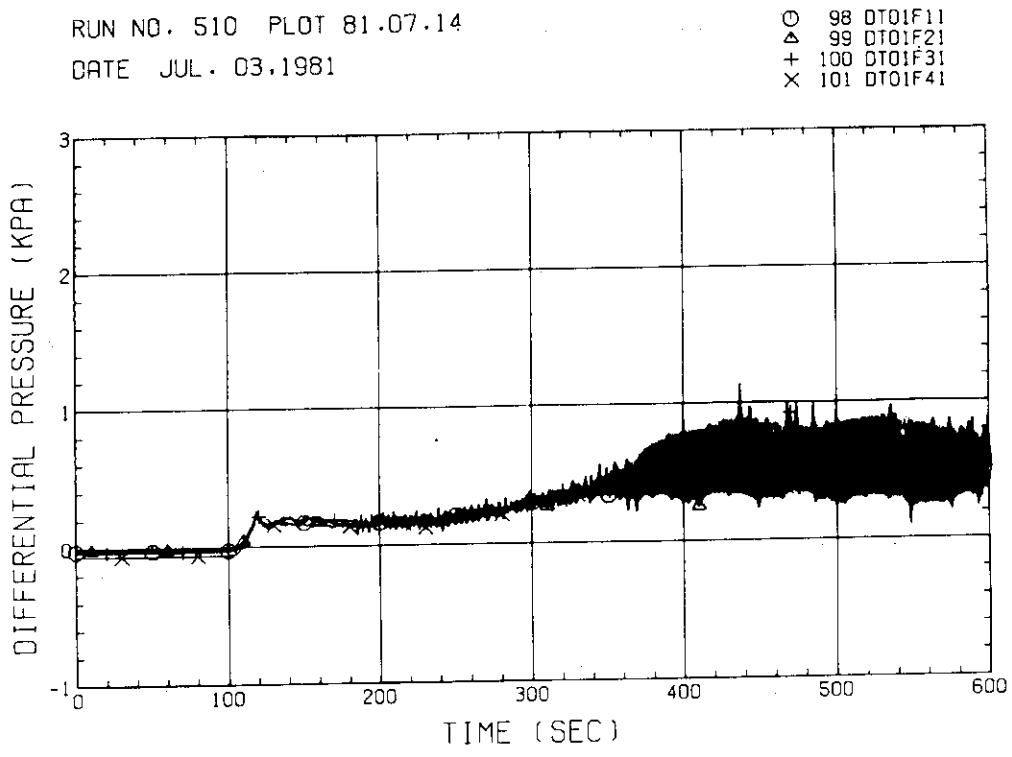

Fig.B-33 DIFFERENTIAL PRESSURE ACROSS END BOX TIE PLATE (BUNDLE 1,2,3,4)

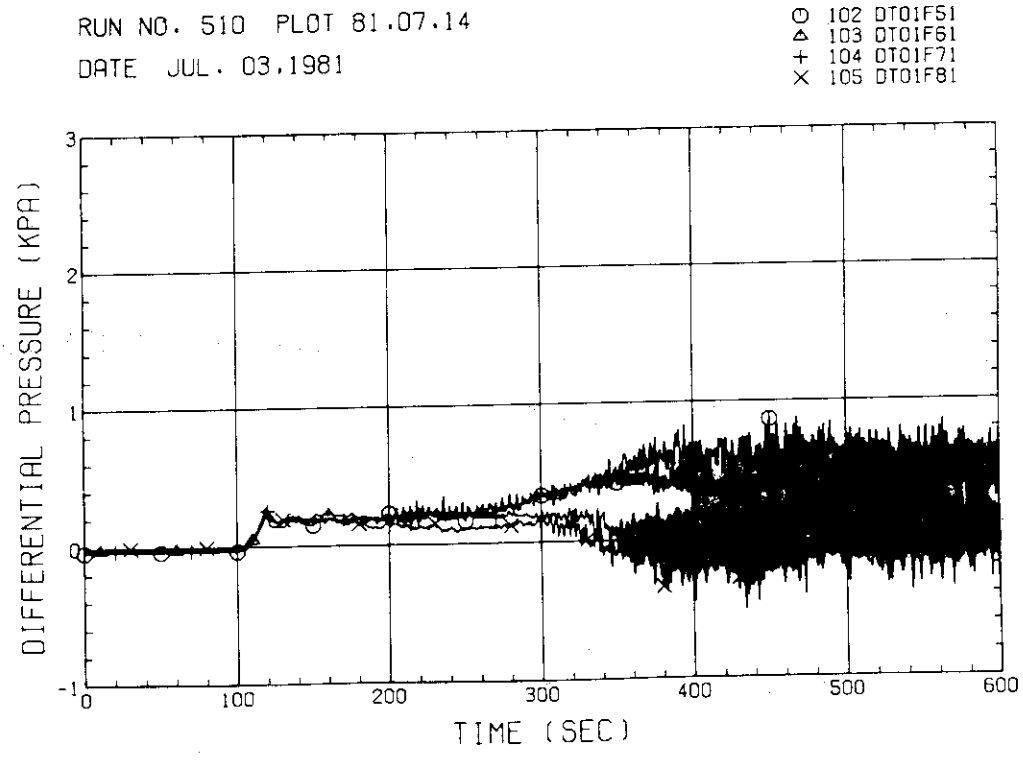

Fig.B-34 DIFFERENTIAL PRESSURE ACROSS END BOX TIE PLATE (BUNDLE 5,6,7,8)

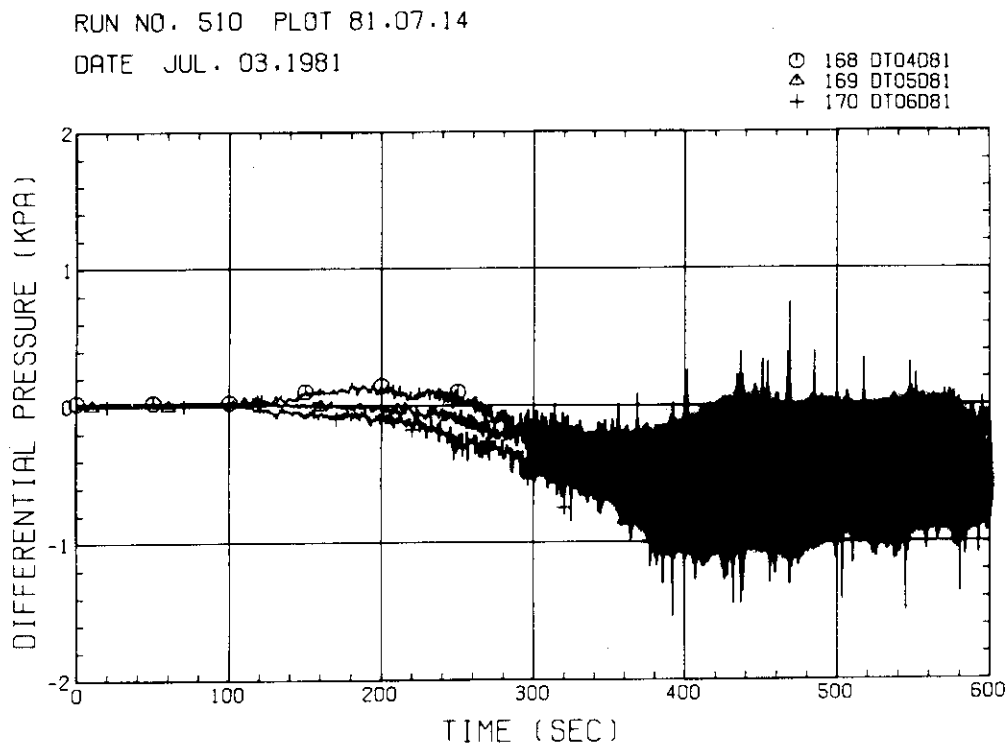

Fig.B-35 DIFFERENTIAL PRESSURE, HORIZONTAL,BUNDLE 5-8 (04-BELOW SPACER 4, 05-BELOW SPACER 6, 06-BELOW END BOX)

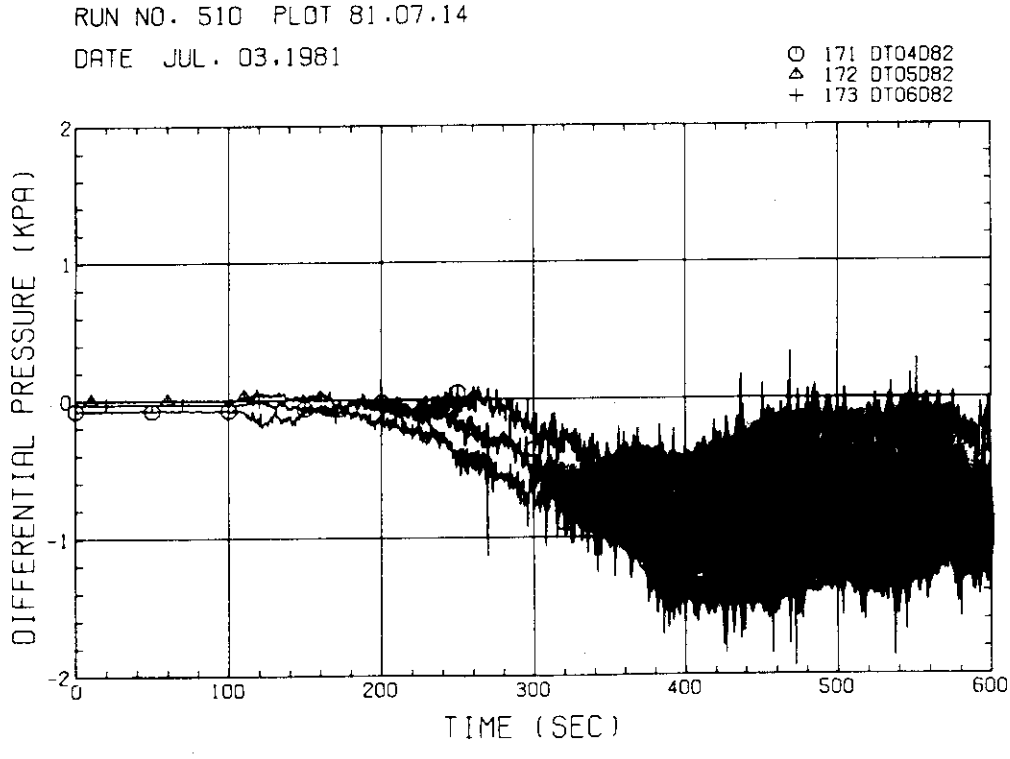

Fig.B-36 DIFFERENTIAL PRESSURE, HORIZONTAL,BUNDLE 1-8 (04-BELOW SPACER 4, 05-BELOW SPACER 6, 06-BELOW END BOX)

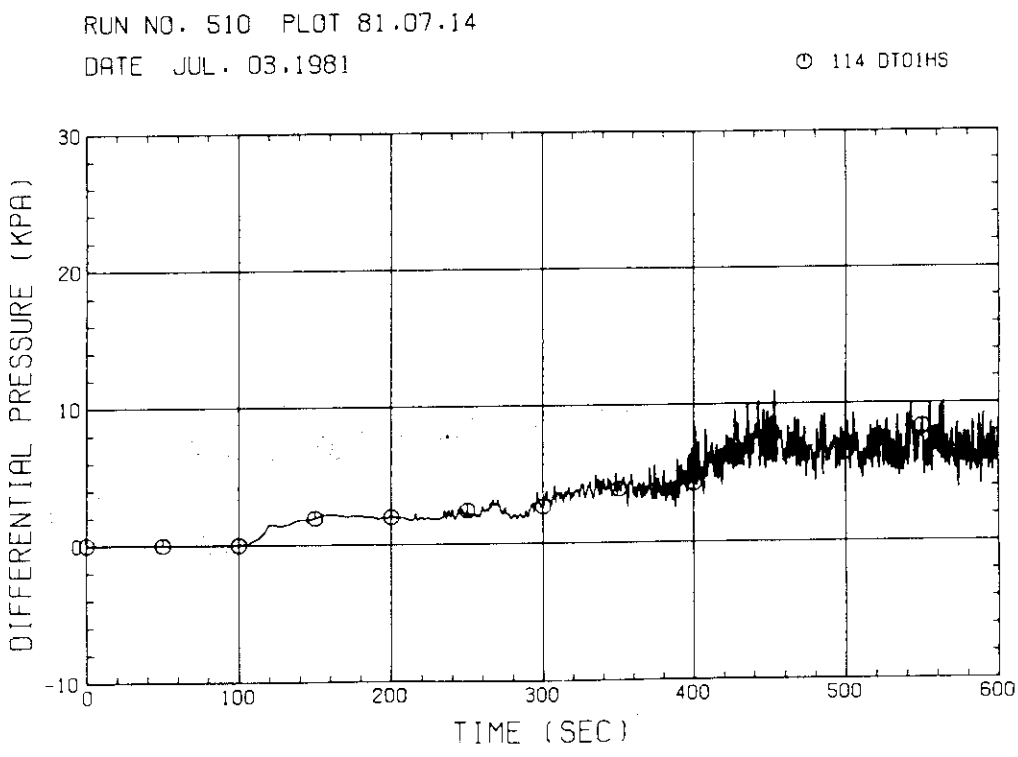

Fig.B-37 DIFFERENTIAL PRESSURE OF HOT LEG.
HOT LEG INLET - STEAM/WATER SEPARATOR INLET

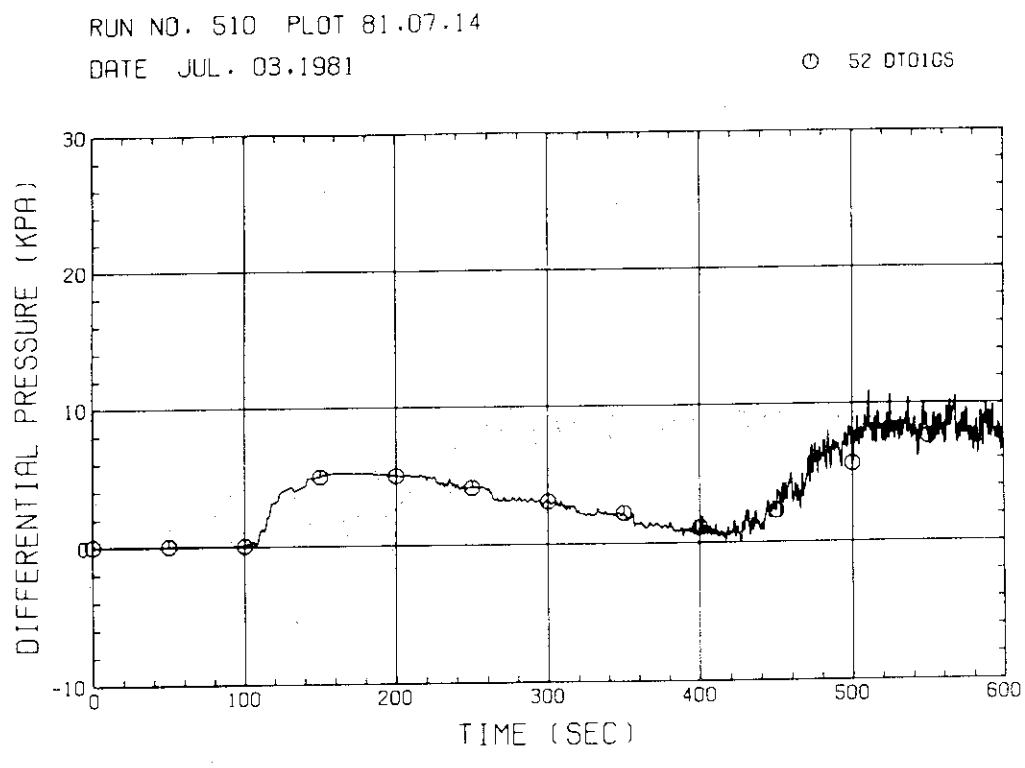

Fig.B-38 DIFFERENTIAL PRESSURE, STEAM/WATER SEPARATOR INLET -
BROKEN COLD LEG - S/W SEPARATOR SIDE NOZZLE

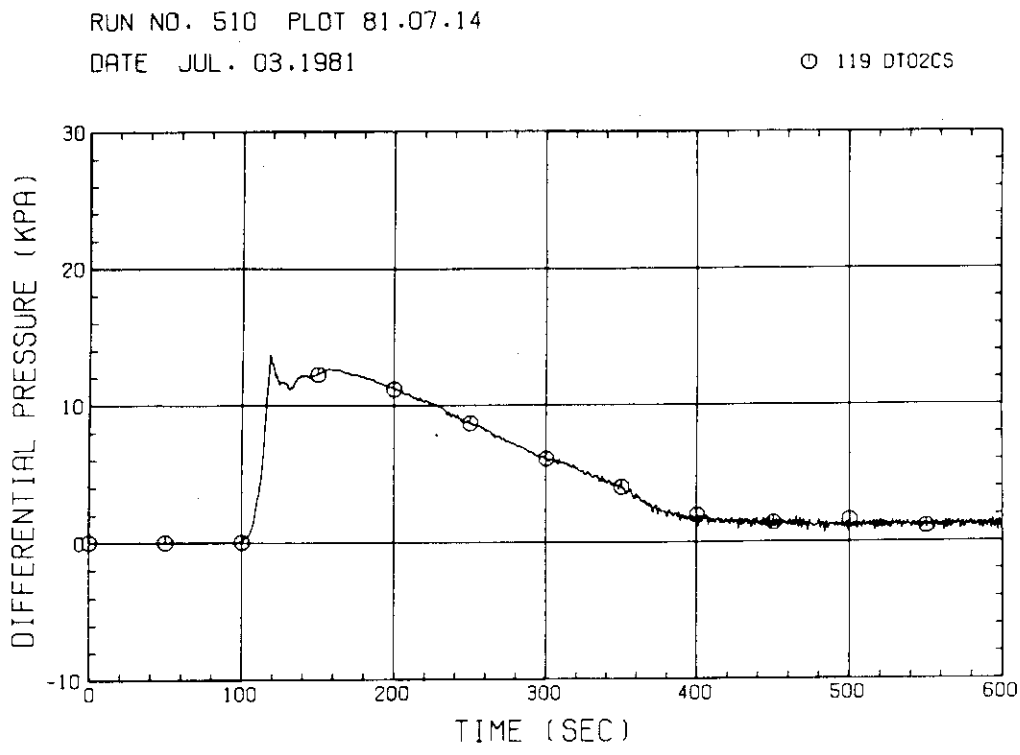

Fig.B-39 DIFFERENTIAL PRESSURE OF INTACT COLD LEG

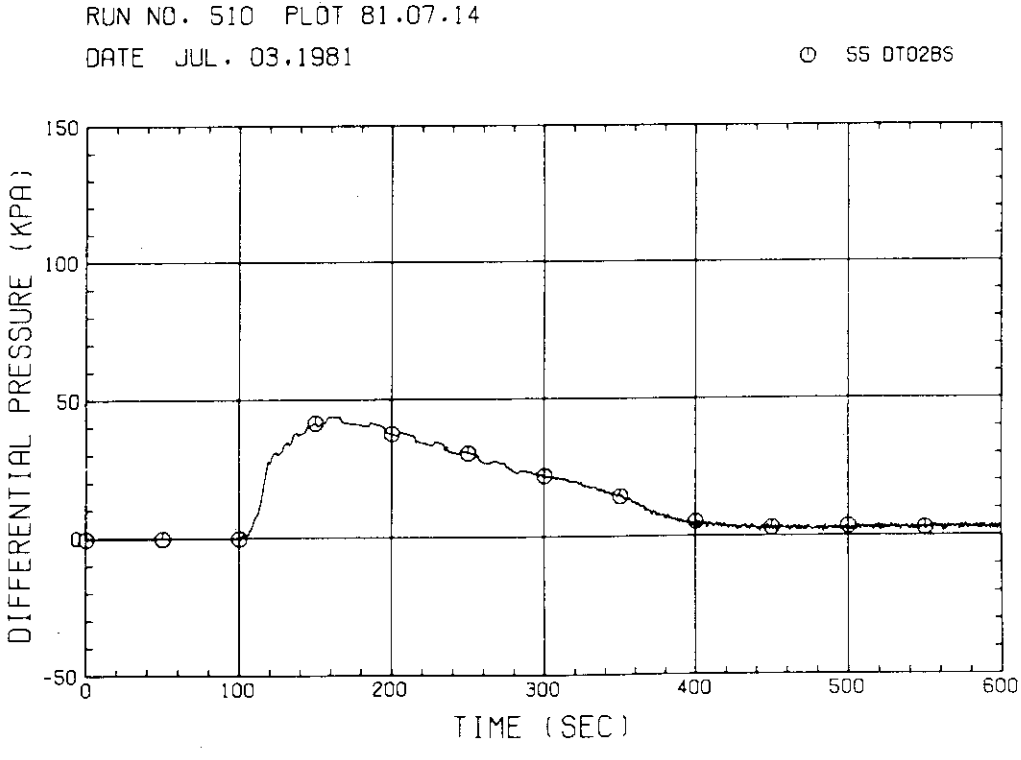

Fig.B-40 DIFFERENTIAL PRESSURE, STEAM/WATER SEPARATOR - CONTAINMENT TANK-II

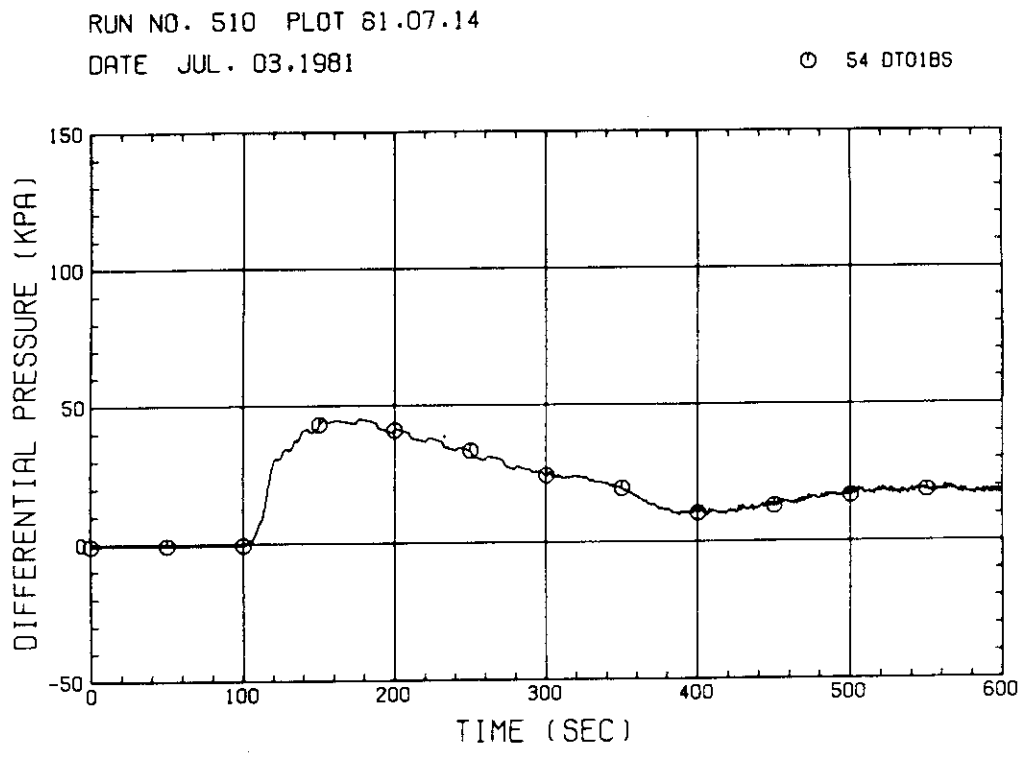

Fig.B-41 DIFFERENTIAL PRESSURE, TOP OF UPPER PLENUM - CONTAINMENT TANK-II

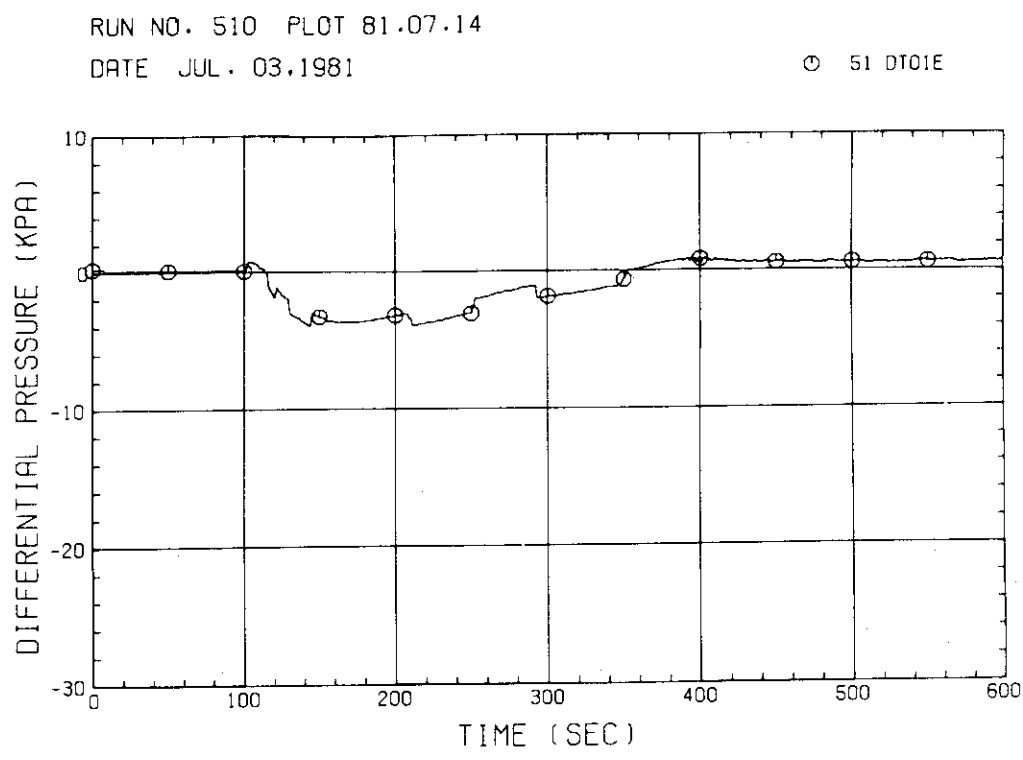

Fig.B-42 DIFFERENTIAL PRESSURE, CONTAINMENT TANK-II - CONTAINMENT TANK-I

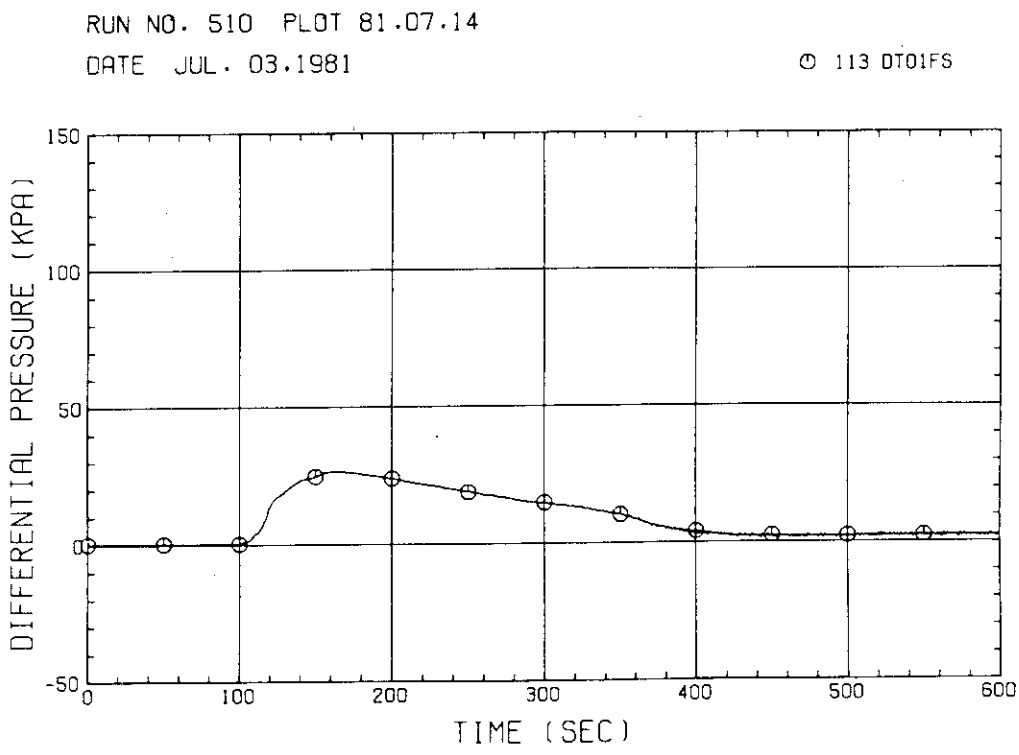

Fig.B-43 DIFFERENTIAL PRESSURE OF BROKEN COLD LEG - PV SIDE, DOWNCOMER - CONTAINMENT TANK-I

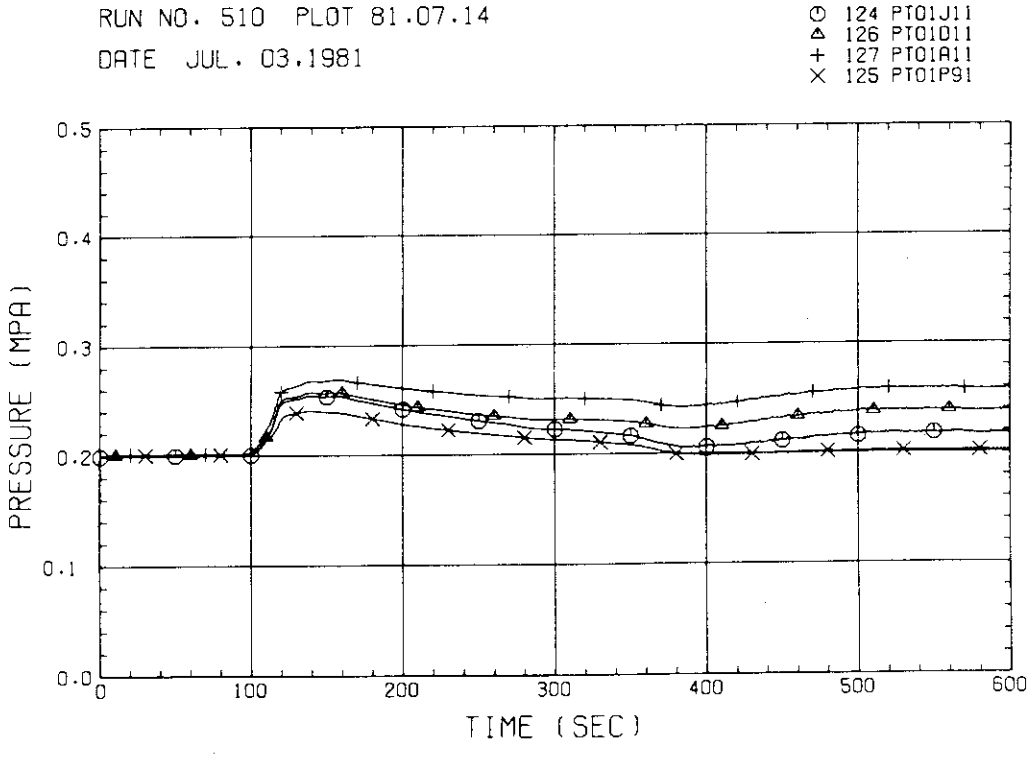

Fig.B-44 PRESSURE IN PV (J - TOP OF PV, D - CORE CENTER, A - CORE INLET, P - BELOW COLD LEG NOZZLE IN DOWNCOMER)

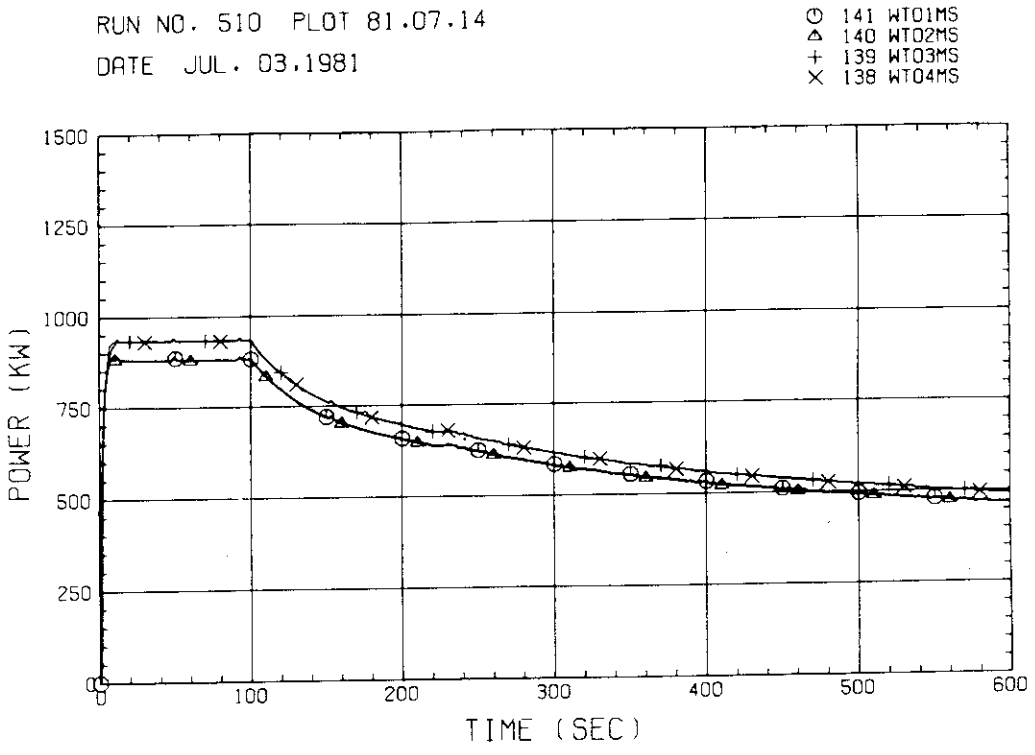

Fig.B-45 BUNDLE POWER (BUNDLE 1.2.3.4)

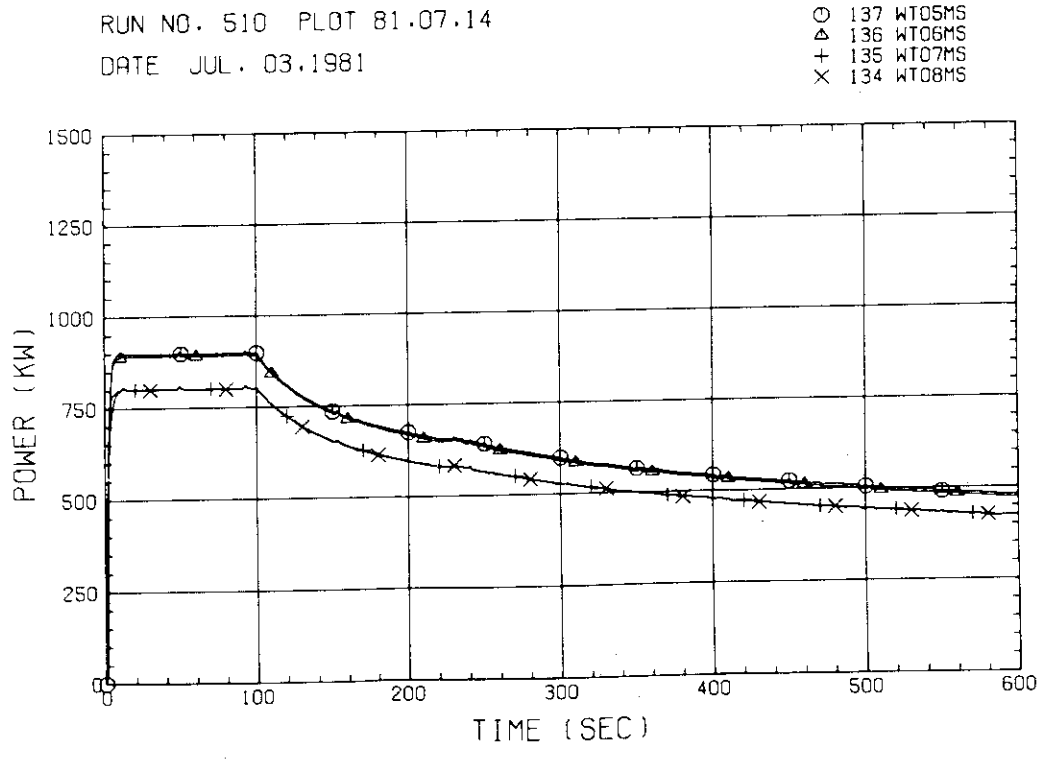

Fig.B-46 BUNDLE POWER (BUNDLE 5.6.7.8)

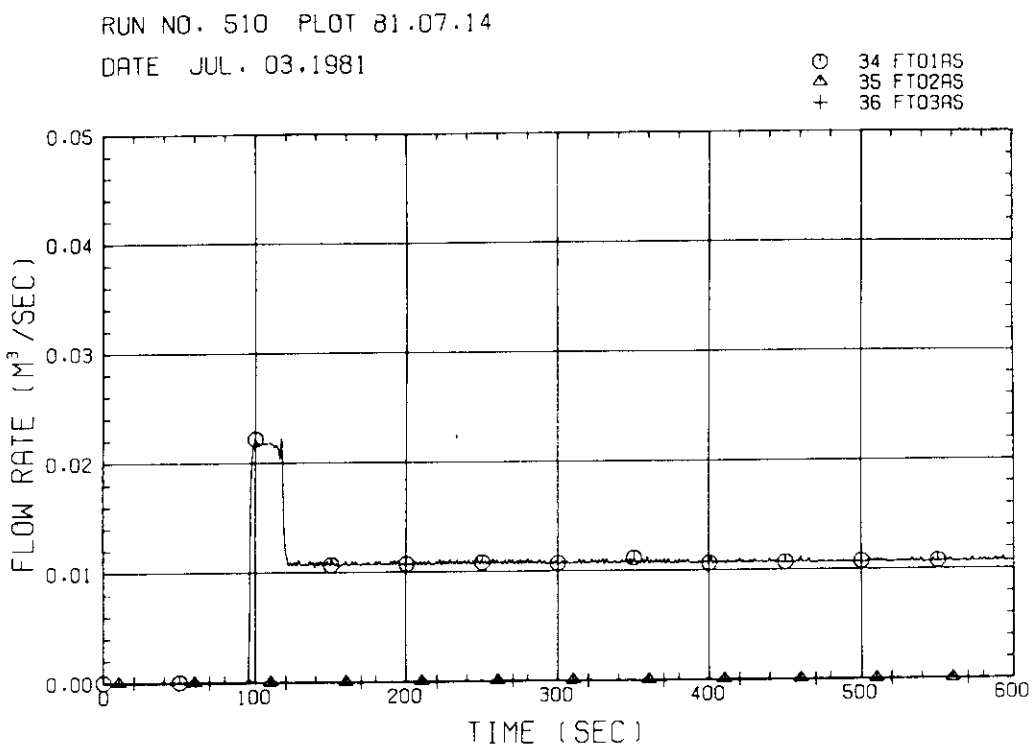

Fig.B-47 FLOW RATE OF ECC WATER (01-DOWNCOMER/LOWER PLENUM/ HOT LEG, 02-INTACT COLD LEG, 03-BROKEN COLD LEG)